



A VAPOUR-LIQUID EQUILIBRIUM STUDY ON
SUB-CRITICAL SYSTEMS USING A STATIC
APPARATUS

E.P.Wilson

April 2, 2009

A thesis submitted in fulfillment of the academic requirements for the degree of Master of Science at the School Of Chemical Engineering, University of KwaZulu-Natal (Durban).

ABSTRACT

High pressure vapour-liquid equilibrium experiments were undertaken with a static high-pressure apparatus designed by Prof. J. D. Raal and commissioned by Prof. D. Ramjugernath. Isothermal VLE binary data data was measured at moderate temperatures and pressures ranging from atmospheric to 7.2 bar. The equipment had a combined operating pressure and temperature limit of approximately 150 bar and 215° C respectively. The apparatus was initially designed for the measurement of gas-liquid binary systems- where one of the components was supercritical at the operating conditions.

Test data were measured for the pentane + ethanol system at 100.41°C. The 2-methyl-2-butene + TAME, hydrocarbon + olefin system, was observed at 70°C, 94.6°C and 104.5°C. The apparatus was modified for the measurement of binary systems containing sub-critical components at the operating conditions specified. An injection port was installed on the apparatus assembly such that the second component of the binary system could be introduced into the equilibrium cell.

The binary VLE data was regressed using various thermodynamic models. The direct method or *phi-phi* approach was considered. The equations of state models used in the regression were the Peng-Robinson-Stryjek-Vera (PRSV) and Soave-Redlich-Kwong (SRK). The 1-fluid van der Waals, Wong and Sandler mixing rules were selected to estimate binary interactions. The excess Gibbs energy equations coupled with the Wong and Sandler mixing rules were the NRTL and WILSON equations.

Preface

The work described in this thesis was performed in the School of Chemical Engineering at the University Of KwaZulu-Natal, Durban from March, 2004 to December, 2007. The supervision of this project was under Prof. D. Ramjugernath and Dr. P. Naidoo.

I, Etienne Wilson, declare that the work presented in this thesis is my own, unless stated otherwise in the text.

Etienne Wilson

As the candidate's supervisor, I, Prof. D. Ramjugernath have approved this thesis for submission.

Prof. Deresh Ramjugernath

As the candidate's co-supervisor, I, Dr. P. Naidoo have approved this thesis for submission.

Dr. Prathieka Naidoo

ACKNOWLEDGEMENTS

This project has been a long journey in my life. I think that it is safe to say that it has been the toughest personal challenge that I have encountered thus far. The completion of this thesis must be attributed to the efforts of many individuals. These individuals have given me technical advice and in general personal support. I take this opportunity to send them my sincerest gratitude and I apologize in advance for any persons that have been omitted.

- I am a spiritual person and therefore must acknowledge God for the opportunity to undertake a Masters.
- My family and especially my mother, Veronica Wilson. She has been a vital source of motivation and walked this journey with me from the start. There were times when I took her efforts for granted, I apologise. Thank you for not giving up, I could not have completed without you.
- My Supervisors, Prof. D. Ramjugernath and Dr. Prathieka Naidoo for the opportunity to undertake the research project. Thank you for your patience and support.
- The mechanical workshop staff in the School of Chemical Engineering (UKZN). A special thanks to Mr Les Henwood for his technical advice and moreover your friendship.
- The computer and electronics workshop staff in the School of Chemical Engineering (UKZN). Mr Dhavaraj Naidoo, Mr Preyothan Nayager and Mr Colin Mandri.
- Special thanks to the following people for their friendship and support: Prashant Reddy, Gregory Moodely, Viran Pillay, Jason Knock, Davide Magagna, Wesley Jordan Oaks, Dr. Tyrone Mcknight, Dr. Scott Clifford, Carl Murphy, Vivek Gadodia, Warren Bokwe, Seth Keshwar-Hill, Damir Turkovic and his family, Dr. Roger Harris, the Brauns family, the Manjoo family and Lauren Williams. A special acknowledgement to Prof. Maciej Starzak for his technical advice with the MAT-LAB programming for this project.

- Sasol R&D for their patience and support. In particular Mr Japie Scholtz and Mr Harko Mulder. I am grateful for the opportunities that you gave me to complete the last part of the thesis.
- The National Research Foundation (NRF) Of South Africa for their financial support.

Contents

1	Introduction	1
2	Literature Survey Of Equipment	2
2.1	Equipment classification	2
2.2	Analytical methods	4
2.2.1	Features of the analytical method	4
2.2.2	Experimental difficulties with the analytical method	5
2.2.3	Gas chromatography	8
2.2.4	Spectroscopic or photochemical methods	9
2.3	Static type apparatus	10
2.3.1	Static analytical method	10
2.4	The static non-analytic method	10
2.4.1	General considerations	10
2.4.2	Disadvantages	11
2.5	The static combined method	11
2.5.1	General considerations	11
2.5.2	Apparatus used in this HPVLE study	12
3	Interpretation of vapour-liquid equilibrium thermodynamics	13
3.1	Phase Equilibria	13
3.2	Computational methods for analyzing HPVLE	14
3.2.1	Combined Method	14
3.2.2	Direct Method	17
3.3	Equations Of State	18
3.3.1	Cubic Equations Of State	18
3.3.2	Extension of Cubic Equations Of State to Mixtures	27
3.4	General considerations for the liquid phase	33
3.4.1	Activity Coefficients	34
3.4.2	Excess Gibbs energy models	34
3.5	Standard states	37

4	Experimental Apparatus	40
4.1	History of HPVLE Apparatus	40
4.2	Apparatus: Specification and Considerations	43
4.2.1	The Equilibrium Cell And Piston Assembly	43
4.2.2	Mixing of Equilibrium cell contents	44
4.2.3	Sampling of the Vapour and Liquid Phases	45
4.2.4	Jet-mixers	46
4.3	Thermal specifications	48
4.3.1	The Air-bath	48
4.3.2	Temperature Control	50
4.3.3	Thermal Leaks, Conductive paths and Thermal disturbances	50
4.3.4	The Refrigeration unit	52
4.4	Pressure measurement	53
4.5	Composition measurement	53
4.6	Auxiliary Equipment	53
4.7	Equipment Safety Specifications	54
5	Systems Chosen For Experimentation	55
5.1	n-Pentane + Ethanol	55
5.2	2-Methyl-2-Butene + TAME	57
6	Experimental Procedure	58
6.1	Equipment Start-up	58
6.1.1	Preparation of the Equilibrium Cell	58
6.1.2	Preparation of components	60
6.1.3	Introducing the liquid component into the cell	60
6.1.4	Injection of the Second Liquid Component	61
6.2	Equilibrium phase sampling	62
6.2.1	Liquid phase sampling	62
6.2.2	Vapour phase sampling	64
6.3	GC calibration procedure	65
6.3.1	Standard solution method of calibration	65
7	Experimental Results	67
7.1	Vapour Pressure Measurements	67
7.1.1	n-Pentane Vapour Pressures	67
7.1.2	Ethanol Vapour Pressures	68
7.1.3	2-Methyl-2-Butene Vapour Pressures	69
7.1.4	TAME Vapour Pressures	70
7.2	Binary System Measurements	71
7.2.1	n-Pentane(1) + ethanol(2) system	71
7.2.2	2-Methyl-2-Butene(1) + TAME(2) system	73

8 Discussion: Computation Results	76
8.1 Theoretical Treatment of the Data	76
8.1.1 Direct-Method	76
8.2 Regression Analysis	77
8.2.1 Experimental Vapour Pressure Regression	77
8.2.2 Regression Analysis Of The Binary Systems Measured	79
9 Conclusion	95
Bibliography	97
A Appendix A	107
A.1 Criteria for phase equilibria	107
A.1.1 Partial Molar Properties	108
A.1.2 Fugacity	109
A.2 Fugacity Coefficient and activity coefficient	111
B Appendix B	113
B.1 Degassing apparatus	113
B.2 Determination of Jet-Mixer operating temperature	114
B.3 Temperature and pressure calibration	117
B.3.1 Temperature calibration	117
B.3.2 Pressure calibration	120
B.4 Gas Chromatograph Specifications	120
B.4.1 GC settings and calibration	120
C Appendix C	123
C.1 Physical Properties Of Components	123
C.1.1 General Physical Properties	123
C.1.2 Vapour Pressures	124

List of Tables

3.1	Examples of EOS that are modifications of the van der Waals equations, with respect to the attractive term.	24
3.2	Temperature dependence of the α function in cubic EOS . . .	25
3.3	Modifications to the repulsive term of the van der Waals EOS	26
4.1	Specifications of column	53
5.1	Experimental data for n-pentane + ethanol	56
5.2	Experimental data for 2-methyl-2-butene + TAME	57
7.1	n-Pentane measured vapour pressures and relative % error . .	68
7.2	Ethanol measured vapour pressures and relative % error . . .	69
7.3	2-Methyl-2-butene measured vapour pressures and relative % error	70
7.4	TAME measured vapour pressures and relative % error	71
7.5	n-Pentane(1) + ethanol(2) Binary Isotherm Data At 100.41°C	72
7.6	Experimental measurements of 2-methyl-2-butene(1) + TAME(2) at 70.0°C	73
7.7	Experimental measurements of 2-methyl-2-butene(1) + TAME(2) at 94.6°C	74
7.8	Experimental measurements of 2-methyl-2-butene(1) + TAME(2) at 105.4°C	75
8.1	The Direct-Method input parameters	77
8.2	The pure component κ_1 values for the <i>PRSV</i> equation of state	77
8.3	The pure component L, M and N values for the Twu, Bluck, Cunningham and Coon (1991), $\alpha(T)$ function .	78
8.4	The percentage relative error in bubble pressure and n-pentane vapour composition with <i>PRSV</i> and <i>SRK</i>	79
8.5	The pentane(1) + ethanol(2) experimental data at 100.14°C compared to the <i>PRSV-EOS-1fluid van der Waals</i> regression.	81
8.6	The pentane(1) + ethanol(2) experimental data at 100.14°C compared to the <i>SRK-EOS-1fluid van der Waals</i> regression. .	81

8.7	The <i>1-fluid van der Waals</i> mixing rule for pentane(1) + ethanol(2) at 100.14°C	81
8.8	The percentage relative error in bubble pressure and n-pentane vapour composition for the <i>WSMR</i> regression	82
8.9	The <i>PRSV-WSMR-NRTL</i> interaction parameters calculated for pentane(1) + ethanol(2) at 100.14°C	82
8.10	The <i>SRK-WSMR-WILSON</i> interaction parameters calculated for pentane(1) + ethanol(2) at 100.14°C	83
8.11	The pentane(1) + ethanol(2) experimental data at 100.14°C compared with the <i>PRSV-EOS-WSMR(NRTL)</i> regression.	83
8.12	The pentane(1) + ethanol(2) experimental data at 100.14°C compared with the <i>SRK-EOS-WSMR(WILSON)</i> regression.	83
8.13	The 2-methyl-2-butene(1) + TAME(2) experimental measurements at 70°C against the calculated values with <i>PRSV-1 fluid van der Waals mixing rule</i>	86
8.14	The 2-methyl-2-butene(1) + TAME(2) experimental measurements at 94.6°C against the calculated values with <i>PRSV-1 fluid van Der Waals mixing rule</i>	86
8.15	The 2-methyl-2-butene(1) + TAME(2) experimental measurements at 104.5°C against the calculated values with <i>PRSV-1 fluid van Der Waals mixing rule</i>	87
8.16	The 2-methyl-2-butene(1) + TAME(2) k_{12} parameter obtained with the <i>PRSV-EOS-1 fluid van Der Waals mixing rule</i> and <i>SRK-EOS-1 fluid van Der Waals mixing rule</i>	90
8.17	The relative errors in 2-methyl-2-butene(1) vapour composition and in the calculated bubble pressures for the respective isotherms	91
8.18	The 2-methyl-2-butene(1) + TAME(2) experimental measurements at 70°C against the calculated values with <i>PRSV-WSMR-NRTL</i>	92
8.19	The 2-methyl-2-butene(1) + TAME(2) experimental measurements at 94.6°C against the calculated values with <i>PRSV-WSMR-NRTL</i>	92
8.20	The 2-methyl-2-butene(1) + TAME(2) experimental measurements at 104.5°C against the calculated values with <i>PRSV-WSMR-NRTL</i>	92
8.21	The relative errors in 2-methyl-2-butene(1) vapour composition and in the calculated bubble pressures with the <i>PRSV-WSMR-NRTL</i> model	93
8.22	The <i>PRSV-WSMR-NRTL</i> interaction parameters determined for 2-methyl-2-butene(1) + ethanol(2) for the respective isotherms	93
B.1	GC operating settings	120

C.1	Physical properties of the pure components of the respective binary systems	123
C.2	Vapour pressure parameters of the respective binary system components	124

List of Figures

2.1	The general classification of HPVLE equipment	3
2.2	Schematic of a static equilibrium cell	4
4.1	Schematic of experimental apparatus layout	41
4.2	Schematic of the equilibrium cell	42
4.3	Diagram of the equilibrium cell composite stirrer	44
4.4	Sampling modes of GC valve operation	46
4.5	Cross-section schematic of the jet-mixer design	47
4.6	Apparatus air-bath heating elements	49
4.7	Schematic of the air-bath temperature probe layout	52
6.1	Schematic of experimental apparatus, sampling lines and valve layout	59
7.1	Plot of measured n-pentane vapour pressures	68
7.2	Plot of measured ethanol vapour pressures	69
7.3	Plot of measured 2-methyl-2-butene vapour pressures	70
7.4	Plot of measured TAME vapour pressures	71
7.5	n-Pentane(1) + ethanol(2) binary isotherm at $100.41^{\circ}C$	72
7.6	The 2-methyl-2-butene(1) + TAME(2) vle isotherm at $70^{\circ}C$	73
7.7	The 2-methyl-2-butene(1) + TAME(2) vle isotherm at $94.6^{\circ}C$	74
7.8	The 2-methyl-2-butene(1) + TAME(2) VLE Isotherm At $105.4^{\circ}C$	75
8.1	The n-pentane(1) + ethanol(2) isothermal P-x-y regression at $100.41^{\circ}C$ with the <i>PRSV-EOS</i> and the van der Waals 1-fluid mixing rules	80
8.2	The n-pentane(1) + ethanol(2) $x_i - y_i$ diagram at $100.41^{\circ}C$ with the <i>PRSV-EOS</i> and 1-fluid van der Waals mixing rules	80
8.3	The n-pentane(1) + ethanol(2) isothermal P-x-y regression at $100.41^{\circ}C$ with the <i>PRSV-EOS</i> and WSMR-NRTL mixing rules	84
8.4	The n-pentane(1) + ethanol(2) $x_i - y_i$ diagram at $100.41^{\circ}C$ with <i>PRSV-EOS</i> and WSMR-NRTL mixing rules	84

8.5	The n-pentane(1) + ethanol(2) isothermal P-x-y regression at 100.41°C with the <i>SRK-EOS</i> and <i>WSMR-WILSON</i> mixing rules	85
8.6	The n-pentane(1) + ethanol(2) $x_i - y_i$ diagram at 100.41°C with <i>SRK-EOS</i> and <i>WSMR-WILSON</i> mixing rules	85
8.7	The 2-methyl-2-butene(1) + TAME(2) isothermal P-x-y regression at 70°C with the <i>PRSV-EOS-1fluid van Der Waals mixing rules</i>	87
8.8	The 2-methyl-2-butene(1) + TAME(2) isothermal P-x-y regression at 94.6°C with the <i>PRSV-EOS-1fluid van Der Waals mixing rules</i>	88
8.9	The 2-methyl-2-butene(1) + TAME(2) isothermal P-x-y regression at 105.4°C with the <i>PRSV-EOS-1fluid van Der Waals mixing rules</i>	88
8.10	The 2-methyl-2-butene(1) + TAME(2) isothermal x-y diagram at 70°C with the <i>PRSV-EOS-1fluid van Der Waals mixing rule</i> regression	89
8.11	The 2-methyl-2-butene(1) + TAME(2) isothermal x-y diagram at 94.6°C with the <i>PRSV-EOS-1fluid van Der Waals mixing rule</i> regression	89
8.12	The 2-methyl-2-butene(1) + TAME(2) isothermal x-y diagram at 105.4°C with the <i>PRSV-EOS-1fluid van Der Waals mixing rule</i> regression	90
B.1	Schematic of degassing apparatus	113
B.2	A plot of the jet-mixer pressure against the component saturation pressure	116
B.3	PT-100 standard calibration chart	117
B.4	Air-bath temperature sensor calibration	117
B.5	Equilibrium temperature sensor calibration, T_1	118
B.6	Equilibrium temperature sensor calibration, T_2	118
B.7	Equilibrium temperature sensor calibration, T_3	119
B.8	Equilibrium temperature sensor calibration, T_4	119
B.9	Equilibrium cell pressure transducer calibration	120
B.10	Response factor chart for the ethanol rich region	121
B.11	Response factor chart for the pentane rich region	121
B.12	Response factor chart for the TAME rich region	122
B.13	Response factor chart for the 2-methyl-2-butene rich region	122

Chapter 1

Introduction

As we move into the future, the increasing demand for novel products subsequently leads to the design of new chemical process concepts and therefore novel chemical technologies. The science of vapour-liquid equilibrium (*VLE*) is the foundation for a variety of separation methods which include: simple distillation, azeotropic distillation, extractive distillation and general flash operations.

The use of process simulators for the design of unit operations and prediction of process performance has become the norm of today. However these process simulator predictions must still be validated against real data and accuracy of the process design. Consequently there is an increasing demand for accurate experimental data. Accurate *High-Pressure Vapour-liquid-Equilibrium (HPVLE)* data for many systems are still rare. This may be attributed to the difficulty in obtaining accurate *VLE* data at these elevated pressure conditions.

This project was an attempt to obtain accurate binary isothermal *HPVLE* data of the petrochemical industry, specifically in reactive distillation units (behavior of 2-methyl-2-butene with tert-amyl-methyl ether (TAME)). The study was undertaken at the Thermodynamics Research Group in the School of Chemical Engineering at the University of KwaZulu-Natal (Durban).

In this study the binary systems were experimentally measured with a static equilibrium apparatus. The data were used to determine parameters of several equations of state, correlations and thermodynamic models that are supported in process simulators.

Chapter 2

Literature Survey Of Experimental Equipment

2.1 Equipment classification

The type of equipment and experimental method chosen for a HPVLE study depends on the requirements of the research and the most reliable, accurate and cost-effective approach. In twin, these factors depend on the system investigated and the operating conditions of the study. Vapour liquid equilibrium studies encompass a great variety of equipment and experimental methods. Several researchers have reported these methods and equipment. This chapter outlines the several experimental methods and equipment that have been developed for HPVLE studies.

Experimental methods may be classified into two categories, synthetic methods and analytical methods. This classification of experimental methods has been reviewed by Deiters and Schneider (1986). A synthetic method is defined as the preparation of a mixture of known composition and its behaviour investigated as a function of temperature and pressure. Thereby, the problem of analyzing the equilibrium compositions, which is common in HPVLE studies is eliminated. In an analytical method, pressure and temperature are changed to cause phase separation and an equilibrium sample is withdrawn and analyzed. Raal and Mühlbauer (1994) have given an excellent summary of experimental methods and the experimental equipment used in HPVLE studies. Figure 2.1 shows a simple classification of HPVLE equipment.

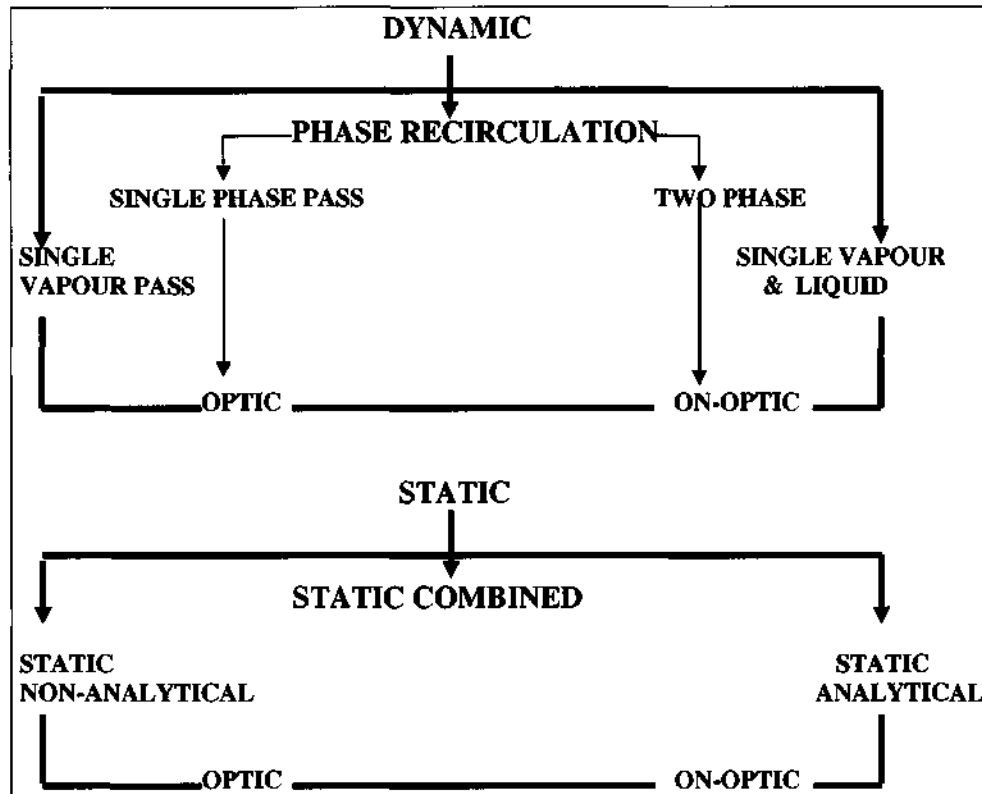


Figure 2.1: The general classification of HPVLE equipment

The classification of experimental equipment depends upon the fluid dynamics of the equilibrium cell which in turn, is based on the circulation of either the vapour or liquid phase, or the simultaneous circulation of both phases. If circulation of phases takes place, the equipment is classified as dynamic or flow method. The static method is defined as one in which the system is charged into the cell and no circulation of phases occurs.

The following sections in this chapter will focus only on the static method since the equipment (equilibrium cell) used in this HPVLE study is of the static type with internal circulation through the sampling valves. A comprehensive review of both types of equipment, dynamic and static is, presented in Ramjugernath (2000). Selected examples of static equipment that have similarities with the apparatus used in this project, are listed in the sections titled analytical and synthetic method below.

2.2 Analytical methods

2.2.1 Features of the analytical method

Figure 2.2 on page 4 illustrates the main features of the analytical method for both dynamic and static methods. The main features of the analytical method are listed below:

- Equilibrium cell where the vapour and liquid are in equilibrium
- The equilibrium cell is housed in a temperature-controlled environment. Examples of environments that have been used:

TYPE	Reference
air-baths	(Mühlbauer, 1990)
copper jackets	(Konrad, Swaid and Schneider, 1983)

- An agitating mechanism to promote mixing of the cell contents. This is achieved by circulation of one or more of the phases in dynamic methods. In static methods mixing is achieved with an internal stirrer. The method of agitation used by (Ashcroft, Shearn and Williams, 1983) was an unorthodox method, where the equilibrium cell was rocked mechanically.
- A method to sample the vapour and liquid phases. A sampling device is required for both the liquid and vapour phases in the static method.
- Accurate analysis of the withdrawn samples.
- Temperature and pressure measurement instruments.

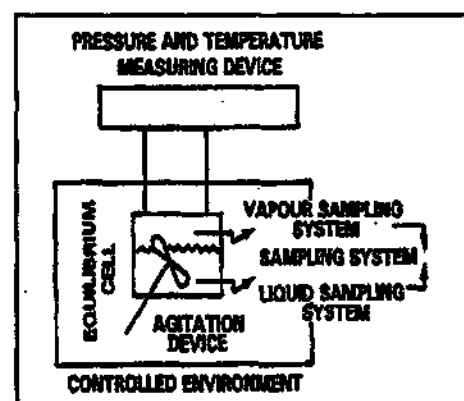


Figure 2.2: Schematic of a static cell, Raal and Mühlbauer (1994)

2.2.2 Experimental difficulties with the analytical method

Isothermal conditions

It has been reported by Raal and Mühlbauer (1994) that a small even vertical temperature gradient in the equilibrium chamber of a static or a dynamic cell can cause significant error in the measurements. This problem was found to be severe particularly in the the measurement of volatile/non-volatile systems. Raal and Mühlbauer (1994) recommend that several temperature sensors be placed at different positions along the wall of the equilibrium cell, to determine the temperature profile in the equilibrium cell. Four temperature sensors were inserted into the wall of the equilibrium cell used in this project. Two of the sensors provide an indication of the liquid temperature and the other two provide an indication of the temperature within the vapour space of the equilibrium chamber. There are a several factors which may contribute to a temperature profile within the equilibrium cell; including conductive paths to and from the cell introduced by fittings and radiative energy exchange between the cell and bath heaters. A value of 0.2°C in temperature deviation has been reported to be acceptable by Ramjugernath (2000).

The attainment of equilibrium

A state of true equilibrium is probably never achieved because of small changes in the surroundings and also due to retarding resistances. Ramjugernath (2000) states that the rate at which equilibrium is reached, decreases as equilibrium is attained. In phase equilibrium studies, high stirring rates are desired to promote the attainment of equilibrium. The problem with mechanical stirring of the equilibrium contents is fluid friction and hence a change in the internal energy of the system. This change in the internal energy must result in temperature gradients in the fluid. Temperature, pressure, vapour and liquid compositions are variables that provide an indication of equilibrium. Measured fluctuations in the temperature and pressure over a period of time, have also been suggested by various researchers as an indication of phase equilibrium. If composition is to be used as a criterion for phase equilibrium, repeated vapour and liquid sample composition analysis must produce reproducible results.

Problems associated with sampling

A major problem that many researchers have encountered during the sampling of equilibrium phases results from the change in volume of the equilibrium cell when a sample is withdrawn. Ramjugernath (2000) states that the disturbance of the equilibrium condition is directly proportional to the change in volume caused by sampling.

The change in volume can be related to the change in pressure of the equilibrium, since volume and pressure are related. This problem associated with sampling was encountered by Mühlbauer (1990). Pressure changes of 0.1 and 0.01 bar induced by sampling have been reported by Besserer and Robinson (1971).

There are two types of volume changes associated with sampling in the static method which results in the disturbance of the equilibrium condition:

- i) the volume change associated with the withdrawn sample;
- ii) the volume change associated with the sampling method.

The ideal method to minimize the effects of volume change is to have the smallest volume change introduced during sampling. This has been practically achieved by various researchers. A list of methods to achieve the smallest possible volume change during sampling are given below:

- The ratio of the equilibrium chamber volume to the volume of the withdrawn sample must be large. A large ratio will decrease the volumetric disturbances as the cell volume is decreased. The disadvantage of a large equilibrium cell is the increase use of chemicals leading to increase in operational costs. Many researchers have reported the use of large equilibrium cells to minimize the percentage of volume lost during sampling; (Sagra et al., 1972), (Ashcroft et al., 1983), (Reiff et al., 1987) and (Mühlbauer, 1990).
- The use of a rapid sampling method employing rapid-acting valves, as reported by Figuiere et al., 1980. Rapid-acting valves were used for sampling.
- A method that eliminates the volume change attributed to the sampling method employed. Rogers and Prausnitz (1970) used a sampling rod that traversed the entire equilibrium cell.
- The use of a variable-volume cell wherein pressure change caused by sampling is compensated by adjusting the cell pressure.
- The use of in-situ composition analysis techniques such that the contents of the equilibrium cell are not disturbed. Konrad et al. (1983) and Besserer and Robinson (1971) used optical methods to determine the composition of the equilibrium phases.

Obtaining a homogeneous sample

A major problem encountered during the sampling of the liquid phase, is the tendency of the more volatile component in the sample to flash, producing concentration gradient in the resultant vapour. Therefore, if the withdrawn sample is not genised, the composition analysis will be in error. A list of procedures that have been used to homogenise the sample is given below:

- The use of a stirred homogenisation vessel situated in the sample line as used by Wagner and Wichterle (1987)
- A forced circulation system to homogenise the vapourised liquid sample was employed by Nakayama et al., (1987).
- The jet mixer utilized by Mühlbauer (1990). The liquid sample is expelled into an evacuated jet-mixer where the swirling of the sample with a carrier gas (helium) promotes mixing and hence homogenisation of the sample.
- The method of analysing the more and less volatile components separately was employed by Rogers and Prausnitz (1970) and Inomata et al., (1986). The components in the sample had to be separated first, which was achieved by expansion into an evacuated vessel. A pressure calculation on the vessel would determine the amount of the more volatile component (which could be a supercritical fluid). The condensed components (less volatile) were then flushed with an organic solvent. The resulting mixture was then analysed by gas chromatography and the composition determined with a calibration standard. This procedure is complex and seemed to be tedious.

- Chou et al., (1990) used microcells for the homogenisation of the withdrawn samples. The equilibrium samples trapped in the microcells were placed into a microcell housing, in which the sample was analysed.

Composition analysis of the withdrawn sample

The general composition analysis methods used by researchers for HPVLE studies are gas chromatography(GC) and spectroscopy. Composition analysis by analysis by refractive index in conjunction with GC analysis has been reported by Besserer and Robinson (1971).

2.2.3 Gas chromatography

Gas chromatography is used to separate the volatile components of a mixture. The components of the mixture evaporate into the gas phase once inside the injector of the GC. A carrier gas, generally helium, flows through the injector and transports the sample onto the GC column or packing. After the components have passed through the column or packing, where separation takes place, the components are transported to a detector. The components reach the detector at varying times due to differences in the separation. The two most commonly used types of detectors in GC analysis are *thermal* conductivity detectors (TCD) and *flame* ionisation detectors (FID). The FID can only be used to detect organics, whereas the TCD can be used to detect hydrocarbons, non-hydrocarbons and organics. The FID is more sensitive than the TCD detector. The disadvantage of analysis by GC is that the state at which the sample enters the GC (high-pressure state) differs from the state at which the sample is withdrawn. Deiters and Schneider (1986) state that the problem with GC analysis is not the quantitative determination of composition but the handling and preparation of the sample.

The calibration of GC detectors continues to be a problem in the analysis of gas mixtures or gas-liquid mixtures. This problem can be overcome with a precision volumetric calibration device (Raal and Mühlbauer, 1998).

2.2.4 Spectroscopic or photochemical methods

These methods make use of in-situ composition analysis to overcome the difficulties associated with sample preparation for GC analysis are overcome. Konrad et al. (1983) use infrared spectroscopy to determine the phase compositions. The difficulties associated with spectroscopic methods are given below:

- extensive calibration procedures,
- these methods are restricted to specific groups of compounds e.g. ultraviolet spectroscopy is restricted to aromatics or coloured compounds and
- the possibility of the absorption bands of different compounds overlapping.

Temperature and pressure measurement

There are various types of temperature sensors; platinum resistance thermometers (Pt-100 Ω), thermocouples, thermistors and quartz thermometers. The most common types of pressure sensors used are pressure transducers, differential manometers and Bourdon-type pressure gauges. Pressure transducers with temperature compensation over wide ranges-these are favoured.

Degassing of components

Degassing is a purification operation whereby impurities (dissolved gases) are removed from the respective liquid component. If this process is not carried out adequately, competition between the dissolved gases and the more volatile component in the liquid will occur at low concentrations of the more volatile component. The degassing procedure is important when the two components of a binary system are partially soluble. Figuiere, Hom, Laugier, Renon, Richon and Szwarc (1980) and Legret et al., (1980) have stated that degassing has a significant impact on the accuracy of VLE data. Ramjugernath (2000) states that liquid degassing is usually executed in-situ or before the sample is introduced into the equilibrium cell. Equipment used for degassing is described by Mühlbauer (1990).

2.3 Static type apparatus

Static equilibrium cells have been used in a variety of configurations for HPVLE measurement. Static cells are generalized into two categories based on the sampling method, analytic or synthetic. The analytic method samples both the vapour and liquid phase compositions. The synthetic method does not require the sampling of the equilibrium phases. Raal and Mühlbauer (1994) state that the synthetic method is least accurate for systems where the isobars and isotherms have large gradients. For mixtures with more than two components the information obtained by the non-analytic method (synthetic method) is limited.

2.3.1 Static analytical method

Figure 2.2 on page 4 illustrates the general features of a static apparatus. The components are charged into the equilibrium cell. The liquid components are transported into the equilibrium chamber by flushing (with volatile component) or by the use of a pump or a compression type device. The contents of the cell are agitated to promote mixing and contact between the phases. Temperature and pressure readings are taken after equilibrium has been established. The vapour and liquid phases are sampled for composition analysis.

2.4 The static non-analytic method

2.4.1 General considerations

The non-analytical (synthetic) method was defined earlier in the chapter as the method based on introducing a mixture of known composition into the equilibrium cell and adjusting the temperature or pressure until phase separation occurs. Isothermal measurements are performed by the method of pressure variation, whereas isobaric measurements are undertaken by varying the temperature. The temperature and pressure are recorded at the commencement of the homogeneous phase separation. The initial loading of the components is recorded. Consequently the composition of the mixture can be calculated. Concentration gradients are avoided by adjusting the pressure and temperature to form a single homogenous phase. The temperature or pressure is adjusted again until the formation of a new phase is observed. A phase separation locus (phase envelope) is described by the temperature, pressure and composition (mole fraction) where phase separation occurs.

2.4.2 Disadvantages

- It is difficult to observe iso-optic systems, where the coexisting phases have a similar refractive index.
- Data measurement obtained for mixtures with more than two components, the experimentation is limited.
- The method is unsuitable for measurements in the region near the critical state.
- Dew points can easily go undetected if the vapour phase condenses as a thin film (not as a mist) on the wall of the equilibrium cell.

2.5 The static combined method

2.5.1 General considerations

Deiters and Schneider (1986) state that whereas isobaric and isothermal data indicate small gradients, slight disturbances in the pressure and temperature of a mixture can produce significant fluctuations in the phase compositions. Therefore, the application of the analytical method is not suitable for the study of phase behavior near the critical region. The static non-analytic method is more accurate near the critical state, as it does not require sampling. In the case where the isobars and isotherms have large gradients, the non-analytic method is least accurate. An error in the overall composition leads to a large temperature deviation in the generated data.

The combination of the features of the analytical and non-analytical static methods into a single equilibrium cell have been attempted. The equipment must make provisions for the observation of the cell contents, to allow for the sampling of the vapour and liquid phases and a method for accurately determining the volume of the equilibrium cell.

2.5.2 Apparatus used in this HPVLE study

A predecessor of the apparatus used by Ramjugernath (2000) was developed by Mühlbauer (1990). Both apparatus sets were developed in the same laboratory at the University Of Natal. The novel jet-mixer designed by Raal and Mühlbauer (1994) was incorporated into Mühlbauer's design.

Ramjugernath (2000) used these jet-mixers for phase homogenisation. The copper lined air-bath of Mühlbauer was used in Ramjugernath's design. The operating pressure and temperature limits of the apparatus developed by Ramjugernath (2000) were reported to be 175 bar and 175 °C respectively. The equilibrium cell contents could be viewed through two pairs of illuminated sapphire windows. The equilibrium cell had a capacity of 200 cm^3 . A piston and a stepper motor were incorporated into Ramjugernath's design. This allowed the volume of the equilibrium cell to be varied and, therefore, enable P - V - T measurements.

The sampling method and procedures employed did not cause disturbance to the equilibrium condition. This is attributable to the elevated pressures that Ramjugernath (2000) measured. The liquid and vapour phases were sampled by a novel means of circulating representative equilibrium samples through the sample loop of a VALCO six-port two-piston sampling valve. The samples were conveyed to the respective jet-mixers (vapour and liquid). Composition analysis of the the equilibrium samples were determined by gas chromatography. Kissun (2001) performed futher HPVLE measurements on the equipment. The equipment was modified by the addition of a single stage vapour-compression refrigerator, which made it possible to perform measurements at sub-ambient temperatures. Kissun (2001) reported that temperatures as low as $-23^{\circ}C$ could be reached. In a second modification made to the equipment. Kissun (2001) replaced the original jet-mixers with larger ones. This enabled the jet-mixers to operate at lower temperatures.

The high operating temperatures of the previous jet-mixers created instabilities in the temperature profile within the air-bath. Naidoo (2004) continued with the HPVLE measurements on the equipment. Naidoo (2004) reported that the equipment had pressure and temperature operating limit of 75 bar and 215 °C respectively. The liquid jet-mixer was resized because the previous jet-mixer indicated a non-uniform pattern that resulted in inaccurate composition analysis. The magnetic stirrer was also modified in Naidoo's study. In addition Naidoo also included a data-logging package, KJ-SENSE, that monitored the temperatures (air-bath, cell and jet-mixers) as well as the cell pressure. A new stepper motor circuit was developed and incorporated, such that the displacement of the piston could be measured accurately.

Chapter 3

Interpretation Of Vapour-Liquid Equilibrium Thermodynamics

3.1 Phase Equilibria

The state of equilibrium is defined as a static condition in which no change occurs in the macroscopic properties of a system over time. Hence a balance of all potentials occurs. In the case of an isolated system consisting of liquid and vapour phases, equilibrium is reached when there exists no tendency for change to occur within the system. Hence the temperature, pressure and phase compositions of a system reach final values which thereafter remain constant.

At the microscopic level conditions are not static. The molecules of the respective phases (liquid and vapour) are changing phases continuously. Smith, van Ness and Abbott (2001) state that the molecules with high velocities near the phase interface overcome forces (surface forces), to pass into the other phase. At equilibrium, the average rate of the passage of molecules is the same in both directions. Therefore there is no net interphase transfer of material. Vapour-liquid equilibrium (*VLE*) is therefore defined as the state of coexistence of liquid and vapour phases. Appendix A gives a qualitative description of phase equilibria. This chapter will discuss the computational methods and models used for the interpretation of experimental VLE data.

3.2 Computational methods for analyzing HPVLE

The general calculation methods developed for phase equilibrium thermodynamics, are theoretical models (e.g. cubic equations of state). The calculation methods that have been developed for HPVLE computation are derived from the criteria of phase equilibria-equation Appendix (A.14). Appendix A discusses the principles of phase equilibria.

There are two computational methods used in phase equilibrium analysis, namely the *combined method* and the *direct method*. The *combined method* (or *gamma-phi method*), uses both the activity coefficient (γ) and the fugacity coefficient (ϕ) to describe the liquid and vapour phase non-idealities respectively. The *direct method* or *phi-phi method* uses fugacity coefficients in solution ($\hat{\phi}_i$) to describe both the vapour and liquid phase non-idealities. The *direct method* was extended to include the hypothetical standard-states for supercritical components. Ramjugernath (2000) discusses the advantages and disadvantages of the *combined method* and *direct method*. Bubble pressure computation with the *combined* and *direct method* is discussed in this following section, since isothermal measurements were undertaken in this HPVLE study.

3.2.1 Combined Method

The non-idealities of the liquid and vapour phases are described by separate auxiliary functions. Therefore, from the equilibrium condition:

$$\hat{f}_i^V = \hat{f}_i^L \quad (3.1)$$

Where,

$$\hat{f}_i^V = y_i \hat{\phi}_i^V P \hat{f}_i^L = x_i \gamma_i f_i^{OL} \quad (3.2)$$

$$y_i \hat{\phi}_i^V P = x_i \gamma_i f_i^{OL} \quad (3.3)$$

The *fugacity of component (i) in solution* ($\hat{\phi}_i^V$), is readily calculated using a suitable equation of state (EOS). The EOS describes the vapour-phase behavior through the exact thermodynamic relationship, equation (3.4).

$$\ln \hat{\phi}_i^V = \frac{1}{RT} \int_{V^v}^{\infty} \left[\left(\frac{\partial P}{\partial n_i} \right)_{T,V,n_j} - \frac{RT}{V} \right] dV - \ln \left[\frac{PV^V}{n_T RT} \right] \quad (3.4)$$

Where,

$\hat{\phi}_i^V$ = Fugacity coefficient in solution of the vapour phase

V^V \equiv Vapour phase molar volume

$$n_T = \sum_{i=1}^N n_i$$

P = Pressure

T = Temperature

R = Universal Gas Constant

For the isothermal case, $\hat{\phi}_i^V$ is calculated from equation 3.5 together with an equation of state for \bar{Z}_i^V .

$$\ln \hat{\phi}_i^V = \int_0^P (\bar{Z}_i^V - 1) \frac{dP}{P} \quad (\text{const } T) \quad (3.5)$$

The activity coefficient is derived from the *Gibbs Duhem* equation. Smith, Ness and Abbott (2001) derive the *Gibbs Duhem* equation, which is used as a constraint in phase equilibrium data analysis.

$$\left[\frac{\partial(G)}{\partial P} \right]_{T,x} dP + \left[\frac{\partial(G)}{\partial T} \right]_{P,x} dT - \sum_i x_i d\bar{G}_i = 0 \quad (3.6)$$

At constant T and P,

$$\sum_i x_i d\bar{G}_i = 0 \quad (3.7)$$

The activity coefficient for component i (γ_i) is determined by relating it to the excess Gibbs free energy:

$$\sum x_i d \ln \gamma_i = \sum x_i \left(\frac{\bar{G}_i^E}{RT} \right) = \left(\frac{-\bar{H}^E}{RT^2} \right) dT + \left(\frac{\bar{V}^E}{RT} \right) dP \quad (3.8)$$

γ_i provides an indication of the degree of non-ideality of a component in a mixture, by relating \hat{f}_i^L (at mole fraction x_i , T and P) to some other condition. Where the fugacity is known. This reference condition is the *standard state* and it represents the thermodynamic condition of a component where its activity coefficient equals one.

Two combined methods have been proposed in fluid phase thermodynamics, (Chao and Seader, 1961) and (Prausnitz and Chueh, 1968). Raal and Mühlbauer (1998) discuss the two methods in detail. Other combined methods that have been developed constitute improvements of the earlier combined methods and are reviewed by Wichterle (1978b). The modified combined methods focus on the following conditions:

- *Different standard states to describe noncondensable components.*
- *Liquid-phase activity coefficient models to describe complex and polar mixtures.*
- *Different equations of state to compute $\hat{\phi}_i^V$*

The difficulties associated with the combined method and direct method have been discussed in (Wichterle, 1978b), (Mühlbauer and Raal, 1995) and (Ramjugernath, 2000). These difficulties associated with the combined method are summarized below:

1. An appropriate liquid standard state fugacity f_i^{OL} is required if one of the components is supercritical at the equilibrium condition.
2. An appropriate EOS is required at high pressures since the vapour phase non-idealities are more significant, i.e. $\hat{\phi}_i^V$. At moderate pressures, the effect of pressure on the liquid phase can be neglected. However at high pressures, this assumption does not hold and therefore the pressure effect must be considered. Therefore, in the Gibbs-Duhem equation (3.6), for the isothermal condition the pressure term must be included.
3. The pure component liquid molar volumes (V_i^L) and partial molar liquid volumes (\bar{V}_i^L) must be determined from reliable correlations.
4. Multiple parameters that must be determined for the regression of the HPVLE data using the combined method. Therefore, a suitable (with respect to time) and reliable regression method or algorithm is preferred.

3.2.2 Direct Method

This method uses the component fugacity coefficient ($\hat{\phi}_i$), to describe the non-idealities in both the liquid and vapour phases of a system. Therefore the equilibrium constraint is rewritten in the form:

$$\begin{aligned} \hat{f}_i^L &= \hat{f}_i^V \\ x_i \hat{\phi}_i^L &= y_i \hat{\phi}_i^V \end{aligned} \quad (3.9)$$

Where,

$$\ln \hat{\phi}_i^V = \left(\frac{1}{RT} \right) \int_{V^V}^{\infty} \left[\left(\frac{\partial P}{\partial n_i} \right)_{T, V, n_j} - \frac{RT}{V^V} \right] dV - \ln \left[\frac{PV^V}{n_T RT} \right]$$

and

$$\ln \hat{\phi}_i^L = \left(\frac{1}{RT} \right) \int_{V^L}^{\infty} \left[\left(\frac{\partial P}{\partial n_i} \right)_{T, V, n_j} - \frac{RT}{V^L} \right] dV - \ln \left[\frac{PV^L}{n_T RT} \right]$$

The fugacity coefficients of both the vapour and liquid phases are calculated by using the equations above with an equation of state. The equation of state expresses $\hat{\phi}_i$ as a function of the the state variably (measured variables); temperature, pressure and composition. The difficulties that have generally been associated with the direct method are:

1. An appropriate EOS is required to describe both the liquid and vapour phase non-idealities. The problem is selecting an EOS from a large variety of models that have been published.
2. The behavior of the mixture must be described by appropriate mixing rules.
3. The problem with using high-order EOS's (greater than cubics) is the location of the vapour and liquid roots.
4. It has been found that in the critical region, the computational techniques do not converge for bubble and dew point calculations.

3.3 Equations Of State

An equation of state is a semi-empirical function of pressure, temperature and volume describing the mechanical state of a substance. Equations of state form the basis of high pressure phase equilibria calculations. In addition to the determination of liquid-liquid and gas-liquid properties, the transitions between these systems can be determined from the same inputs. Thermodynamic properties of fluids can also be calculated by the *EOS*-e.g. vapour pressures, critical properties, densities, etc. The publications in literature on *EOS*, is extensive. Therefore, only the most generally used *EOS* are discussed below.

3.3.1 Cubic Equations Of State

Cubic equations of state have found considerable application in vapour liquid equilibria computation. These equations are capable of describing both liquid and vapour phases with flexibility over a wide range of temperature and pressure. Cubic equations of state (*CEOS*) are defined as equations that are cubic in volume. Equations of state are generally presented explicitly with respect to pressure and can be defined as the sum of an attractive and repulsive term. Most modern *CEOS* have at least two adjustable parameters and follow the basic van der Waals *EOS*:

$$P = \frac{RT}{V-b} - \frac{a}{V^2} \quad (3.10)$$

Where,

P = Pressure

V = Molar volume

b = contribution of molecular volume

a = contribution of attractive forces, type of potential

The repulsive term and basic attractive term are derived from (3.10) above:

$$\text{repulsive term} = \frac{RT}{V-b} \quad (3.11)$$

$$\text{attractive term} = \frac{a}{V^2} \quad (3.12)$$

In the modern cubic equations of state, there are other parameters that account for factors such as molecular shape, dipole moments etc. Sadus (1992) states that the two parameter model is adequate for both non-polar spherical and non-spherical molecules. However, for mixtures of strongly polar molecules are poorly represented by the two-parameter model above. This can be attributed to the strong self-association of some dipolar molecules (via hydrogen bonding).

There are three principal types of *EOS*: empirical, theoretical and semi-empirical. Modern *CEOS* generally retain the van der Waals separation of the repulsive and attractive contributions. Consequently the repulsive and attractive terms are described by “hard body + attractive term” models respectively. The trend of empirical models is to retain the van der Waals hard sphere term but incorporate an attractive term that accounts for temperature dependence. The general form of many of these equations is given by equation (3.13), where $g(V)$ is a function of the molar volume.

$$P = \frac{RT}{V - b} - \frac{a(T)}{g(V)} \quad (3.13)$$

Sadus (1992) states that theoretical *CEOS* concentrate on the effect of molecular shape. The modern *CEOS* are generally modifications of the van der Waals EOS. These modern equations can be grouped into four categories:

- (i) modifications to the attractive term
- (ii) improved repulsive models
- (iii) modifications to both terms, and
- (iv) equations for non-spherical models

Modifications Of The Attractive Term

The *Redlich-Kwong* equation given by equation (3.14) below, is one of the most important modifications of the van der Waals *CEOS*. The *Redlich-Kwong CEOS* retains the van der Waals hard sphere term, as do many other *CEOS*, but the attractive term has been modified to account for temperature dependency i.e.

$$P = \frac{RT}{V - b} - \frac{a}{[VT^{0.5}(V + b)]} \quad (3.14)$$

The *Redlich-Kwong (RK)* equation has been widely used at low temperatures for the properties of pure substances-(Redlich and Kwong, 1949).

However it has limited accuracy and is successful only for nearly ideal systems. This equation was the basis for several modifications of the van der Waals attractive term i.e. including temperature dependence. In particular the modification of Soave (1972) and Peng and Robinson (1976) have achieved widespread acceptance. Both of these equations have additional parameters to improve the predictions of pure fluid properties.

The *Soave* equation has shown promising results for mixtures at both low temperatures and high temperatures (including the critical region). The *Soave* equation is:

$$P = \frac{RT}{V-b} - \frac{a(T, \omega)}{V(V+b)} \quad (3.15)$$

where,

$$a(T, \omega) = a_c \alpha(T) \quad (3.16)$$

$$a_c = 0.42747 \frac{R^2 T_c^2}{P_c} \quad (3.17)$$

$$b = 0.08664 \frac{RT_c}{P_c} \quad (3.18)$$

for normal fluids,

$$\sqrt{\alpha} = 1 + \kappa(1 - \sqrt{T_r}) \quad (3.19)$$

$$\kappa = 0.48508 + 1.55171\omega - 0.15613\omega^2 \quad (3.20)$$

$$(3.21)$$

The *Soave CEOS* may be arranged in the form of the compressibility factor (Z):

$$Z^3 - Z^2 + Z(A - B - B^2) - AB = 0 \quad (3.22)$$

Where,

$$A = \frac{a(T)P}{(RT)^2} \quad (3.23)$$

$$B = \frac{bP}{RT} \quad (3.24)$$

$$Z = \frac{PV}{RT} \quad (3.25)$$

For a supercritical fluid, vapour and liquid roots of compressibility function are taken as the maximum and minimum real positive roots of equation (3.22) respectively. Hence, for a pure component, the fugacity coefficient using the *Soave* or *Soave Redlich-Kwong CEOS* of the vapour and liquid phase is:

$$\ln \phi_i = Z_i^V - 1 - \ln(Z_i^V - B) - \frac{A}{B} \ln\left(\frac{Z_i^V + B}{Z_i^V}\right) \quad (3.26)$$

$$\ln \phi_i = Z_i^L - 1 - \ln(Z_i^L - B) - \frac{A}{B} \ln\left(\frac{Z_i^L + B}{Z_i^L}\right) \quad (3.27)$$

The *SRK CEOS*, has proved successful in the computation of several hydrocarbon vapour pressures and in the prediction of the phase behaviour of multicomponent systems (including mixtures of non-polar and slightly polar fluids). The prediction of vapour pressures for polar and non-polar molecules was improved by the introduction of a two-parameter α function, (Soave, 1993). The two parameters shown below in equation (3.28), are applicable to non-polar or slightly polar fluids. The parameters m and n must be fitted from experimental data for strongly polar fluids.

$$\alpha(T) = 1 + m\left(1 - \frac{T}{T_c}\right) + n\left(1 - \sqrt{\frac{T}{T_c}}\right)^2 \quad (3.28)$$

$$m = 0.484 + 1.515\omega - 0.044\omega^2 \quad (3.29)$$

$$n = 2.756m - 0.700 \quad (3.30)$$

Peng and Robinson (1976) further modified the *SRK-EOS*, by including different volume and temperature dependence on the α term. Improved liquid volumes were reported, where $Z_c = 0.307$ and accurate vapour pressure predictions for hydrocarbons- 6 to 10 carbon number range. The *CEOS* proposed by Peng and Robinson (1976) was developed to account for the weakness of the *SRK-EOS*, in the area of the critical region and inaccurate liquid density predictions. The Peng-Robinson EOS is formulated below:

$$P = \frac{RT}{V - b} - \frac{a(T)}{V(V + b) + b(V - b)} \quad (3.31)$$

where,

$$a(T) = a_c \alpha(T) \quad (3.32)$$

$$a_c = 0.457235 \frac{(RT_c)^2}{P_c} \quad (3.33)$$

$$b = 0.077796 \frac{RT_c}{P_c} \quad (3.34)$$

$$\alpha(T) = \left[1 + \kappa \left(1 - \sqrt{\frac{T}{T_c}} \right)^2 \right] \quad (3.35)$$

$$\kappa = 0.37464 + 1.5422\omega - 0.26992\omega^2 \quad (3.36)$$

Equation (3.31) can be written in the form of the compressibility factor, hence for a pure component:

$$Z^3 - (1 - B)Z^2 + Z(A - 3B - 2B^2) - (AB - B^2 - B^3) = 0 \quad (3.37)$$

the fugacity coefficient by PR EOS,

$$\ln \phi_i = Z_i - 1 - \ln(Z_i - B) - \frac{A}{2\sqrt{2}B} \ln \left(\frac{Z_i + (1 + \sqrt{2})B}{Z_i + (1 - \sqrt{2})B} \right) \quad (3.38)$$

The Soave-Redlich-Kwong and Peng-Robinson equations have become the most preferred EOS used in industry. The popularity of the SRK EOS and the PR EOS can be attributed to the minimal input data (only critical properties and acentric parameters for generalised parameters) required for VLE computation and the accurate prediction of phase equilibria for hydrocarbon systems. The disadvantages of the above mentioned EOS include inaccurate prediction of liquid densities, inaccurate generalised parameters for nonhydrocarbons (polar and associating fluids) and the unreliable phase behaviour prediction of long chain molecules. The capabilities and limitations of CEOS are described by Abbott (1979). A detailed review of equations of state is also given by Wei and Sadus (2000).

The inclusion of the acentric factor as a third parameter and the introduction of additional parameters in the attractive term and repulsive term are other modifications discussed in Wei and Sadus (2000). The additional parameters improve both the saturation vapour pressure and liquid molar volume predictions. Moreover, the equations of state can be applied to polar fluids if the appropriate parameters are chosen. The major disadvantage of including additional parameters is that additional mixing rules are required for the extension of the EOS to mixtures and the computation time as well as complexity increases.

The *Peng-Robinson-Stryjek-Vera* or PRSV CEOS is a modification to the original *Peng-Robinson* equation of state, equation (3.31). The addition of parameters into the temperature function (α) of the *Peng-Robinson EOS* improves the vapour pressure predictions of polar, non-polar and associating compounds Stryjek and Vera [1986a,b]. The *PRSV EOS* has proved to be successful in the computation of VLE and LLE mixtures.

Recall from *Peng-Robinson EOS*,

$$\alpha = \left[1 + \kappa \left(1 - \sqrt{\frac{T}{T_c}} \right) \right]^2$$

where,

$$\kappa = 0.37464 + 1.54226\omega - 0.26992\omega^2$$

The *PRSV EOS* has the same α expression, except the κ term is modified as follows:

$$\kappa = \kappa_0 + \kappa_1(1 + T_R^{0.5})(0.7 - T_R) \quad (3.39)$$

where,

$$\kappa_0 = 0.378893 + 1.4897153\omega - 0.1713184\omega^2 + 0.0196554\omega^3 \quad (3.40)$$

The parameter κ_1 is an adjustable parameter characteristic of the respective pure compound. Stryjek and Vera (1986a) list κ_1 values for over ninety compounds of industrial interest. Based on volumetric data that were used for the supercritical region regression, Stryjek and Vera (1986a) recommended that when $T_R > 1$, $\kappa = \kappa_0$ for all compounds.

The ability of an *EOS* to predict phase equilibria is partly attributed to the temperature dependence of the attractive term. Several expressions to estimate the attractive terms in equations of state have been developed, which are basically modifications to the attractive term of the van der Waals equations. The modifications to the attractive terms of the van der Waals equation of state are given in Table 3.1 and correlations for α are given in Table 3.2. The list of references given in Table 3.1 and Table 3.2, include a selection of modifications that are well-known.

Table 3.1: Examples of EOS that are modifications of the van der Waals equations, with respect to the attractive term.

Reference	Attraction term
Redlich and Kwong (1949)	$\frac{a}{T^{0.5}V(V-b)}$
Soave (1972)	$\frac{a(T)}{V(V-b)}$
Peng and Robinson (1976)	$\frac{a(T)}{V(V+b)+b(V-b)}$
Fuller (1976)	$\frac{a(T)}{V(V+cb)}$
Schmidt and Wenzel (1980)	$\frac{a(T)}{V^2+ubV+wb^2}$
Harmens and Knapp (1980)	$\frac{a(T)}{V^2+cbV+(c-1)b^2}$
Patel and Teja (1982)	$\frac{a(T)}{V(V+b)+c(V-b)}$
Stryjek and Vera (1986a)	$\frac{a(T)}{V(V+b)+b(V-b)}$
Trebble and Bishnoi (1987)	$\frac{a(T)}{V^2+(b+c)V+(bc+d^2)}$
Yu and Lu (1987)	$\frac{a(T)}{V(V+c)+b(3V+c)}$
Twu, Coon and Cunningham (1992b)	$\frac{a(T)}{V(V+4b)+c(V+b)}$
Twu, Sim and Tassone (2000)	$\frac{a(T)}{(V+3b)+(V-0.5b)}$

Table 3.2: Temperature dependence of the α function in cubic EOS

Reference	α as a function of temperature
Redlich and Kwong (1949)	$\alpha = \frac{1}{\sqrt{T}}$
Soave (1972)	$\alpha = \left[1 + \kappa(1 - \sqrt{T_r}) \right]^2$ $\kappa = 0.485 + 1.551\omega + 0.156\omega^2$
Peng and Robinson (1976)	$\alpha = \left[1 + \kappa(1 - \sqrt{T_r}) \right]^2$ $\kappa = 0.374 + 1.542\omega + 0.269\omega^2$
Harmens and Knapp (1980)	$\alpha = \left[1 + \kappa_1(1 - \sqrt{T_r}) + \kappa_2(T_r^{-1} - 1) \right]^2$
Harmens and Knapp (1980)	$\alpha = \left[1 + \kappa_1 \ln(T_r) + \kappa_2(\ln T_r) \right]^2$ $T_r > 1$
Soave (1984)	$\alpha = 1 + m(1 - T_r) + n(T_r^{-1} - 1)$
Stryjek and Vera (1986a)	$\alpha = \left[1 + \kappa(1 - T_r) \right]^2$ $\kappa = \kappa_0 + \kappa_1(1 + \sqrt{T_r})(0.7 - T_r)$ $\kappa_0 = 0.378 + 1.489\omega - 0.171\omega^2 + 0.019\omega^3$
Trebble and Bishnoi (1987)	$\alpha = \exp \left[q_1(1 - T_r) \right]$
Yu and Lu (1987)	$\alpha = 10^{[\kappa_1(a_0 + a_1 T + a_2 T^2)(1 - T_r)]}$
Twu et al. (1991)	$\alpha = T_r^{N(M-1)} \exp \left[L(1 - T_r^{NM}) \right]$
Twu et al. (1995a,b)	$\alpha = \alpha^0 + \omega(\alpha^1 - \alpha^0)$ $\alpha^0 = T_r^{A_1} \exp \left[B_1(1 - T_r^{C_1}) \right]$ $\alpha^1 = T_r^{A_2} \exp \left[B_2(1 - T_r^{C_2}) \right]$
Gasem, Gao, Pan and Robinson (2001)	$\alpha = \exp \left[(A + BT_r)(1 - T_r^{C+D\omega+E\omega^2}) \right]$

The equations given in table 3.1 and table 3.2 are widely used in industrial and engineering applications. However they are generally not applicable to highly asymmetric fluids. Equations for predicting and describing asymmetric systems, contain a modification to the repulsive term of the van der Waals equation. Recall that the repulsive term for a hard-sphere fluid, of the van der Waals equation of state is:

$$\text{Repulsive term} = \frac{V}{V - b}$$

Modifications to the repulsive term of the van der Waals equation have been tabulated in Table 3.3 below. Modifications of the attraction and repulsive term of the general cubic equation of state are discussed in Wei and Sadus (2000). The application of cubic equations of state for the computation of vapour-liquid equilibria is discussed in Orbey and Sandler (1998) and Raal and Mühlbauer (1998).

Table 3.3: Modifications to the repulsive term of the van der Waals equation, where $\eta = \frac{b}{4V}$.

Reference	van der Waals Repulsive term
Reiss, Frisch and Lebowitz (1959)	$\frac{1+\eta+\eta^2}{(1-\eta)^3}$
Thiele (1963)	$\frac{1+\eta+\eta^2}{(1-\eta)^3}$
Guggenheim (1965)	$\frac{1}{(1-\eta)^4}$
Carnahan and Starling (1969)	$\frac{1+\eta+\eta^2-\eta^3}{(1-\eta)^3}$
Boublik (1981)	$\frac{1+(3\alpha-2)\eta+(3\alpha^2-3\alpha+1)\eta^2-\vartheta^2\eta^3}{(1-\eta)^3}$

Naidoo (2004) states that the modifications of an existing *EOS* and the developments of new *EOS* are contingent on the properties of interest to the authors. The authors generally fail to comment on the applicability of the *EOS* other than their own areas of interest. Therefore certain equations of state are only applicable to specific fluids.

3.3.2 Extension of Cubic Equations Of State to Mixtures

Mühlbauer and Raal (1995) state that extension of the van der Waals equation of state and its derivatives (modified *EOS*) to mixtures requires mixing rules. This section is devoted to the extension of the a and b parameters commonly encountered in most cubic *EOS*. The simplest of these mixing rules are the *classical one-fluid* mixing rules proposed by van der Waal. The van der Waals *one-fluid* rule models an the *EOS* mixture parameter as a mole-fraction-weighted sum of the corresponding pure component parameters.

$$a_m = \sum_{j=1}^m \sum_{i=1}^n z_i z_j a_{ij} \qquad b_m = \sum_{j=1}^m \sum_{i=1}^n z_i z_j b_{ij} \quad (3.41)$$

The van der Waal's *one-fluid* model assumes that the radial distribution function of the component molecules are all identical. Hence the model is relatively accurate when the size difference between the molecules is small. In addition to the model above combining rules are required for the evaluation of the parameters a_{ij} and b_{ij} . The general combining rules are:

$$a_{ij} = \sqrt{a_i a_j} (1 - k_{ij}) \quad (3.42)$$

$$b_{ij} = \frac{1}{2} (b_i + b_j) (1 - l_{ij}) \quad (3.43)$$

The binary interaction parameters k_{ij} and l_{ij} are obtained from the *VLE* regression. In general the interaction parameters in the combining rules are temperature dependent. For *simple mixtures of non-polar components*, l_{ij} is set to zero. The general expression for the *one fluid* mixing parameter b_m then reduces to:

$$b_m = \sum z_i b_i \quad (3.44)$$

The development of the van der Waals one-fluid mixing rule stems from the Virial *EOS*. Smith et al. (2001) illustrate the derivation of the mixing rule from the virial equation of state.

Numerous mixing rules have been published. The mixing rules presented in this section were used in the binary *VLE* regression of this project. Mühlbauer and Raal (1995) give an excellent summary of the classification of mixing rules found in literature.

The fugacity coefficient of a component in a mixture ($\hat{\phi}_i$) for the Soave

and Peng-Robinson EOS, using the van der Waals *one fluid* mixing rule, are given below:

$\hat{\phi}_i$ evaluated with Soave Redlich-Kwong EOS,

$$\ln \hat{\phi}_i = \frac{b_i}{b_m} (Z_i - 1) - \ln(Z_i - B_m) - \frac{A_m}{B_m} \left[\frac{2 \sum_{j=1}^n z_j a_{ij}}{a_m} - \frac{b_i}{b_m} \right] \ln \left(\frac{Z_i + B_m}{Z_i} \right) \quad (3.45)$$

$\hat{\phi}_i$ evaluated with Peng and Robinson EOS,

$$\ln \hat{\phi}_i = \frac{b_i}{b_m} (Z_i - 1) - \ln(Z_i - B_m) - \frac{A_m}{2\sqrt{2}B_m} \left[\frac{2 \sum_{j=1}^n z_j a_{ij}}{a_m} - \frac{b_i}{b_m} \right] \ln \left(\frac{X}{Y} \right) \quad (3.46)$$

Where;

$$X = Z + (1 + \sqrt{2})B_m \quad (3.47)$$

$$Y = Z + (1 - \sqrt{2})B_m \quad (3.48)$$

The van der Waals (vdW) mixing rules provide a reasonable correlation for mixtures of hydrocarbons, hydrocarbons with inorganic gases, non-polar and slightly polar components-for molecules that are of similar size. The disadvantage of the *one fluid* theory is, its application is limited to mixtures that exhibit moderate solution non-ideality. The vdW's theory has shortcomings in the liquid phase non-ideality predictions. Models that incorporate the excess Gibbs energy, G^E , have been developed to describe the liquid phase non-ideality. These models have been defined as activity coefficient models and were developed to describe highly non-ideal systems.

Mühlbauer and Raal (1995) have classified mixing rules into five main groups. The five main groups are: classical, density-dependent, composition-dependent, density-independent and local composition mixing rules. Many of the mixing rules and combining rules that have been developed provide good correlations of complex mixtures. However, some of these mixing rules do not satisfy specific criteria. The general criterion that applies to all mixing rules, is that the mixing rule must not result in the second virial coefficient being non-quadratic in composition. Hence a complete mixing and combining rule should satisfy certain boundary conditions. The boundary conditions that constrain the mixing rules are-at low densities the second virial coefficient must be quadratic in composition and at high liquid-like densities the rules produce G^E behavior similar to that of activity coefficient models.

Wong-Sandler mixing rule

The Wong and Sandler (1992*b*) mixing rule satisfies these boundary conditions. These mixing rules are density-independent and allows for the extrapolation of VLE data over large ranges of temperature and pressure.

The Wong and Sandler mixing rule are based on two modifications:

1. The constraints for the two *EOS* functions a and b , are implied by the van der Waals one fluid mixing rule:

$$\begin{aligned} B(x_i, T) &= \sum \sum x_i x_j B_{ij}(T) \\ &= \sum \sum x_i x_j \left(b - \frac{a}{RT} \right)_{ij} \\ &= b_m - \frac{a_m}{RT} \end{aligned} \quad (3.49)$$

The last equality has been extended by incorporating a combining rule:

$$\left(b - \frac{a}{RT} \right)_{ij} = \frac{1}{2} \left[\left(b_{ii} - \frac{a_{ii}}{RT} \right) + \left(b_{jj} - \frac{a_{jj}}{RT} \right) \right] (1 - k_{ij}) \quad (3.50)$$

Sandler (1999) proposed the modification:

$$\left(b - \frac{a}{RT} \right)_{ij} = \frac{1}{2} \sqrt{\left(b_{ii} - \frac{a_{ii}}{RT} \right) \left(b_{jj} - \frac{a_{jj}}{RT} \right)} (1 - k_{ij}) \quad (3.51)$$

where k_{ij} is the binary interaction parameter.

$$(3.52)$$

2. The Wong and Sandler (1992*b*) mixing rule are based on the *Excess Helmholtz* free energy A^E , instead of the *Excess Gibbs* excess free energy G^E . The choice of A^E over G^E can be attributed to the fact that A^E is not as strongly dependent on pressure as G^E . Therefore it is not necessary to assume $V^E = 0$ for a liquid. The relationship between the *EOS* mixture parameters, a_m and b_m is derived from the following defining expressions:

$$G^E = A^E + PV^E \quad (3.53)$$

At low pressures PV^E is negligible and therefore:

$$\begin{aligned} G^E(T, P = 1\text{bar}, x_i) &= A^E(T, P = 1\text{bar}, x_i) \\ &= A^E(T, P^{\text{high}}, x_i) \end{aligned} \quad (3.54)$$

The second inequality implies the pressure independence of A^E . The second constraint for the a and b parameters follows from the equalities below:

$$\begin{aligned} A_{EOS}^E(T, P = \infty, x_i) &= A^E(T, P = \infty, x_i) \\ &= A^E(T, P^{low}, x_i) \\ &= G^E(T, P^{low}, x_i) \end{aligned} \quad (3.55)$$

Equation (3.54) implies that an activity coefficient model can be used to describe the *Helmholtz* free energy (A_{EOS}^E). The *Helmholtz* free energy at infinite pressure derived for a van der Waals type cubic EOS is:

$$A_{\infty}^E = \Lambda \left[\frac{a_m}{b_m} - \sum_{i=1}^n z_i \frac{a_i}{b_i} \right] \quad (3.56)$$

where Λ is numerical constant dependent on the EOS used.

For the *Peng-Robinson* EOS:

$$\Lambda = \frac{1}{\sqrt{2}} \ln(\sqrt{2} - 1) \quad (3.57)$$

Wong and Sandler obtained the following relation for the parameters a_m and b_m from equation (3.54):

$$a_m = b_m \left[\sum_{i=1}^n z_i \frac{a_i}{b_i} - \frac{G_{\gamma}^E(T, P_{low}, x_i)}{\Lambda} \right] \quad (3.58)$$

The second boundary condition, quadratic composition dependence of the second virial coefficient, was satisfied by the relation below:

$$b_m = \frac{\sum \sum z_i z_j \left(b - \frac{a}{RT} \right)_{ij}}{1 - \frac{G_{\gamma}^E(T, P_{low}, x_i)}{\Lambda RT} - \sum_{i=1}^n z_i \frac{a_i}{b_i}} \quad (3.59)$$

Substitution of equation (3.59) into equation (3.58) results in a_m . The variables (Q,D) defined below, simplify the expression for $\hat{\phi}_i$ by grouping common terms.

$$Q = \sum \sum z_i z_j \left(b - \frac{a}{RT} \right)_{ij} \quad (3.60)$$

$$D = \frac{G_{\gamma}^E(T, P_{low}, x_i)}{\Lambda RT} + \sum_{i=1}^n z_i \frac{a_i}{b_i RT} \quad (3.61)$$

Hence:

$$\frac{a_m}{RT} = Q \frac{D}{1-D} \quad (3.62)$$

$$b_m = \frac{Q}{1-D} \quad (3.63)$$

The expression for $\hat{\phi}_i$ obtained from the *Peng-Robinson EOS* coupled with the *Wong and Sandler* mixing rules is given below, equation (3.64). The fugacity coefficient in solution of the vapour and liquid phases is calculated by using the vapour and liquid compressibility factor root (Z^V and Z^L respectively) in equation (3.64). Recall that the *Peng-Robinson* and the *Peng-Robinson-Stryjek-Vera EOS's* differ by the temperature dependence of the attractive term, hence the expression for $\hat{\phi}_i$ is the same for both *EOS*.

$$\begin{aligned} \ln \hat{\phi}_i = & -\ln \left[Z - B_m \right] + \frac{1}{b_m} \left(\frac{\partial n b_m}{\partial n_i} \right) (Z - 1) + \frac{1}{2\sqrt{2}} \left(\frac{a_m}{b_m RT} \right) \\ & \left[\frac{1}{a_m} \left(\frac{1}{n} \frac{\partial n^2 a_m}{\partial n_i} \right) - \frac{1}{b_m} \frac{\partial n b_m}{\partial n_i} \right] \times \ln \left[\frac{Z + (1 + \sqrt{2}) B_m}{Z + (1 + \sqrt{2}) B_m} \right] \end{aligned} \quad (3.64)$$

Where:

$$\frac{\partial n b_m}{\partial n_i} = \frac{1}{(1-D)} \left(\frac{1}{n} \frac{\partial n^2 Q}{\partial n_i} \right) - \frac{Q}{(1-D)^2} \left(1 - \frac{\partial n D}{\partial n_i} \right) \quad (3.65)$$

$$\frac{1}{RT} \left(\frac{1}{n} \frac{\partial n^2 a_m}{\partial n_i} \right) = D \frac{\partial n b_m}{\partial n_i} + b_m \frac{\partial n D}{\partial n_i} \quad (3.66)$$

The expressions for the partial derivatives of Q and D are:

$$\left(\frac{1}{n} \frac{\partial n^2 Q}{\partial n_i} \right) = 2 \sum_j z_j \left(b - \frac{a}{RT} \right)_{ij} \quad (3.67)$$

$$\frac{\partial n D}{\partial n_i} = \frac{a_i}{b_i RT} + \frac{\ln \gamma_{i\infty}}{\Lambda} \quad (3.68)$$

Where $\ln \gamma_{i\infty}$ is dependent on the Gibbs excess energy model used for the liquid phase.

$$\ln \gamma_{i\infty} = \frac{1}{RT} \frac{\partial n A_{\infty}^E}{\partial n_i} \quad (3.69)$$

The *Wong and Sandler (WSMR)* mixing rules have been reported to yield accurate correlation for vapour-liquid, liquid-liquid and vapour-liquid-liquid equilibria. The mixing rules describe the phase behavior of simple and complex systems, systems composed of binary and ternary mixtures. A cubic *EOS* combined with the *WSMR* can be used for the correlation of a wide range of highly non-ideal systems that were previously described by an activity coefficient model. The capabilities of this mixing rule have been discussed in Wong and Sandler (1992b). The limitations of the *Wong and Sandler* mixing rules and modifications to the mixing rules have been discussed in Orbey and Sandler (1995a) and Coutsikos, Kalospiros and Tassios (1995).

Coutsikos et al. (1995) showed that at high pressures, equation (3.54) is invalid for asymmetric systems ($k_{ij} \geq 1$). This implied that the *Gibbs* excess energy models at low pressures cannot be applied to high pressures:

$$G^E(T, P_{low}, x_i) \approx A^E(T, P_{low}, x_i) \neq A^E(T, P \rightarrow \infty, x_i) \quad (3.70)$$

Orbey and Sandler (1995a) modified the *Wong and Sandler* mixing rule such that for a multicomponent system, a single mixing rule could be used to describe the behavior of non-ideal binary pairs as well as binary pairs in the same mixture that could be described by van der Waals *one-fluid* theory. This modification implies that the mixing rule transforms to the conventional van der Waals *one-fluid* mixing rule for certain values of its parameters. The modification to the cross virial term is given by equation (3.71) below.

$$\left(b - \frac{a}{RT}\right)_{ij} = \frac{1}{2}(b_i + b_j) - \frac{\sqrt{a_i a_j}}{RT}(1 - k_{ij}) \quad (3.71)$$

A new expression for A^E , for a binary system was proposed. The equation was a result only for a special case, where the fluid satisfies the one-fluid theory and combining rules.

$$A^E = \frac{\delta x_1 x_2}{x_1 b_1 + x_2 b_2} \quad (3.72)$$

The reformulated mixing rules of Orbey and Sandler (1995a), can only be used directly with certain free-energy models i.e. modified NRTL and Van Laar.

3.4 General considerations for the liquid phase

One method of describing the liquid and vapour phases of a system is by the combined method (section 3.2.1). In the direct method equations are used to relate the fugacity coefficient of the liquid phase to the liquid mole fractions, temperature, pressure and other variables. Another useful method, involves the definition of an ideal liquid solution and hence the description of deviations from the ideal behavior in terms of excess functions.

The defining equation for an ideal solution is:

$$\bar{G}_i^{id} = G_i + RT \ln \hat{f}_i^{id} \quad (3.73)$$

Where G_i is the Gibbs energy of the pure species as it actually exists at T and P . By the Lewis-Randall rule:

$$\hat{f}_i^{id} = x_i f_i^{OL} \quad (3.74)$$

The fugacity f_i^{OL} in equation (3.74) is defined as the standard state fugacity of pure species i . The standard state fugacity is evaluated at a temperature and pressure where the fugacity is accurately known. By the definition given above, equation (3.73) and the Lewis-Randall rule, for a real liquid:

$$\bar{G}_i = \Gamma_i(T) + RT \ln \hat{f}_i \quad (3.75)$$

Hence,

$$\begin{aligned} \bar{G}_i - \bar{G}_i^{id} &= RT \ln \left[\frac{\hat{f}_i}{x_i f_i^{OL}} \right] \\ &= \bar{G}_i^E \end{aligned} \quad (3.76)$$

The activity coefficient is defined by the dimensionless ratio:

$$\gamma_i = \frac{\hat{f}_i}{x_i f_i^{OL}} \quad (3.77)$$

$$\Leftrightarrow \bar{G}_i^E = RT \ln \gamma_i \quad (3.78)$$

The liquid fugacity is related to the liquid mole fraction as:

$$\hat{f}_i^L = \gamma_i x_i f_i^{OL} \quad (3.79)$$

3.4.1 Activity Coefficients

The activity coefficient (γ), corrects for the non-ideality in the liquid phase and is a function of liquid composition (x_i), temperature and pressure. Liquid phase activity coefficient can be derived from the fundamental excess property relation (Smith et al., 2001):

$$d\left(\frac{nG^E}{RT}\right) = \frac{nV^E}{RT}dP - \frac{nH^E}{RT^2}dT + \sum_i \frac{\bar{G}^E}{RT}dn_i \quad (3.80)$$

where:

$$\ln \gamma_i = \left[\frac{\partial \left(\frac{nG^E}{RT} \right)}{\partial n_i} \right]_{P,T,n_j} \quad (3.81)$$

Thus $\ln \gamma_i$ is a partial molar property with respect to $\frac{G^E}{RT}$. Hence from the summability relationship and the Gibbs-Duhem equation:

$$\frac{G^E}{RT} = \sum_i x_i \ln \gamma_i \quad (3.82)$$

and

$$\sum_i x_i d \ln \gamma_i = 0 \quad (3.83)$$

Equation (3.83) in the integrated form relates the γ_1 to γ_2 . There exists several well-known semi-empirical activity coefficient models that relate the activity coefficients of a system to G^E . At isothermal conditions the equilibrium pressure varies with the change in composition of the liquid. The correlation of experimental *VLE* data by the integrated form of equation (3.83) requires that the γ_i values be evaluated at the same reference pressure (P^R). The experimentally obtained isothermal activity coefficients are at different pressures and therefore have to be corrected from the experimental total pressure (P) to the reference pressure. Section 3.5, discusses the pressure correction to experimental activity coefficients further.

3.4.2 Excess Gibbs energy models

The function $\frac{G^E}{RT}$ is assumed to be weakly dependent on pressure and therefore, the pressure dependence is often neglected. Empirical models have been proposed that express the excess Gibbs energy as function of liquid

mole fraction, volume fraction and molecular surface fractions. The latter two are preferred in cases where the molecules of a system differ significantly in size or chemical nature. The models used to correlate the data in this project are the Wilson and NRTL equations.

Wilson equation

Wilson (1964) proposed the following Gibbs excess free energy for mixtures:

$$\frac{G^E}{RT} = -x_1 \ln(x_1 + \Lambda_{12}x_2) - x_2(x_1 \Lambda_{21} + x_2) \quad (3.84)$$

The activity expressions for coefficients derived from Wilson (1964) excess free energy model are:

$$\ln \gamma_1 = -\ln x_1 + \Lambda_{12}x_2 + x_2 \left[\frac{\Lambda_{12}}{x_1 + \Lambda_{12}x_2} - \frac{\Lambda_{21}}{x_1 \Lambda_{21} + x_2} \right] \quad (3.85)$$

$$\ln \gamma_2 = -\ln x_2 + \Lambda_{21}x_1 - x_1 \left[\frac{\Lambda_{12}}{x_1 + \Lambda_{12}x_2} - \frac{\Lambda_{21}}{x_1 \Lambda_{21} + x_2} \right] \quad (3.86)$$

where:

$$\Lambda_{ij} = \frac{V_i}{V_j} \exp\left(-\frac{\lambda_{ji} - \lambda_{jj}}{RT}\right) \frac{V_i}{V_j} \exp\left(-\frac{\Delta\lambda_{ji}}{RT}\right) \quad (3.87)$$

$$(3.88)$$

Where;

λ_{ij} = Molecular interactions between molecules i and j .

λ_{ji} = Molecular interactions between molecules j and i .

The parameters Λ_{12} and Λ_{21} are adjustable that are functions of the pure-component molar volumes V_i and the characteristic energy differences, $\Delta\lambda_{ji}(= \lambda_{ji} - \lambda_{jj})$ between the molecules. The parameters $\Delta\lambda_{ji}$ have been reported to be independent of temperature over modest temperature ranges. The Wilson model has been reported to correlate the *Gibbs* energy with reasonable accuracy for a variety of miscible mixtures, solutions of polar or associating components and systems that do not exhibit large asymmetric deviations from ideality. The disadvantages of the model are listed below:

- inaccuracy in the prediction of certain systems with limited miscibility. Hence the model should be applied to systems that are completely miscible-(Prausnitz and Chueh, 1968).
- inaccuracy for systems where a plot of $\ln \gamma_i$ versus x_i exhibits maxima or minima.

Naidoo (2004) states that the parameters Λ_{12} and Λ_{21} should always be positive for accurate representation of the data over the entire composition range.

NRTL Model

The *NRTL* or (*nonrandom, two-liquid*) is one of the most widely used excess *Gibbs* energy models. It is a local composition model derived by Renon and Prausnitz (1968b) and unlike the *Wilson* equation can be applied to partially miscible as well as completely miscible systems. Equation (3.89) below is the expression for the excess *Gibbs* energy from the *NRTL* model.

$$\frac{G^E}{RT} = x_1 x_2 \left[\frac{\tau_{21} G_{21}}{x_1 + G_{21} x_2} + \tau_{12} G_{12} x_1 G_{12} + x_2 \right] \quad (3.89)$$

where the parameters τ_{ji} and G_{ji} are given by:

$$\tau_{ji} = \frac{g_{ji} - g_{ii}}{RT} = \frac{\Delta g_{ji}}{RT} \quad (3.90)$$

$$G_{ji} = \exp(-\alpha_{ji} \tau_{ji}) \quad (3.91)$$

The adjustable parameter g_{ji} is defined as the energy parameter between molecules of components j and i respectively. The *NRTL* model has three adjustable parameters Δ_{12} , Δ_{21} and α_{ij} . Where Δ_{12} and Δ_{21} are the intermolecular energies between molecules 1 and 2 for Δ_{12} . Similarly for Δ_{21} . The parameter τ_{ji} is usually correlated with data in VLE computations instead of the Δg_{ji} .

The α_{ij} parameter refers to the *non-randomness* in a mixture. For $\alpha_{12} = \alpha_{21}$, the parameter has been found to vary in the range 0.2 to 0.7-(Renon and Prausnitz, 1968b). Sandler (1994) reported that when experimental data are scarce, $\alpha_{12} = 0.3$ is a reasonable assumption. The activity coefficients derived from equation (3.89) are given below:

$$\ln \gamma_1 = x_2^2 \left[\tau_{21} \left(\frac{G_{21}}{x_1 + G_{21} x_2} \right)^2 + \frac{\tau_{12} G_{12}}{(G_{12} x_1 + x_2)^2} \right] \quad (3.92)$$

$$\ln \gamma_2 = x_1^2 \left[\tau_{12} \left(\frac{G_{12}}{G_{12}x_1 + x_2} \right)^2 + \frac{\tau_{21}G_{21}}{(x_1 + G_{21}x_2)^2} \right] \quad (3.93)$$

The original *NRTL* model has been found to be inaccurate in the dilute region and is inferior to the *Wilson* model in the representation of strongly asymmetric systems that are highly non-ideal. The deficiency of the *NRTL* model has been accounted for by the inclusion of a volumetric molar ratio in the analytic form-(Vetere, 2000).

3.5 Standard states

The concept of standard-states is defined as, the known or specified thermodynamic condition of a component. Furthermore at the standard-state for a specific component, the activity coefficient (equation (3.77)) is unity i.e.

$$\gamma_i = \frac{\hat{f}_i^L}{x_i f_i^{OL}}$$

The activity coefficient of component i , is only defined when its standard state is specified- f_i^{OL} . The conditions (T, P) required for the specification of f_i^{OL} are arbitrary, but these conditions must be chosen such that γ_i is approximately unity. At extreme conditions, the system temperature often exceeds the critical temperature of one of the components in a system. The components of the systems studied in this project were all condensable at the isothermal conditions chosen for experimentation i.e. condensable components. In the case of supercritical components, the choice of the standard state has been discussed by Mühlbauer and Raal (1995).

The condensable components are defined as the components in a system which have critical temperatures greater than the system operating temperature. Generally the activity coefficients of a system are normalized for consistency with respect to the standard state condition mentioned earlier i.e.

$$\lim_{x_i \rightarrow 1} \gamma_i = 1$$

$$\gamma_i = \frac{\hat{f}_i^L}{x_i f_i^{OL}} \approx 1$$

As the composition of the mixture approaches that of the pure component i , the liquid fugacity \hat{f}_i becomes equal to the mole fraction multiplied by the standard state fugacity f_i^{OL} . This method of normalization of the activity coefficients of the *condensable components* is defined as *symmetric normalization*.

Activity coefficient of condensable components

The activity coefficient at system temperature (T) and pressure (P) is determined by including a correction term, equation (3.94). The correction term accounts for the change from the arbitrary reference pressure (P^R to the system conditions:

$$\gamma_i^{(P)} = \gamma_i^{(P^R)} \exp\left(\int_{P^R}^P \frac{\bar{V}_i^L}{RT} dP\right) \quad (3.94)$$

Application of the symmetric normalization of condensable components, $\gamma_i^{(P^R)} \rightarrow 1$ for $x_i \rightarrow 1$, implies that the standard state reference fugacity equals that of the pure component at temperature (T) and pressure (P^R).

$$f_i^{OL} = \hat{f}_i^L \quad (3.95)$$

Furthermore at equilibrium the equilibrium constraint, $\hat{f}_i^V = \hat{f}_i^L$ applies. The liquid phase fugacity can be easily calculated from the equilibrium constraint i.e. for a reference pressure (P^R), equal to the pure component vapour pressure (P_i^{sat}):

$$\hat{f}_i^{L(P_i^{sat})} = \hat{f}_i^{V(P_i^{sat})} = \phi_i^{sat} P_i^{sat} \quad (3.96)$$

\Leftrightarrow

$$f_i^{OL} = P_i^{sat} \phi_i^{sat} \exp\left(\int_{P_i^{sat}}^{P^R} \left(\frac{\bar{V}_i^L}{RT}\right) dP\right) \quad (3.97)$$

Generally the reference pressure is set to zero:

$$f_i^{OL} = P_i^{sat} \phi_i^{sat} \exp\left(-\frac{\bar{V}_i^L P_i^{sat}}{RT}\right) \quad (3.98)$$

For condensable components the expression of, equation (3.98), assumes that \bar{V}_i^L is a function of temperature only. Therefore \bar{V}_i^L is replaced with V_i^L , which is calculated from liquid models. The *Modified Racket* equation

was used in the regression analysis to predict \bar{V}_i^L :

$$\bar{V}_i^L = \frac{RT_c}{P_c} Z_{RA}^{[1+(1-T_r)\frac{1}{2}]} \quad (3.99)$$

where Z_{RA} is a constant specific to the compound,

$$Z_{RA} = 0.29056 - 0.08775\omega \quad (3.100)$$

Chapter 4

EXPERIMENTAL APPARATUS

4.1 History of HPVLE Apparatus

The experimental apparatus used in this study is a result of years of research and development undertaken at the School of Chemical Engineering at the University of KwaZulu-Natal.

The interest in *HPVLE* equipment began at the school in the early 1980's. The development of high pressure technology was initiated by *SASOL*. *SASOL* had assigned the school to undertake *VLE* measurements at the extreme conditions of 500 °C and 200 bars. The data was of particular interest for *SASOL's* coal liquefaction processes. The studies were furthered between 1983 to 1985 and the construction of liquid and vapour sampling devices followed.

The major difficulty encountered during experimentation was the sampling of the equilibrium liquid phase (Mühlbauer, 1990), (Ramjugernath, 2000). The composition analysis of the liquid phase indicated an incorrect bias towards the more volatile component.

In addition to the problems of sampling the liquid phase, there were **temperature uniformity** problems associated with the equilibrium cell situated in an air-bath.

Mühlbauer (1990) perfected the liquid and vapour sampling devices, redesigned the air-bath and constructed certain auxiliary equipment. Ramjugernath (2000) continued the *HPVLE* research and made significant progress with the equipment. Kissun (2001) devised a refrigeration unit for measurements below room temperature. Naidoo (2004) continued with the *HPVLE* measurements and redesigned the liquid jet-mixers.

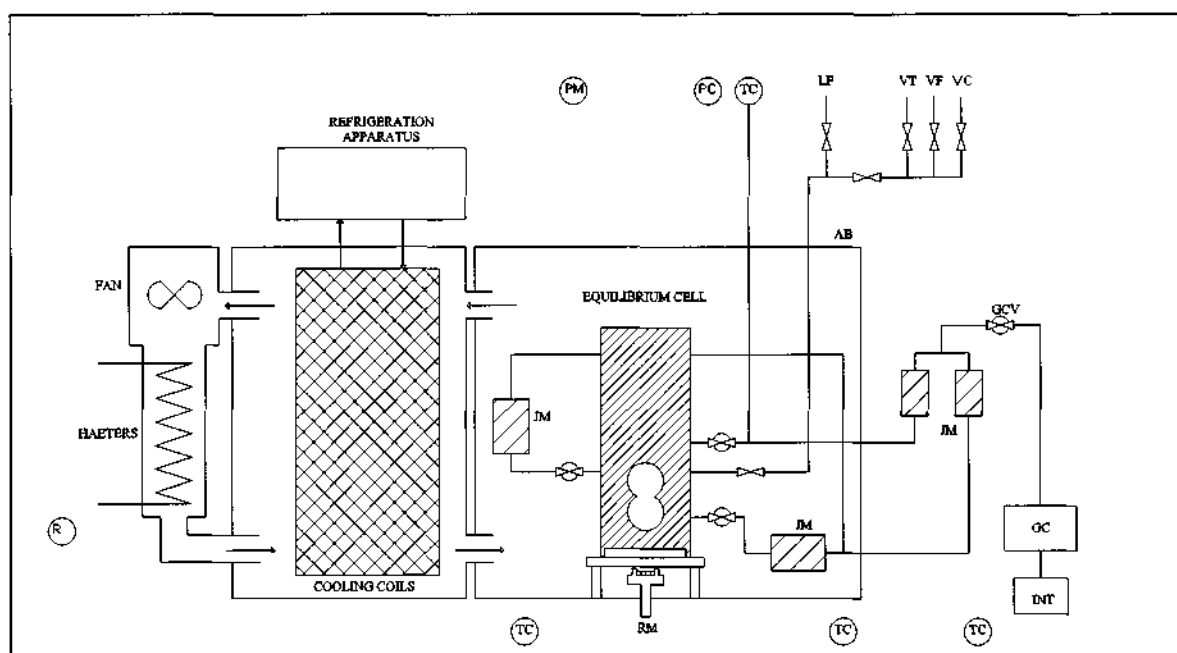


Figure 4.1: Schematic of experimental apparatus layout: AB - Air-bath; GC - gas chromatograph; GCV - gc sampling valve; INT- integrator; JM - jet-mixer; LF- liquid feed line; PC- pressure transducer; PM- pressure measuring device; RM - rotating magnet; TC -thermocouple; VC- vacuum line; VF - gas(N_2) feed line; VT-vent line, Naidoo (2004)

The work of Ramjugernath (2000) made a significant contribution by overcoming the limitations that were encountered by Mühlbauer (1990). Ramjugernath (2000) redesigned the apparatus and made the following improvements:

1. A more compact and versatile experimental apparatus
2. An improved sampling method for analysis
3. The detection of the formation of a secondary liquid phase (if it exist)
4. The sampling of multiple phases with the sampling method.

A summary of the equipment specifications are listed below.

1. The equipment is of the static type. The isothermal environment is a air-bath with dimensions of $1m \times 0.75m \times 0.5m$. The equilibrium cell has a variable volume and therefore is capable of undertaking P - V - T measurements and VLE measurements via the dew and bubble point methods.

2. Sampling of the equilibrium phases was achieved by six-port two-piston GC sampling valves. The equilibrium phase samples were circulated through the sample loop of the GC sampling valves.
3. The formation of multiple phases and the phase interfaces can be detected visually. This is possible as the equilibrium cell has two pairs of illuminated sapphire viewing windows. The windows are 33mm in diameter and are 14mm thick. The windows offer a viewing diameter of 22mm-(Ramjugernath, 2000).
4. A composite stirrer was designed such that the equilibrium phases mix independently (two liquid and vapour phases). The stirring of the phases also promoted the flow of each phase through the sampling loops of the respective sampling valves. Figure 4.2 below illustrates the equilibrium cell design.

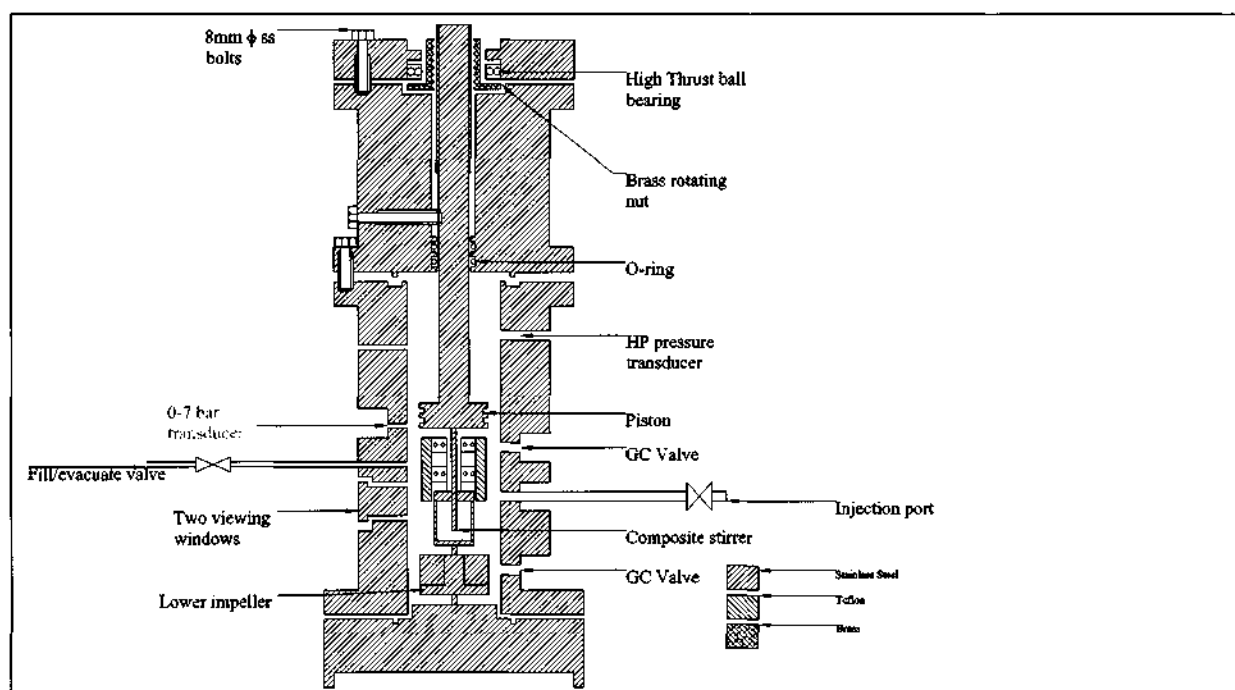


Figure 4.2: Schematic of equilibrium cell, (Naidoo, 2004)

4.2 Apparatus: Specification and Considerations

4.2.1 The Equilibrium Cell And Piston Assembly

The experimental apparatus consisted of an equilibrium cell and a piston assembly, Figure 4.2. The piston was used to manipulate the internal volume of the cell via a stepper motor. Thereby the equilibrium cell with the stepper motor was able to undertake P - V - T measurements (Naidoo, 2004). The piston and the stepper motor were not used in this study since isothermal measurements were undertaken. In this study the piston was screwed to the top of the cell, such that the entire volume of the cell was used during measurements.

The equilibrium cell was machined from a solid billet (stainless steel type 316) with diameter 120mm and height 200mm. The billet was bored to a diameter of 40mm and length 190mm. The effective resulting internal volume (with composite stirrer) of the equilibrium cell was approximately 200ml. There were two pairs of synthetic sapphire windows (33mm in diameter and 14mm thick) placed in special housings bolted onto the equilibrium cell body.

The sealing between the sapphire window housing and the equilibrium cell body was achieved with Viton "O"-rings. The sapphire housings were constructed of 316 stainless steel and the sapphire windows were encased in a gasket type material that fitted into the stainless steel housing. Viton "O"-rings were used to seal the sapphire windows against the gasket type material housing. The sapphire window encasing was made from a combination of two materials, Axiol and bronze impregnated with teflon. The viewing paths for the sapphire windows were illuminated with small 5 watt light bulbs. The light bulbs were housed in a pyrex tube. Hence the bulbs were not in direct contact with the isothermal air-bath space.

The equilibrium cell had a removable base. The removable base was incorporated into the design for two reasons:

1. It made construction and attachment of the composite impeller much simpler. The composite impeller attaches to the removable base and is supported by a screw that screws into the base.
2. It makes cleaning of the entire equilibrium cell possible. Mechanical cleaning of the equilibrium cell would be required if the components in the cell were to form residues during experimentation.

The base of the cell was a flange with a raised edge that bolted into the equilibrium cell body. The sealing between the base and the cell body was achieved with Viton "O"-rings.

The equilibrium cell body had 3mm holes drilled into it for the GC valve sampling lines, pressure transducer lines and the inlet/evacuate line figure 4.2. The fill/evacuate valve used the equilibrium cell was a Whitey valve. The valve is bi-directional and was reported to withstand a combined temperature and pressure effect of 175 °C and 1000psi respectively (Naidoo, 2004).

4.2.2 Mixing of Equilibrium cell contents

Static apparatus have been found to require lengthy periods of time for before phases equilibrium to be achieved. Agitation of the equilibrium contents is essential to reduce the time taken to reach equilibrium.

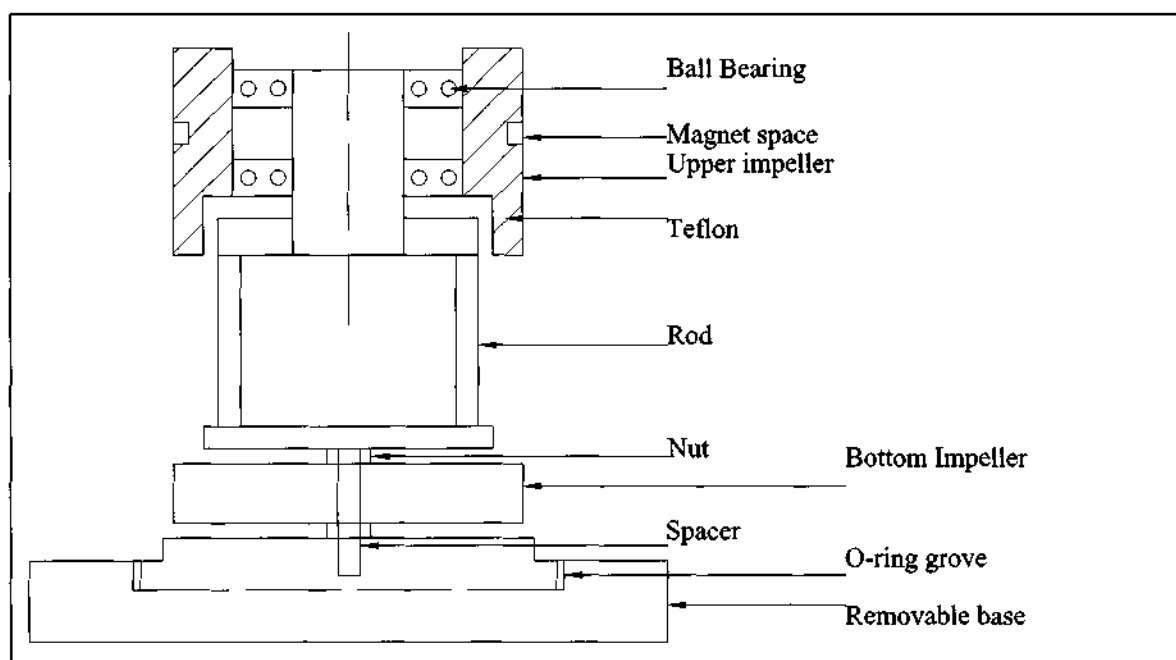


Figure 4.3: Diagram of the equilibrium cell composite stirrer, (Naidoo, 2004)

The equilibrium cell was designed to mix both the vapour and liquid phases with two separate stirrers. Both stirrers are mounted on to a single assembly, Figure 4.3. The stirrers were rotated by externally mounted solenoids. However the top stirrer was not used in this study because it was actually installed to agitate a second liquid phase if it existed (*VLL*). The design of the impeller for the liquid phase (bottom stirrer) was designed by Mühlbauer (1990). The liquid phase was agitated with a four bladed stainless steel (type 316) impeller. The impeller rotated on a stainless steel

pin. The speed of the impeller was controlled by a geared Maxon motor. Ramjugernath (2000) modified the agitation mechanism with the inclusion of a external rotating horseshoe magnet mounted on the motor. Teflon spacers were used to reduce the friction between the bottom stirrer and the equilibrium cell.

The upper stirrer was constructed from stainless steel (type 316). The stirrer had spaces to contain four cylindrical shaped rare earth magnets. Stainless steel protrusions were attached to a cylindrical teflon layer at the lower end of the stirrer design. This impeller was designed to aid in the agitation of a second liquid phase if it existed.

Upon agitation a vortex was created in the liquid phase by the high impeller speeds, thereby allowing the vapour phase to be entrained. This would effectively induce rapid mass transfer. The centrifugal force of the stirrer forced the liquid phase to also flow into the sampling loops of the liquid GC valve(s). This action ensured that a representative sample was always present in the sample loops.

4.2.3 Sampling of the Vapour and Liquid Phases

The sampling method used was initially employed by Ramjugernath (2000). The sampling device was a commercial six-port two position GC sampling valve. The GC sampling valves used for both the vapour and liquid phases can withstand high temperatures and pressures (175 bar and 215°C). The six-port two piston GC sampling valves were manufactured by VALCO and supplied by Anatech Instruments (Ramjugernath, 2000).

The GC sampling valve has two modes of operation illustrated in figure 4.4. From figure 4.4: in *sampling* mode, the stirrers force fluid through the sampling loop and back into the equilibrium cell. This ensured the flow of a representative equilibrium phase sample through the sample loop. The volume of the sample withdrawn from the equilibrium cell was determined by the size of the sample loop. The sample loop was a fine bore, thick walled stainless steel tubing (3.2 mm tubing with internal diameter of 1mm). The length of the sampling loop inserted was approximately 210 cm, this resulted in an approximate volume of 0.165 cm^3 . Using the valve in *flushing* mode as depicted in Figure 4.4, the equilibrium cell is shut from the sampling loop and the sampling loop is opened to the carrier gas (Helium). The carrier-gas flushes the representative sample out of the sample loop into a jet-mixer (vapour or liquid).

There are three GC sampling valves on the apparatus. The valves are positioned at appropriate heights along the wall of the equilibrium cell body so that the appropriate phases could be sampled. The first sampling valve was

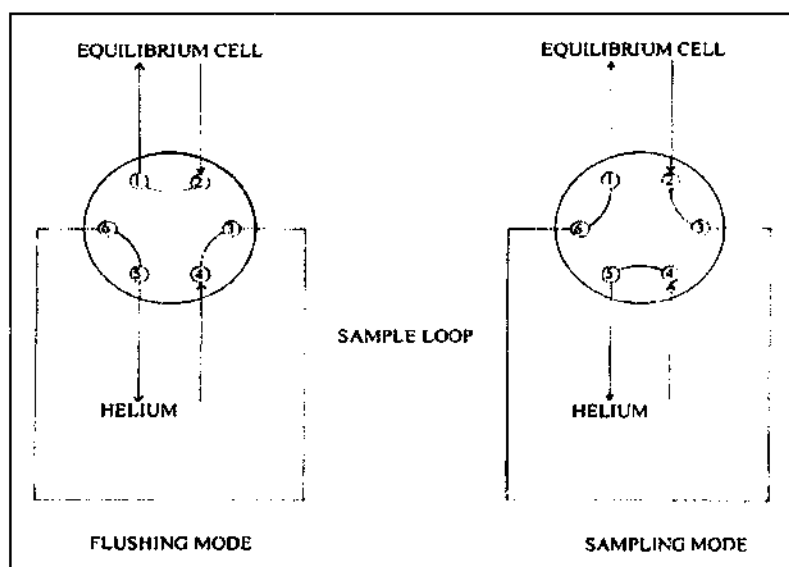


Figure 4.4: Schematic diagram illustrating the two operation modes of the GC valves, (Naidoo, 2004)

positioned at the bottom of the cell body, adjacent to the bottom stirrer. This valve samples the bottom liquid phase. The second sampling valve is positioned adjacent to the upper stirrer, approximately a third of the way up the equilibrium cell body to sample the second or upper liquid-phase (if it should exist). The third GC sampling valve, sample the vapour phase and is positioned approximately half way up the cell body.

4.2.4 Jet-mixers

It has been reported that sample analysis, particularly of the liquid phase in the static method, has been the most demanding (Deiters and Schneider, 1986), (Ramjugernath, 2000). The sampling method of the equilibrium phase should recognise that the sample must be homogeneous. The problem arises during the flushing (sampling) of a volatile/non-volatile mixture into an evacuated space. Ramjugernath (2000) reported that the more volatile component tends to flash preferentially. This creates a non-homogenous gas-liquid mixture, and can cause the analysis of the withdrawn sample phase to be in error.

The apparatus used to further mix the equilibrium sample in this study was the jet-mixer. Figure 4.5 illustrates the schematic after the redesign by Naidoo (2004). The jet-mixer was designed to vapourise and homogenize the withdrawn sample before composition analysis.

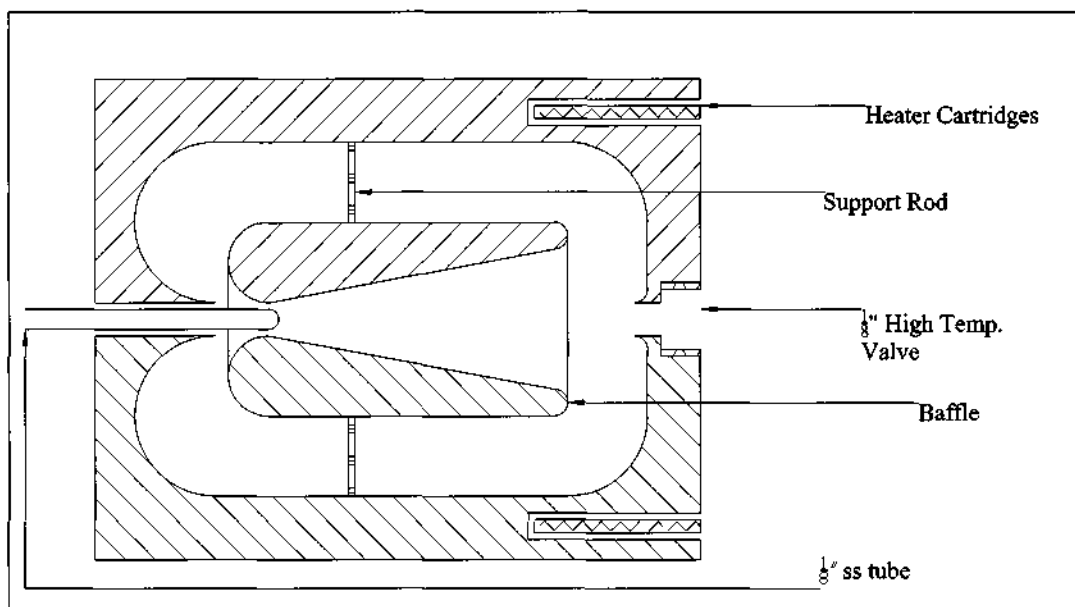


Figure 4.5: Cross-section through the jet-mixer, (Naidoo, 2004)

The equilibrium sample is flushed with helium from the GC sampling valve sample loop into an initially evacuated jet-mixer. The flushed sample passes through the jet-mixer nozzle at a high velocity producing swirling and re-circulating flow. The sample circulates in the jet-mixer until the pressure was uniform. The carrier-gas is flushed at a controlled rate through the sampling loop into the jet-mixer. The swirling action creates within the jet-mixer, induces further mixing of the sample-homogenisation.

The jet-mixer has no moving parts or external devices. It was machined from 316 stainless steel. The mixing chamber consists of an internally mounted cylindrically shaped baffle. The baffle had a restriction nozzle that accelerated and vapourized the withdrawn sample (in the case of liquid sample). The baffle created a change in the fluid flow direction, thereby enhancing swirling of the fluid. The rounded corners were machined in the internal space to eliminate stagnant areas within the space.

The inlet to the jet-mixer was a 1/8" stainless steel tube that was welded into the jet-mixer body. The inlet line extended into the jet-mixer mixing chamber and ensured that the fluid flowed through the restricted nozzle into the chamber. The inlet line was extended from the GC sampling valve at-

tached to the cell. The sample flow out of the jet-mixer was controlled by a Whitey valve, screwed into the jet-mixer body.

The temperature of the jet-mixer is controlled by a Eurotherm 808 temperature controller while a PT-100 measured the jet-mixer wall temperature. The temperature was controlled to $\pm 1^\circ\text{C}$ of the set point. Three 100 Watt heater cartridges are embedded in the body of the jet-mixer wall. The cartridges are evenly spaced along the circumference of the jet-mixer body. The large body of the jet-mixer ensured good temperature uniformity. The jet-mixer is insulated with Fibrefrax to avoid thermal gradients and non-uniformities within the air-bath. Two different sizes of jet-mixers were used for the vapour and liquid phases. There were four jet-mixers in total. The larger jet-mixers with internal volume of 300 cm^3 are used to homogenise the liquid phase, these are situated inside the air-bath. One of the jet-mixers inside the bath was used for a secondary liquid phase i.e. *VLL*. The other two jet-mixers are smaller (65 cm^3) and positioned outside the air-bath along the sampling lines. The external jet-mixers were used for the vapour sample and to further mix the liquid samples respectively.

The pressure within the jet-mixers was measured with a *Sensotech TJE* pressure transducer. The transducer was not directly attached to any of the jet-mixers. The transducer was connected at the start of the sampling line i.e. at the helium/vacuum line. The operating range of the transducer was from 0-5 bar absolute. Naidoo (2004) reported an accuracy of $\pm 0.25\%$ of the full-scale pressure.

4.3 Thermal specifications

4.3.1 The Air-bath

The air-bath was designed to be compact and functional to minimize thermal gradients. Ramjugernath (2000) incorporated some of the design concepts used by Mühlbauer into the air-bath. The actual bath was constructed from mild steel (4mm thick) with dimensions, $1\text{ m} \times 0.75\text{ m} \times 0.5\text{ m}$

The air-bath lid had a 3mm thick aluminium sheet screwed under it. This sheet held a layer of Fibrefrax insulation onto the air-bath lid to reduce heat loss. The bath had holes to accommodate for the sampling line valve stems, the viewing ports for the cell, the holders of the light source, the cabling to the jet-mixers and the Pt-100 sensors and solenoid coils. These holes were stuffed with Fibrefrax. Temperature instabilities within the bath due to non-uniform air circulation caused temperature differences as large as 3°C between the top and bottom of the equilibrium cell. A circular aluminium baffle was inserted at the hot air inlet into the air-bath. This

was found to reduce the difference to approximately 2°C on average and cause the cell (top and bottom) to heat-up faster.

Insulation

A layer of insulation was situated between the walls of the air-bath and the interior copper lining. The thermal insulation material used was spray foam. The thickness of the insulation was approximately 50mm .

Interior Copper Lining

A copper lining was used inside the air-bath to promote high thermal stability and avoid local temperature disturbances. The lining was approximately 2mm thick and was placed against the spray foam insulation. The lining also held the foam insulation in place. Copper was used because of its high thermal conductivity, 401 W/mK , hence it disperses and transmits local temperature disturbances rapidly (Ramjugernath, 2000).

Air Agitation

Two 500 Watt heating elements were located in a heating compartment. Figure 4.6 shows the element arrangement inside the aluminium compartment. The elements were fitted into the housing to avoid radiative heat transfer

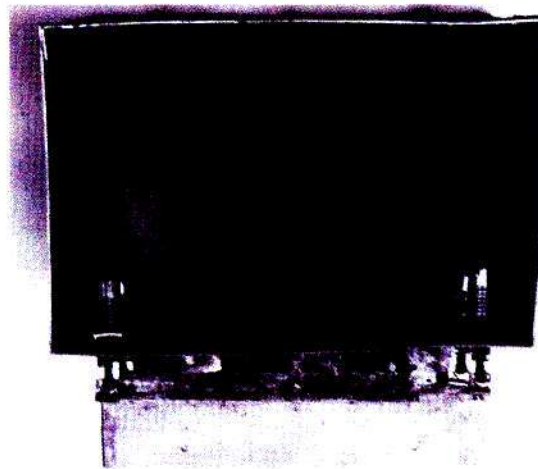


Figure 4.6: Air-bath heating element layout

and consequently local heating effects to the equilibrium cell. The heating elements (and housing) were placed in an insulated box, external to the air-bath. A Siflo Universal fan was used to circulate the air through the box over the heating elements and into the air-bath. A circuit was implemented, with two switches for the respective elements.

The air was circulated between the air-bath and the heater box. Air was drawn in from the top of the air-bath by the fan, blown over the heaters and back into the air-bath through a tunnel at the bottom of the air-bath. Hot spots on the equilibrium cell were avoided by inserting a aluminium deflector plate on the air-bath inlet. An aluminium baffle was inserted adjacent to the cell, figure 4.7. The baffle minimized the hot air from flowing directly onto the equilibrium cell face closest to the air inlet from the heater box.

4.3.2 Temperature Control

The temperature in the air-bath was controlled by a Shinko JCS-33A PID controller. The temperature sensor in the air bath was a PT-100 Ω resistor. The temperature controller had a signal output range of 4-20mA, which drove a fast firing Shinko 8A-340-Z relay. The relay supplied energy to the heating elements by on/off action.

4.3.3 Thermal Leaks, Conductive paths and Thermal disturbances

Thermal, chemical and mechanical equilibrium are constraints required for the measurement of accurate *VLE* equilibrium data. This section outlines and discusses possible areas of concern on the equipment with respect to thermal disturbances.

Factors where the possibility of thermal leaks and conductive paths existed, are listed below:

1. The air bath
 - The holes in the air-bath for the valve stem extensions, sample lines and electrical cabling
 - The aluminium blow-off lid
2. The sampling lines from the air-bath
3. The valve stems of the valves in the air-bath, including the GC sampling valves
4. The cover-plate for the well that housed the horse-shoe magnet and the MAXON motor-(Naidoo, 2004).
5. The jet-mixers inside the air-bath

To prevent heat transfer between the air (room temperature) in the well of the magnetic stirrer and the support plate, the well was sealed in the air-bath. The seal was a graphite (grade M 795) bush able to withstand a temperature of 473 K and 2000 rpm from the motor. Air was used as the insulation medium between the support plate and the equilibrium cell. The air could be heated thereby reducing the temperature gradient across the well.

Teflon thermal breaks were inserted in all the valve stem extensions protruding from the air-bath lid. The thermal breaks were used to reduce the conduction of heat to a minimum. The sample lines external to the air-bath were wrapped with nichrome wire (insulated with heating tape). The nichrome wires were powered by Variac power supplies.

Temperature Measurement

The temperature of the bath was measured by a class A $PT - 100\Omega$ sensor. The equilibrium cell wall temperatures were monitored by four class A $PT - 100\Omega$ sensors, (Naidoo, 2004). The four sensors fitted into holes machined in the cell wall (1-4 in figure 4.7). Two of the $PT - 100$'s were positioned near the bottom of the cell. The remaining two $PT - 100$'s were positioned at the top of the cell. The cell $PT - 100$'s were positioned on the cell wall to determine temperature gradients across the equilibrium cell wall. The bath $PT - 100$ (T_{bath}) and the cell $PT - 100$'s were calibrated with an agilent 34401a 6.5 digit multi-meter coupled with a $PT - 100$ standard. The temperature sensor(bath and cell) calibration charts are given in Appendix B.3.1. The multi-meter and $PT - 100$ standard were calibrated and supplied by Wikka. The temperature probe calibration charts are given in Appendix B.3.1.

The bath sensor was connected to a *Shinko* temperature controller. There were three other $PT-100\Omega$ sensors positioned in different sections of the air-bath, points (5-7) on figure 4.7. These sensors were calibrated previously by a temperature standard and were only used as indication of the air-bath temperature uniformity. All of the sensors shown in figure 4.7 were connected to a Eurotherm multichannel selector that displayed the probe temperatures.

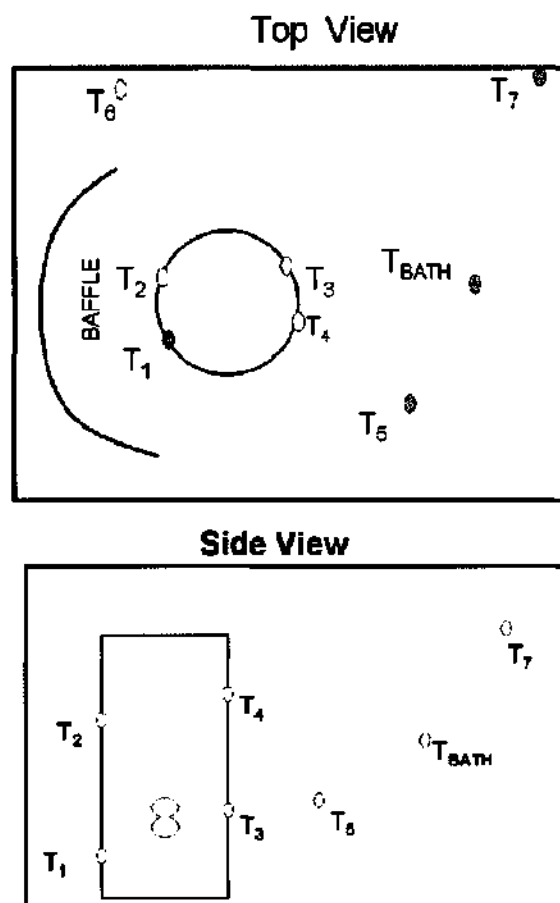


Figure 4.7: Schematic of air-bath temperature probe layout

4.3.4 The Refrigeration unit

Kissun (2001) modified the apparatus of Ramjugernath (2000) by including a single stage vapour compression refrigerator. The unit was capable of producing data at temperatures as low as 250 K.

The refrigeration unit was positioned external to the air-bath, with inlet and outlet tubes fitted onto the heating box adjacent to the air-bath (figure 4.1). The compressor and condenser made-up a single unit manufactured by *L'Unite Hermetique*. The centrifugal condenser had a maximum outlet pressure of 18 bar. The condenser was air-cooled by a fan. The specifications of the condenser was 7m of $\frac{1}{2}$ inch cast iron outer diameter cooling coils encased in a bank of rectangular fins.

The evaporator was similar to the condenser, except the cooling coils were copper. A layer of silicon insulation was used to minimize heat transfer to the surroundings.

4.4 Pressure measurement

Two *Sensotech TJE* transducers were installed onto the experimental apparatus. One for the equilibrium cell (range, 0 – 7bar) and another for the sampling lines and the jet-mixers (range, 0 – 5bar). The transducers were certified to have 0.25% accuracy of full-scale pressure, (Naidoo, 2004). A low pressure standard (0 – 1 bar) was available and used to calibrate the equilibrium cell transducer-the calibration was extrapolated to 7 bar. The equilibrium cell pressure transducer calibration chart is given in Appendix B.3.2.

4.5 Composition measurement

Liquid and vapour samples taken from the equilibrium cell were analyzed by a gas chromatograph. A *Chrompack CP9000* with a TCD detector was connected to the experimental equipment. Hence composition analysis was performed online. The output signal from the GC was converted to a peak

Table 4.1: Specifications of column

Description	Specification	Unit
Supplier	LANGET	-
column length	3	m
outer diameter	$\frac{1}{8}$	inch
packing	Poropak-Q	-
mesh ratio	$\frac{80}{100}$	-

area signal by *Delta* software package. The method of calibration and the GC calibration procedure of the binary systems is discussed in Chapter 6.

4.6 Auxiliary Equipment

A degassing apparatus was used to remove incondensable(impurities) components from the respective chemical. The apparatus was also used to fill the equilibrium cell with the first component of the respective binary. The

degassing apparatus consisted of a 250ml heavy duty Erlenmeyer flask with a single walled condenser. The operation of the degassing apparatus is discussed in Appendix B.1. A custom screw syringe with a teflon plunger (with two viton "O"-rings) was manufactured in the School of Chemical Engineering Workshop. This syringe was connected onto the degassing apparatus initially used for the second component of the respective binary. This method proved to be unsuccessful because the syringe was difficult to use due to the friction between the "O"-rings and the stainless-steel syringe cylinder. The friction on the "O"-rings caused the seals to wear rapidly and therefore the operation of the apparatus was inconsistent due to leaks. A 5ml *SGE* high pressure glass syringe was purchased and used to inject the second component into the equilibrium cell.

4.7 Equipment Safety Specifications

Safety considerations during high-temperature and high-pressure phase equilibrium experimentation must be emphasized due to the extreme operating conditions. The safety considerations considered are in the list below.

- An over design factor of over 100% was considered-Ramjugernath (2000)
- Safety relief valves were fitted before the pressure transducers
- The pressure transducers had a 150% over-pressure safety feature-(Naidoo, 2004)
- Exhaust fans in the laboratory were switched on at all times. The vent/exhaust lines on the equipment were open to the atmosphere outside of the laboratory
- The viewing windows inserted into the air-bath wall were laminated, tempered and shatterproof-(Ramjugernath, 2000)
- The degassing apparatus was covered by a perspex box- in case of an explosion.
- During the GC calibration of the binaries, a gas mask was used due to the volatility of n-pentane and 2-methyl-2-butene.

Chapter 5

SYSTEMS CHOSEN FOR EXPERIMENTATION

The n-pentane + ethanol system was selected as a test system in the study. The test system was used to establish consistent experimental procedures for the equipment and the reproducibility of experimental data. A previously unmeasured system was then examined, 2-methyl-2-butene + TAME. The properties of the components for the two systems are listed in Appendix C.1. Ramjugernath (2000) and Naidoo (2004) used carbon dioxide + toluene as a test system on the equipment comprising one supercritical component in the binary i.e. CO₂.

5.1 n-Pentane + Ethanol

The n-pentane was supplied by Riedel-deHaën and had a minimum purity of 99%. The ethanol was supplied by Saarchem and had a minimum purity of 99.5%. The purity of the components were verified by gas chromatography. Further purification of the components was not undertaken. The n-pentane + ethanol system are selected as a test system because ethanol and pentane were readily available in the laboratory and their boiling points are comparable to the boiling points of 2-methyl-2-butene and TAME boiling points respectively.

This system was subcritical at the desired operating conditions, moderate temperatures and pressure range of 0 – 7 bar conditions characterizing the 2-methyl-2-butene + TAME system measurement. After numerous trials, consistent operating procedures of the equipment were developed with the test system. These procedures were also followed in the measurement of the 2-methyl-2-butene + TAME system. A literature survey of isothermal data for n-pentane + ethanol is given in table 5.1.

Table 5.1: Experimental data for n-pentane + ethanol

Author(s)	Temperature[K]	Pressure range[bar]
Ishii (1935)	263.15	0.0680 – 0.1853
	273.15	0.1060 – 0.3033
	283.15	0.0319 – 0.4604
Pierotti, Deal and Derr (1959)	298.15	0.0584 – 0.0773
	313.15	0.0795 – 0.1736
	343.15	0.4129 – 0.6959
Campbell, Wilsak and Thodos (1987)	372.70	2.2410 – 6.8430
	397.70	4.8262 – 12.011
	422.60	9.6420 – 19.629
Reimers, Bhethanabotla and Campbell (1992)	303.15	0.1051 – 0.8706
Seo, Lee and Kim (2000)	422.60	9.7424 – 19.681
	465.40	25.510 – 41.440
	500.00	48.550 – 57.190

5.2 2-Methyl-2-Butene + TAME

The 2-methyl-2-butene and TAME (tert-amyl-methyl ether) were supplied by Sigma-Aldrich and Fluka, respectively. The respective purities of 2-methyl-2-butene and TAME were > 99% and > 97%. The purity of the components were verified by gas chromatography and further purification was not undertaken. Table 5.2 below lists a survey of experimental isothermal measurements for this system.

Table 5.2: Experimental data for 2-methyl-2-butene + TAME

Author(s)	Temperature[K]	Pressure range[bar]
(Pavlova, Saraev and Chaplits, 1981)	313.15	0.1927 – 1.0649
	333.15	0.4245 – 2.0025
(Qin, Li and Shi, 1996)	328.15	–
(Qin, Li and Shi, 1997)	288.15	–
	305.00	–

Chapter 6

EXPERIMENTAL PROCEDURE

This chapter describes the start-up of the experimental rig and the sampling procedures of the liquid and vapour phases. The experimental procedures discussed, particularly the sampling of phases, were achieved following numerous experimental trials, resulting in a consistent procedure with respect to the data measured. The equilibrium cell pressure and temperature probe calibrations are discussed in Appendix B.3. The start-up procedures of Ramjugernath (2000) and Naidoo (2004) were followed closely.

6.1 Equipment Start-up

6.1.1 Preparation of the Equilibrium Cell

The most common problem encountered in *HPVLE* studies is pressure leakage. This can be attributed to the severe operating conditions impacting the fittings and valves of the apparatus. Therefore it was important for the equilibrium cell and the sampling section be tested regularly for pressure leaks.

The equilibrium cell was tested for pressure leaks by filling the cell with nitrogen to approximately 6 bar, which was considered to be sufficient for the test. The temperature of the bath was set to 60°C. After approximately three hours (thermal equilibrium), the equilibrium cell was monitored for any pressure-drops within an hour. Similarly, any leaks in the sampling section of the equipment were detected by testing in sections of sampling line. The lines were filled to 2 bar and heated to 100°C. The liquid and vapour sampling sections were tested independently. Figure 6.1 illustrates the layout of the cell and sampling section. Note that the second liquid sampling section was not used in this study i.e. JM-2, V7, V8, V9 and SV-3.

The preparation procedure regarding for the replacement of internal seal-

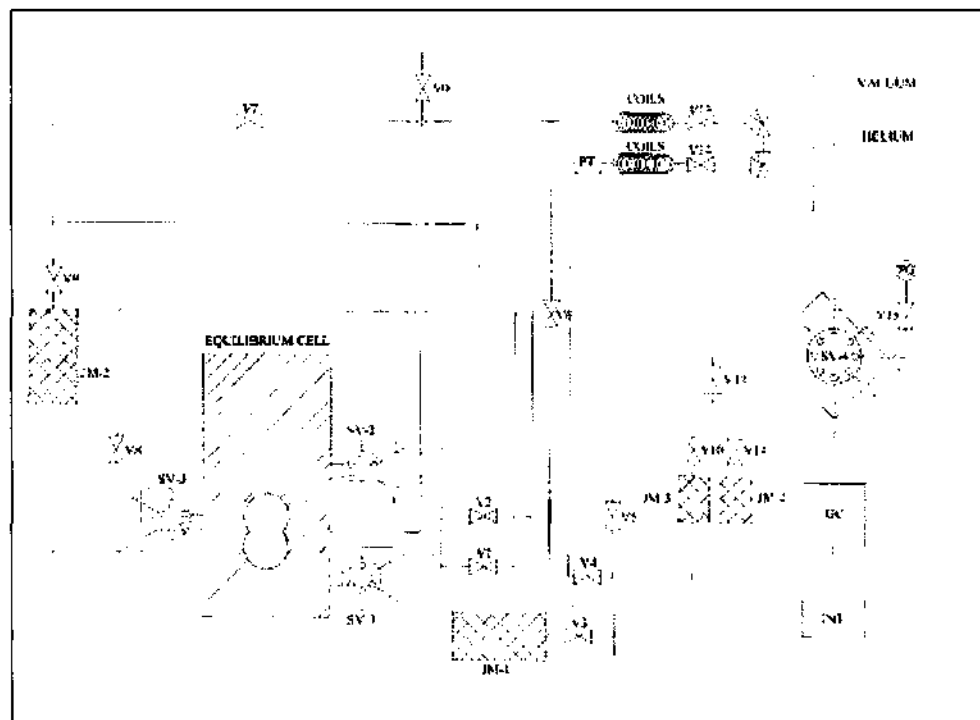


Figure 6.1: Schematic of experimental apparatus, sampling lines and valve layout, (Naidoo, 2004)

ings ("O"-rings etc.) was discussed in Ramjugernath (2000) was not followed in this study. The "O"-rings on the cell piston were replaced if the cell was opened e.g., liquid stirrer maintenance. The replacement of the "O"-rings on the piston was avoided because of the difficulty in removing the cell from the bath, and the possibility of causing leaks on fittings such as valves.

The equilibrium cell was "cleaned" by the application of a vacuum in the equilibrium chamber and raising the temperature of the bath to 115°C . Thus any component that might have been present in the cell were removed by evaporation. Successive flushing of the equilibrium cell with nitrogen removed any trace amounts of impurities. The cell was then flushed with one of the components under investigation.

The internal liquid jet-mixer operating temperature was set on a Eurotherm controller. Appendix B.2 discusses the estimation of the jet-mixer operating temperature. The internal liquid jet-mixer operating temperature was set at 110°C for both systems. The vapour and liquid sampling lines external to the air-bath (including JM-3 and JM-4) were heated sequentially (with respect to the layout above) in increments of 20°C up to SV-4. The lines

were flushed with helium and evacuated successively. A sample (carrier gas) was then sent to the GC to test for any impurity in the line. A small air peak was always noticed during the integration, this could be attributed to the natural leak rates of the fittings.

6.1.2 Preparation of components

The components of the binary systems measured are subcritical at the experimental conditions. The method of degassing was used to remove dissolved impurities. The liquid components were degassed prior to introduction into the equilibrium cell. The procedure and the apparatus is discussed in Appendix B.1.

Two separate degassing apparatuses were initially used for both liquid components of the binary system. Degassing of the components n-pentane (n-pentane + ethanol system) and 2-methyl-2-butene (2-methyl-2-butene + TAME system) skipped on account of the relatively large losses of components due to degassing.

6.1.3 Introducing the liquid component into the cell

The respective component of a binary mixture was introduced into the equilibrium cell from the degassing apparatus via pressure difference. After degassing the liquid, the vacuum to the degassing apparatus was shut off. The equilibrium cell was then opened to the vacuum and evacuated to 0.01kPa. The equilibrium cell was then shut V0, figure 6.1. The degassing apparatus was slowly filled with nitrogen and the cell was opened to the degassing apparatus.

Positioning the liquid level

The cell was filled with the component from the degassing unit once thermal equilibrium had been established. Hence, for the n-pentane + ethanol system, the cell was filled at the air-bath temperature set to 80°C. Similarly the cell was initially filled with TAME at 70°C for the 2-methyl-2-butene + TAME binary.

The cell was filled with approximately 45 cm³-50 cm³ of the component. This volume was estimated to be half-way of the bottom sapphire viewing window. Therefore once the level reached this mark (on the bottom sapphire window), the equilibrium cell was shut to the degassing apparatus. The degassing apparatus was then shut from the nitrogen cylinder and the degassing hot-plate turned down.

This filling procedure was performed twice; the first fill was performed to flush the cell with component. The component was boiled off under vacuum

upon the first fill. Approximately 80 cm³ of component was then filled and degassed in-situ i.e. the second fill. The cell was shut off from the vacuum when the volume inside the cell was reduced to 45 cm³-50 cm³. The bottom stirrer was switched on. The in-situ degassing removed nitrogen from the cell.

There are a number of physical problems associated with an incorrect liquid level, which can affect the composition analysis of an equilibrium sample. The problems that may occur due to incorrect liquid levels in the equilibrium cell (also in Ramjugernath (2000)):

1. if the liquid level is too low i.e. below the sampling port, no liquid will be sampled because there will be insufficient head to allow flow of liquid through the port,
2. During venting with a high liquid level, the liquid phase can be vented,
3. If the liquid level is adjacent or near the vapour sampling port, the liquid phase can be entrained into the vapour sample port.

The stirrer motor was switched on once the cell was filled to the correct liquid level. The speed of the stirrer was adjusted to form a vortex. A moderate stirrer speed was set, as this minimizes splashing of the liquid.

6.1.4 Injection of the Second Liquid Component

The second liquid component was injected into the equilibrium cell via the injection port with a 5ml *SGE* high pressure glass syringe. Before injecting the syringe was flushed three times with the respective component.

The composition analysis was undertaken on the withdrawn equilibrium samples with the static analytic method. Therefore the composition of the cell contents could only be determined after sampling of the equilibrium phases. The volume of the second component was injected such that the liquid compositions of the mixture were evenly spaced along the respective isotherm. This was achieved by noting the cell pressure after injection and reading the liquid composition off the binary isothermal curve. For the test system (n-pentane + ethanol), the composition with each injection was read off the literature data curve. The second component of the 2-methyl-2-butene + TAME system was injected until a 5 kPa-7 kPa change was noticed. After injection the equilibrium contents were given an hour to mix before sampling.

Three isotherms were measured for the 2-methyl-2-butene + TAME system. Therefore to minimize the amount of components used, after composition analysis for the respective isotherm, the temperature controller was set for

the next isotherm. With each injection the liquid level in the cell increased. Once the level moved above the bottom viewing window, the contents of the cell was vented under vacuum until the desired liquid level was reached. The pressure in the cell was used as a rough indicator of the composition of the isotherm.

6.2 Equilibrium phase sampling

6.2.1 Liquid phase sampling

The equilibrium cell contents were deemed to be at equilibrium when the system pressure remained constant. For a particular isotherm, thermal equilibrium was estimated after approximately four hours the cell temperature sensors remained constant. The liquid sampling procedure was similar to the procedure given in (Ramjugernath, 2000).

1. The bottom stirrer speed was reduced. to ensure that minimal splashing of the liquid occurred during sampling.
2. The sampling lines external to the air-bath and the 8-port GC valve, were heated to desired temperatures three hours before sampling. The internal jet-mixer operating temperature was set on the jet-mixer controller to between 100 °C-120 °C. The external jet-mixer temperatures were set to 10 °C-20 °C higher than the internal jet-mixer temperature. The lines were heated by Nichrome wire. The Nichrome wire was insulated with heating (glass) tape and wrapped around the sampling lines. Power was supplied to the Nichrome wire by variable resistance Variacs. Six thermocouple sensors were placed at different points along the sampling lines. The thermocouples were connected to a multiple selector display panel. The lines were maintained at temperatures comparable to the external jet-mixer temperatures. The 8-port GC sampling valve was maintained at 150 °C-160°C, comparable to the GC injector temperature. The valve was heated with a heater cartridge inserted into the valve casing and Nichrome wire wrapped around the sample loops.
3. All the sampling lines were flushed and evacuated prior to sampling. The vapour sampling side was filled with helium to approximately 0.3 bar during sampling of the liquid phase. The liquid sampling side was evacuated. The valves V14, V2, V3, V11, V12 and SV-4 were opened to vacuum (refer to figure 6.1). The lines were evacuated to approximately 1 bar below vacuum. The first liquid sample was always discarded and therefore only V2 was closed. The line from the metering valve V14 up to the cross V1/V2 was filled up to 1.5 bar with helium.

The liquid sample was flushed from the cell by opening V2 and SV-1 (flushing mode) simultaneously. This sample was discarded by venting at V15. This ensured that any lodged vapour in the liquid sample loop was removed. The lines were flushed with helium and evacuated three times. Once -1 bar vacuum was again reached, the valves were closed in reverse order i.e. starting at SV-4. SV-1 was moved into sampling position i.e. ready for flushing the liquid sample.

4. V14 was opened and approximately 1.5 bar of Helium was filled to V1/V2. The carrier gas allowed to heat up for approximately 5 minutes to heat-up. This aided in the prevention of condensation of the equilibrium sample. V2 was then opened and SV-1 was turned to flushing mode simultaneously. As the sample entered the evacuated liquid jet-mixer (JM-1), the pressure dropped to within the negative range of 0.45 bar-0.650 bar. Homogenisation was facilitated by opening V14 slowly i.e. filling the jet-mixer at a rate of approximately 0.15 bar/sec. This created swirling of the sample within the jet-mixer. This constant flowrate of carrier gas also aided in flushing less volatile component that might have been deposited on the lines i.e. ensured that the entire sample was trapped inside the jet-mixer.
5. The metering valve V14 was shut when the pressure inside the jet-mixer reached 1.5 bar and 2.5 bar, for the 2-methyl-2-butene + TAME and n-pentane + ethanol systems respectively. The pressure inside the jet-mixer was monitored for approximately 10 min. If a decrease in pressure was observed, it would imply that there was condensation and the sample would have to be discarded.
6. The valve V3, was then open after the sample had sufficient time in JM-1 for homogenisation-approximately 10 minutes. The sample was then carried to the external liquid jet-mixer(JM-4).
7. Similarly JM-4 was pressurized slowly to 2 bar and 2.5 bar for the respective system. This additional jet-mixer ensured further homogenisation of the sample. The sample was again monitored for condensation.
8. Valve V11 was opened and the valve V12 was then opened fully to allow the diluted equilibrium sample to sit at 8-port GC valve(SV-4). V14 was opened carefully and the line was pressured to 2 bar.
9. The GC valve was then switched and the sample was conveyed to the GC. After a GC run, SV-4 was switched to sampling mode and V15 opened slowly to decrease the pressure within the line. Samples were taken approximately every 0.1 bar decrease in pressure. A plot of the jet-mixer/line pressure versus composition would indicate a region

of homogeneity i.e. region of consistent compositions with minimal variance. The composition was averaged over this region. This region could be seen graphically after about ten samples were sent to the GC.

10. The sample was purged through V15 and the cleaning procedure repeated. The liquid sampling valve SV-1 was positioned into sampling mode and the liquid line pressured to 0.3 bar. The valves were then shut.

6.2.2 Vapour phase sampling

The sampling procedure for the vapour phase was similar and simpler to that of the liquid phase. The equilibrium vapour sample was only homogenised once in the external jet-mixer(JM-3). The vapour was sampled after the liquid phase, allowing the jet-mixers and lines to attain the desired temperatures. The vapour sampling procedure was as follows:

1. The vapour sampling side was cleaned by flushing and evacuating to vacuum similar to the liquid sampling procedure. SV-2 was always left in flushing mode prior to sampling. The vapour sampling side was prepared by opening the following valves to vacuum: V14, V1, V5, V10 and V12.
2. Similar to the liquid sampling procedure, the first vapour sample was discarded. This removed any liquid lodged in the vapour sampling loop.
3. The lines were cleaned and evacuated to -1 bar. The valves on the vapour sampling side were closed in reverse order.
4. Helium was pressured to 1.5 – 1.6 bar up to V1/V2. The gas was heated for approximately 5 minutes.
5. Before sampling, the vapour sampling valve SV-2 was placed into sampling mode for approximately 20 seconds.
6. V1 was opened and SV-2 moved into flushing mode simultaneously. The sample was conveyed up to V5.
7. V5 was opened and the sample was conveyed to the external jet-mixer (JM-3).
8. V14 was opened slowly to allow a rate of $0.15\text{bar}/\text{sec}$ of helium to fill JM-3. JM-3 was filled to 1.8 – 2 bar with respect to the system. Once filled to the desired pressure, the pressure was monitored for any decrease i.e. condensation.

9. V10 was opened and V14 opened slowly to increase the pressure at V12 to 2 bar.
10. V12 was opened and the pressure in the line dropped in decrements of 0.1 bar. The sample was sent to the GC via the 8 port GC valve SV-4.
11. Similarly samples were analyzed until a region of homogeneity was determined.

6.3 GC calibration procedure

Composition analysis of the equilibrium phases was performed by online gas chromatograph analysis. A Chrompack CP9000 gas chromatograph with a thermal conductivity detector (TCD) was used for composition analysis. A packed column was used for separation of the components-specifications in section 4.5. The Delta software package was used to integrate the signals from the GC. The detector required initial calibration for the respective binaries such that the data from Delta could be interpreted.

6.3.1 Standard solution method of calibration

Mixtures of a known mole ratio, composed of the respective binary components were made. The calibration method discussed in Raal and Mühlbauer (1998) was followed. A range of mole ratios $\frac{n_1}{n_2}$ were chosen i.e 0.1 – 1.3. Where:

$$\frac{n_1}{n_2} = \frac{m_1}{Mwt_1} \times \frac{Mwt_2}{m_2}$$

$$= \frac{x_1}{x_2}$$

$n_i = \text{moles}$

$Mwt_i = \text{molecular weight}$

The masses (m_i) of each component were weighed on a scale to ± 0.0001 grams. The response factor F is defined as the constant between the number of moles passing the detector and the peak area A_i . A_i is obtained from the Delta integrator and is dependent on the amount of sample injected. Hence the relationship between moles and peak area is defined as:

$$n_i = A_i F_i$$

Raal and Mühlbauer (1998) suggest that it is more consistent to work with area ratios:

$$\frac{n_1}{n_2} = \left(\frac{A_1}{A_2} \right) \left(\frac{F_1}{F_2} \right) = \frac{x_1}{x_2}$$

A plot of $\frac{A_i}{A_j}$ versus $\frac{x_i}{x_j}$ was made. Similarly mixtures were made for the inverse $\frac{x_2}{x_1}$ and the corresponding $\frac{A_i}{A_j}$ versus $\frac{x_i}{x_j}$ data plotted. The two graphs were found to be linear in the dilution region for the respective binaries. A linear relationship is desired for the calibration range. Constant response factor ratios are indicated when the slope of one plot equals the inverse slope of the second plot. The calibration graphs for the binary systems measured are given in Appendix B.4.1.

Chapter 7

EXPERIMENTAL RESULTS

This chapter presents the experimental measurements obtained from the HPVLE apparatus i.e. pure component vapour pressure measurements and the binary vapour-liquid equilibrium measurements.

7.1 Vapour Pressure Measurements

The apparatus was prepared for measurement as described in chapter 6.1.1, page 56. The pure components ethanol, n-pentane and TAME were degassed and introduced into the equilibrium cell via the degassing apparatus. 2-Methyl-2-butene was not degassed and was injected directly into the equilibrium cell via an injection port.

The temperature range selected for the pure component vapour pressure measurements included the temperature(s) of the respective binary vle isotherm(s). The vapour pressures of the respective components were measured once the apparatus had reached thermal equilibrium for each temperature approximately 3 hours.

7.1.1 n-Pentane Vapour Pressures

The experimental n-pentane vapour pressures are presented graphically in Figure 7.1 and tabulated in Table 7.1 on page 68. The average % relative error ($\text{Abs}(\frac{P_{cal}^{sat} - P_{exp}^{sat}}{P_{cal}^{sat}}) \times 100$) in vapour pressures measured was found to be $\pm 1.08\%$.

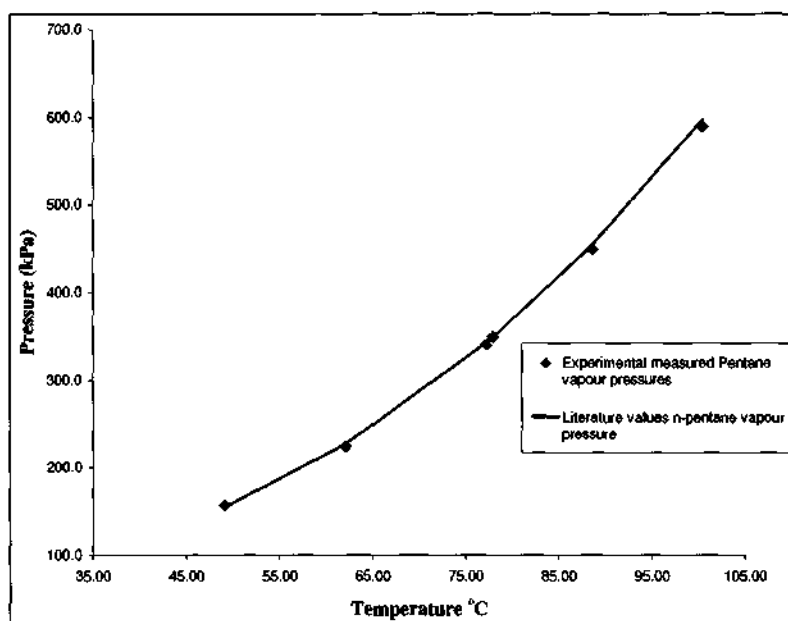


Figure 7.1: Plot Of Experimental n-pentane Vapour Pressure Points Against Literature (Reid et al., 1987)

Table 7.1: n-Pentane Vapour Pressures And Relative % Error With Respect To (Reid et al., 1987)

TEMPERATURE $^{\circ}C$	$P_{experimental}(kPa)$	$P_{literature}(kPa)$	%ERROR
49.11	156.79	154.65	1.38
62.12	223.91	227.59	1.62
77.25	340.11	342.55	0.71
77.95	349.18	348.74	0.13
88.61	448.72	454.33	1.23
100.41	588.96	597.22	1.38

7.1.2 Ethanol Vapour Pressures

A plot of the vapour pressures is given in figure 7.2 and tabulated in table 7.2. The average absolute error in the ethanol vapour pressure measurement was determined to be $\pm 0.841\%$.

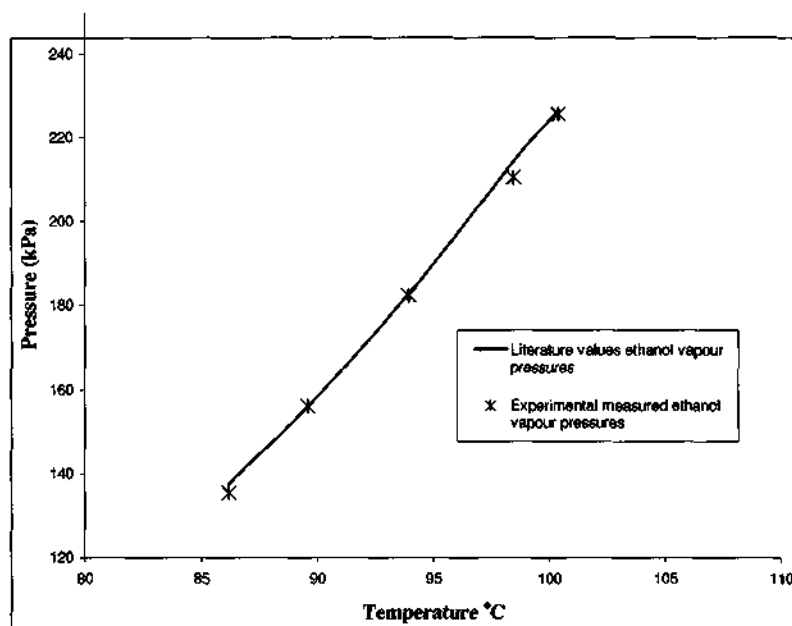


Figure 7.2: Plot Of Experimental Ethanol Vapour Pressure Points Against Literature (Reid et al., 1987)

Table 7.2: Ethanol Vapour Pressures And Relative % Error With Respect To Literature Values (Reid et al., 1987)

TEMPERATURE $^{\circ}C$	$P_{experimental}(kPA)$	$P_{literature}(kPa)$	%ERROR
86.20	135.44	137.70	1.64
89.58	156.19	156.08	0.07
96.96	182.32	182.83	0.28
98.47	210.45	214.21	1.76
100.41	225.51	226.54	0.46

7.1.3 2-Methyl-2-Butene Vapour Pressures

Figure 7.3 and table 7.3 present the vapour pressures for 2-methyl-2-butene. The absolute % error in the vapour pressures measured was $\pm 1.35\%$.

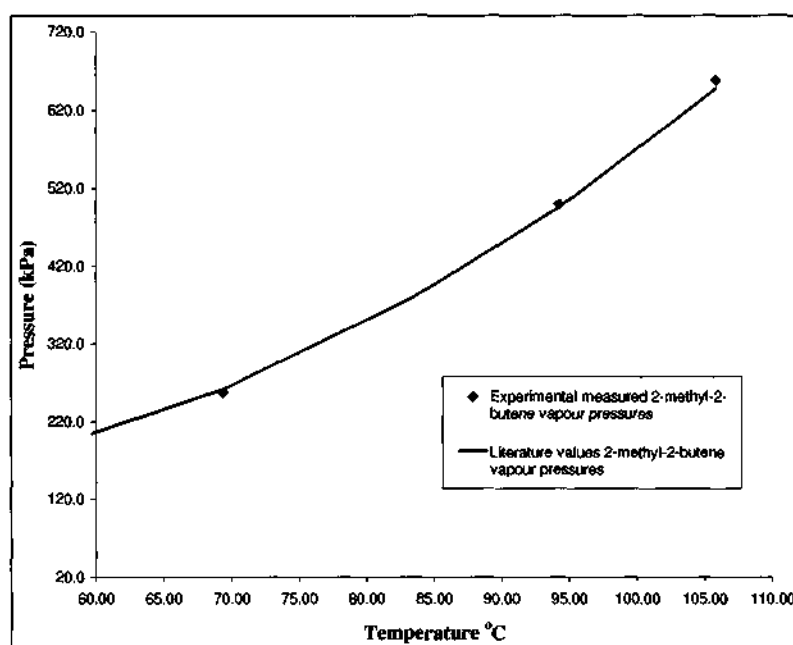


Figure 7.3: Plot Of Experimental 2-methyl-2-butene vapour Pressure Points Against Literature (Reid et al., 1987)

Table 7.3: 2-Methyl-2-butene vapour Pressures And Relative % Error With Respect To Literature Values (Reid et al., 1987)

TEMPERATURE $^{\circ}C$	$P_{experimental}(kPA)$	$P_{literature}(kPa)$	%ERROR
69.35	257.32	261.51	1.60
94.27	498.89	495.50	0.68
105.86	658.40	647.06	1.75

7.1.4 TAME Vapour Pressures

The measured TAME vapour pressures are shown in figure 7.4 and tabulated in table 7.4. The absolute % relative error from table 7.4 was $\pm 0.46\%$.

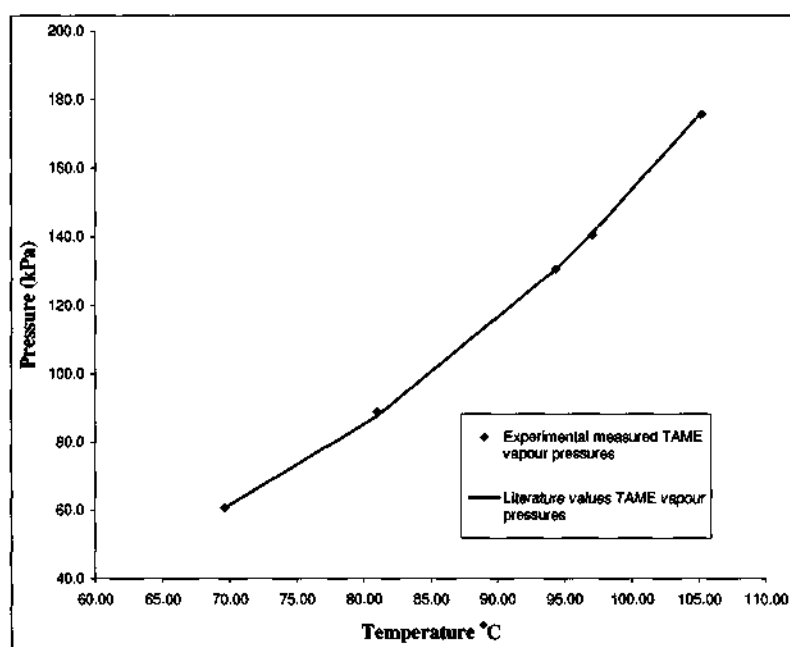


Figure 7.4: Plot Of Experimental TAME Vapour Pressure Points Against Literature (Qin et al.,1997)

Table 7.4: TAME Vapour Pressures And Relative % Error With Respect To Literature Values (Qin et al.,1997)

TEMPERATURE $^{\circ}C$	$P_{experimental}(kPa)$	$P_{literature}(kPa)$	%ERROR
69.63	60.77	60.70	0.11
80.98	88.90	87.64	1.43
94.33	130.56	130.44	0.09
97.08	140.43	141.00	0.40
105.22	175.6	176.09	0.26

7.2 Binary System Measurements

7.2.1 n-Pentane(1) + ethanol(2) system

n-Pentane(1) + ethanol(2) system at $100.41^{\circ}C$

The n-pentane(1) + ethanol(2) system was selected as the test system for this study. The experimental measurements were conducted at $100.41^{\circ}C$ and compared to literature measurements at $99.55^{\circ}C$. The relative error in n-pentane and ethanol vapour pressures were $\pm 0.44\%$ and $\pm 0.63\%$ respectively. The experimental and literature data for the binary system are given on page 72.

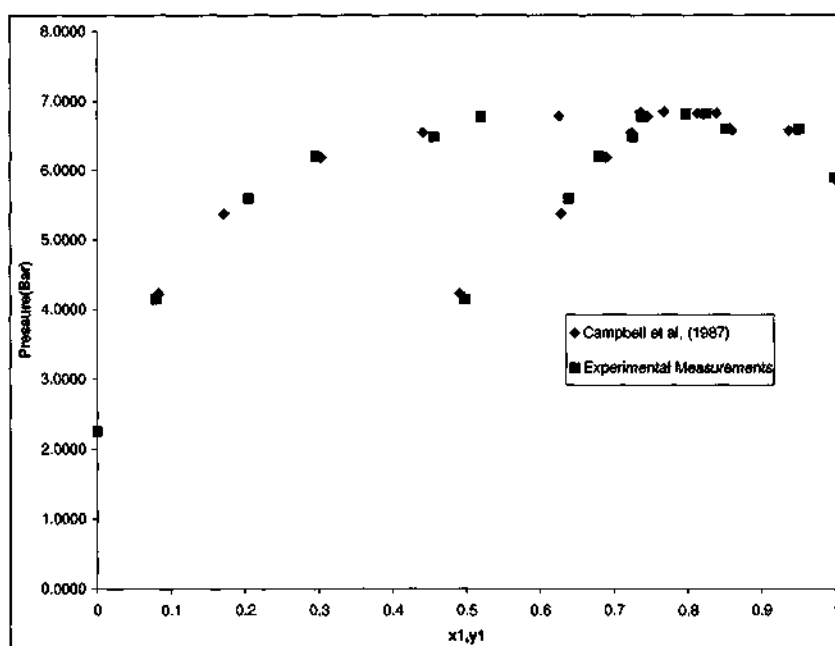


Figure 7.5: The n-pentane(1) + ethanol(2) VLE Isotherm At 100.41°C , Against (Campbell et al., 1987) Measured At 99.55°C

Table 7.5: Binary Experimental Data For The n-pentane(1) + ethanol(2) System at 100.41°C

Pressure bar	x_1	y_1
2.26	0	0
4.14	0.0802	0.4983
5.59	0.2049	0.6390
6.21	0.2953	0.6800
6.48	0.4564	0.7258
6.77	0.5199	0.7386
6.82	0.8253	0.7983
6.59	0.9516	0.8526
5.89	1	1

7.2.2 2-Methyl-2-Butene(1) + TAME(2) system

2-Methyl-2-Butene(1) + TAME(2) system at 70.0°C

The experimental data points for the 70.0°C isotherm are plotted on figure 7.6. Table 7.6 lists the experimental points.

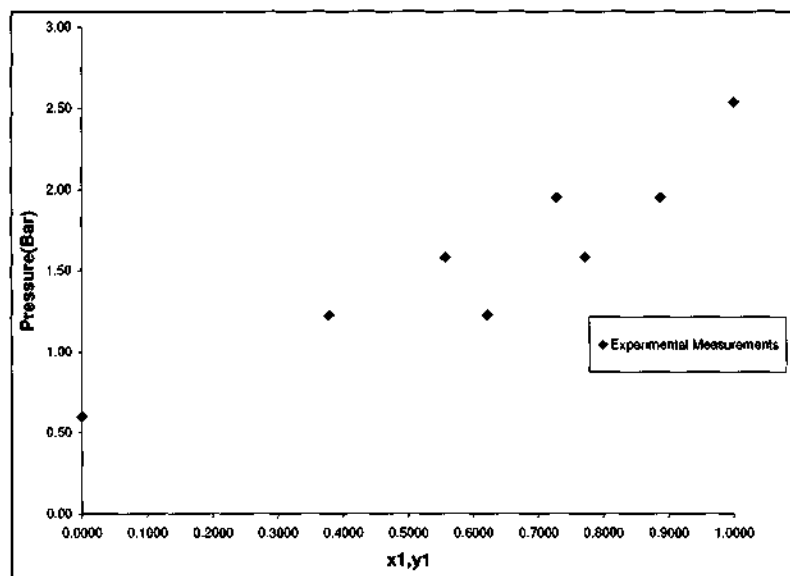


Figure 7.6: The 2-methyl-2-butene(1) + TAME(2) vlc isotherm at 70°C

Table 7.6: Experimental Measurements Of 2-methyl-2-butene(1) + TAME(2) At 70.0°C

Pressure bar	x_1	y_1
0.60	0	0
1.22	0.379	0.622
1.58	0.556	0.772
1.95	0.728	0.888
2.54	1	1

2-Methyl-2-Butene(1) + TAME(2) system at 94.6°C

The 94.6°C isotherm experimental data points are plotted and tabulated in figure 7.7 and table 7.7 respectively.

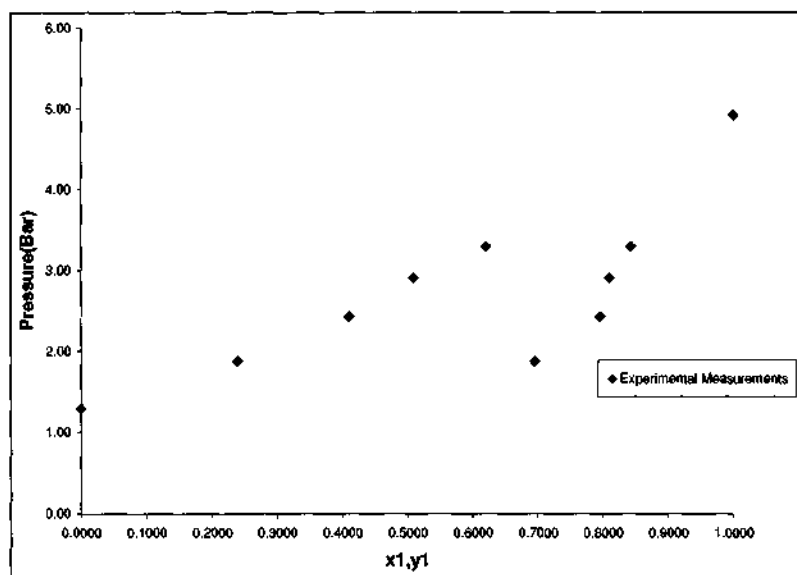


Figure 7.7: The 2-methyl-2-butene(1) + TAME(2) vLE isotherm at 94.6°C

Table 7.7: Experimental Measurements Of 2-methyl-2-butene(1) + TAME(2) At 94.6°C

Pressure bar	x_1	y_1
1.29	0	0
1.88	0.2391	0.6958
2.43	0.4099	0.7954
2.90	0.5093	0.8106
3.29	0.6207	0.8434
4.92	1	1

2-Methyl-2-Butene(1) + TAME(2) system at 105.4°C

The 105.4°C isothermal experimental data is plotted and tabulated in figure 7.8 and table 7.8 respectively.

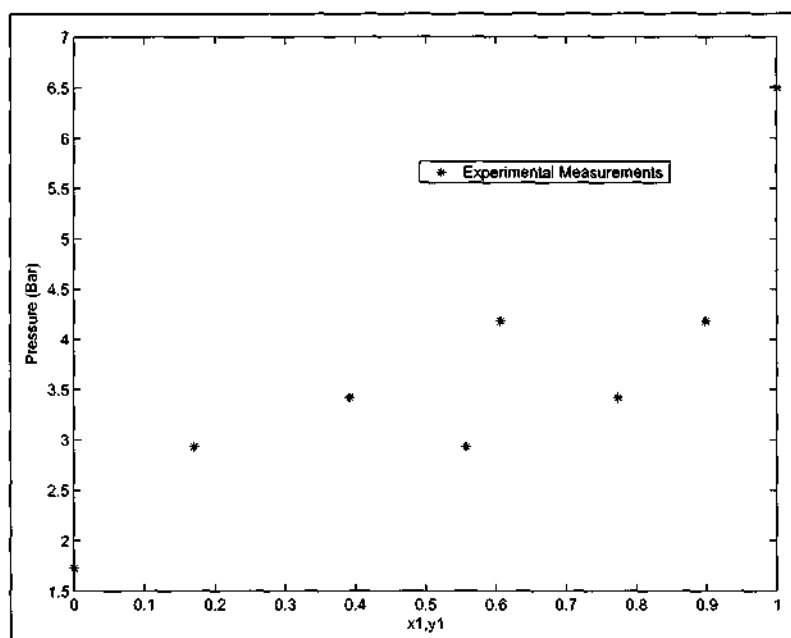


Figure 7.8: The 2-methyl-2-butene(1) + TAME(2) vLE Isotherm At 105.4°C

Table 7.8: Experimental Measurements Of 2-methyl-2-butene(1) + TAME(2) At 105.4°C

Pressure [bar]	x_1	y_1
1.73	0	0
2.93	0.1708	0.5580
3.42	0.3918	0.7740
4.18	0.6065	0.8986
6.50	1	1

Chapter 8

DISCUSSION ON THE DATA CORRELATION

The experimental measurements given in chapter 6 were used in the computational regression with thermodynamic models described in chapter 3. The experimental data were regressed to determine the binary interaction parameters of the respective thermodynamic models considered in this project.

The accuracy of the parameters obtained from regression depends strongly on the precision of the experimental measurements.

8.1 Theoretical Treatment of the Data

8.1.1 Direct-Method

The flexibility with regard to *Cubic Equations Of State* (CEOS) and liquid phase models in the direct-method or approach is outlined in section 3.2. The direct-method was selected for the regression of the VLE data in this study since the approach is practical for isothermal data (Raal and Mühlbauer, 1998).

The *PRSV-EOS* and *SRK-EOS* were used together with the *van der Waals one-fluid* mixing rules and the *Wong-Sandler* mixing rules. The description of the liquid phase was performed with the *NRTL* and *WILSON* equations. *MATLAB* (version 7.0.1) was used to regress the experimental measurements. The input parameters for the regression are outlined below:

Table 8.1: The Direct-Method input parameters

COMPONENT	METHOD	REFERENCE
$\alpha(T_r, \omega)$	-	(Twu et al., 1991)
Liquid molar volume	Modified Rackett	(Reid et al., 1987)
Critical constants	-	(Reid et al., 1987)

8.2 Regression Analysis

8.2.1 Experimental Vapour Pressure Regression

The attractive term in cubic equations of state contains an $\alpha(T)$ function that describes temperature dependence. The $\alpha(T)$ function is component specific. For the *Peng-Robinson-Stryjek-Vera* (PRSV) equation of state, the $\alpha(T)$ function has a pure component interaction parameter (κ_1).

$$\alpha = \left[1 + \kappa \left(1 - \sqrt{\frac{T}{T_c}} \right) \right]^2$$

where,

$$\kappa = \kappa_0 + \kappa_1 (1 + T_R^{0.5})(0.7 - T_R)$$

$$\kappa_0 = 0.378893 + 1.4897153\omega - 0.1713184\omega^2 + 0.0196554\omega^3$$

The κ_1 of the *PRSV* equation of state was calculated for each pure component by regression of the measured pure component vapour pressures. The ω values for the pure components were obtained from Reid et al. (1987). Table 8.2 lists the κ_1 values of the respective components and the average absolute percentage error relative to the measured vapour pressures.

Table 8.2: The pure component κ_1 values for the *PRSV* equation of state

COMPONENT	κ_1	Absolute Pressure Error, %
n-Pentane	-0.1558	0.644
Ethanol	-0.1878	0.802
2-Methyl-2-Butene	-0.2234	2.531
TAME	-0.4636	3.997

Table 8.2 shows that the κ function of the *PRSV-CEOS* was not satisfactory in the vapour pressure regression of 2-methyl-2-butene and TAME. Consequently, a modified $\alpha(T)$ function with stronger temperature dependence was desired. Table 8.3 tabulates the improved vapour pressure regression of 2-methyl-2-butene and TAME respectively. The $\alpha(T)$ function proposed by

Twu et al. (1991) was used in the pure component experimental vapour pressure regressions. This $\alpha(T)$ function of Twu et al. (1991) has the following form:

$$\alpha = T_r^{N(M-1)} \exp \left[L(1 - T_r^{NM}) \right]$$

Where, L , M and N are adjustable parameters. The L , M and N parameters were calculated for each component and are tabulated in table 8.3.

Table 8.3: The pure component L , M and N values for the Twu et al. (1991), $\alpha(T)$ function

COMPONENT	L	M	N	Absolute Pressure Error, %
n-Petane	0.3327	0.3327	1.9891	0.562
Ethanol	0.9272	0.9371	1.4008	0.652
2-Methyl-2-Butene	0.0564	0.8506	0.6742	1.832
TAME	0.1616	0.8506	2.8720	0.525

8.2.2 Regression Analysis Of The Binary Systems Measured

The 1-fluid parameter van der Waals mixing model was used as the base case mixing rule for comparison. A second mixing rule (Wong and Sandler, 1992b) was used in the regression of the binary mixtures and compared with the 1-fluid van der Waals mixing rule performance.

The $G^E(T, P, x_i)$ models that are coupled with the Wong and Sandler mixing rules were the *NRTL* and *Wilson* models. The modified $\alpha(T)$ function of Twu et al. (1991) was substituted into the cubic equations of state used in this study. The $\alpha(T)$ of Twu et al. (1991) was used because the pure component vapour pressure predictions with this $\alpha(T)$ function were accurate to ± 0.896 kPa.

n-Pentane(1) + Ethanol(2) system

Figures 8.1 and 8.2 indicate graphically the extent of deviation between the experimental data and *PRSV-EOS-1fluid van der Waals* bubble-point calculations (regression). The results with the *PRSV-EOS* were not significantly different from the calculation with the *SRK*. This was not expected as the original *Peng-Robinson-EOS* was an improvement of the *SRK*-with respect to vapour pressure prediction. The absolute relative errors in the calculated system pressure and calculated vapour phase composition (with respect to n-pentane) are tabulated in Table 8.4. The vapour phase compositions and system pressures determined with the *PRSV* and *SRK* are given on page 81 together with the calculated *1-fluid van der Waals* mixing rule interaction parameter.

Table 8.4: The percentage relative error in bubble pressure and n-pentane vapour composition with *PRSV* and *SRK*

<i>EOS</i>	%Error y_1	%Error P
<i>PRSV</i>	7.4760	8.3018
<i>SRK</i>	3.5946	8.6245

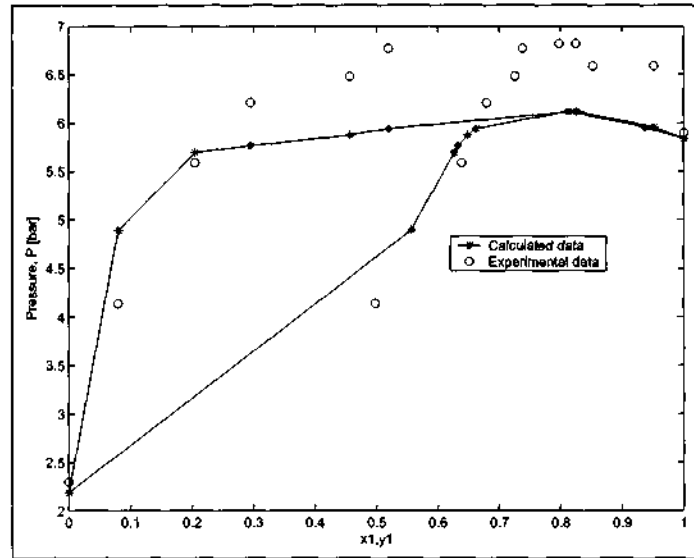


Figure 8.1: The n-pentane(1) + ethanol(2) isothermal regression at 100.41°C with the *PRSV-EOS* and the van der Waals 1-fluid mixing rule.

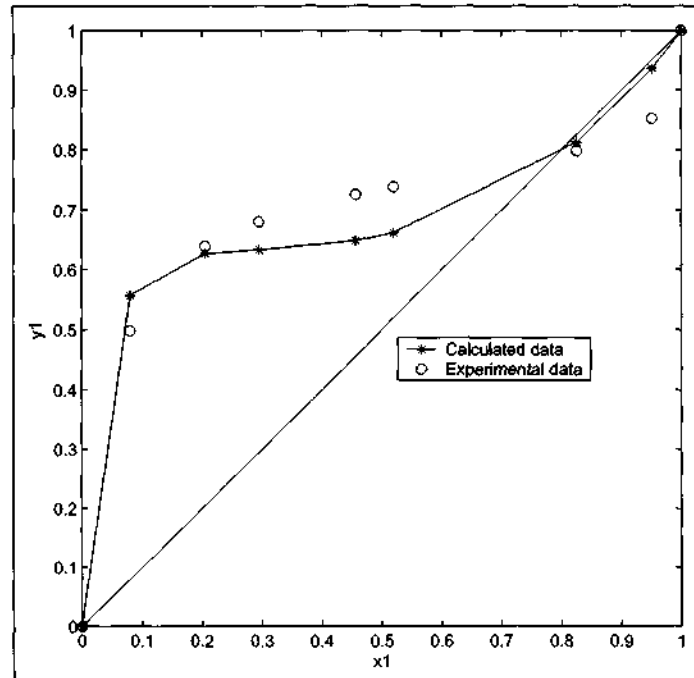


Figure 8.2: The n-pentane(1) + ethanol(2) $x_i y_i$ diagram at 100.41°C against *PRSV-CEOS* with the 1-fluid van der Waals mixing rule prediction

Table 8.5: The pentane(1) + ethanol(2) experimental data at 100.14°C compared to the *PRSV-EOS-1fluid van der Waals* regression, where x^* , P^* , and y^* are measured.

x_1^*	y_1^*	$P(\text{bar})^*$	y_1^{cal}	$P(\text{bar})^{\text{cal}}$
0	0	2.26	0	2.19
0.0802	0.4983	4.14	0.5409	4.71
0.2049	0.6390	5.59	0.6187	5.53
0.2953	0.6800	6.21	0.6292	5.64
0.4564	0.7258	6.48	0.6496	5.79
0.5199	0.7386	6.77	0.6641	5.86
0.8253	0.7983	6.82	0.8174	6.07
0.9516	0.8526	6.52	0.9392	5.94
1	1	5.89	1	5.84

Table 8.6: The pentane(1) + ethanol(2) experimental data at 100.14°C compared to the *SRK-EOS-1fluid van der Waals* regression, where x^* , P^* , and y^* are measured.

x_1^*	y_1^*	$P(\text{bar})^*$	y_1^{cal}	$P(\text{bar})^{\text{cal}}$
0	0	2.26	0	2.73
0.0802	0.4983	4.14	0.4902	5.28
0.2049	0.6390	5.59	0.5798	6.23
0.2953	0.6800	6.21	0.5967	6.40
0.4564	0.7258	6.48	0.6262	6.61
0.5199	0.7386	6.77	0.6439	6.70
0.8253	0.7983	6.82	0.8104	6.88
0.9516	0.8526	6.52	0.9373	6.69
1	1	5.89	1	6.56

Table 8.7: The *1-fluid van Der Waals* mixing rule interaction parameter for pentane(1) + ethanol(2) at 100.14°C computed with *PRSV-EOS* and *SRK-EOS*

parameter	<i>PRSV-EOS</i>	<i>SRK-EOS</i>
k_{12}	0.1008	0.0998

The regression results with the *PRSV-WSMR(NRTL)* and the *SRK-WSMR(WILSON)* models are given in tables (8.8)-(8.10). The graphical representation of the bubble-point calculations with the two models are given on pages (84) and (85) respectively. The calculation results with the *SRK-EOS-WSMR(NRTL)* were not tabulated as these did not differ significantly from those obtained with the *PRSV-EOS-WSMR(NRTL)*. This can be attributed to the fact that both *EOS* used the $\alpha(T)$ of Twu et al. (1991) i.e. with the same improved temperature dependency. In general it would be expected that *SRK* would predict the vapour pressures less accurately than the *PRSV*. The *SRK* is adequate but not sufficiently accurate for the vapour pressure prediction of small to medium size hydrocarbons above their normal boiling points.

The bubble point calculation with the *WSMR* was expected to yield a significant improvement over the *1-fluid van der Waals* mixing rule. However Table 8.8 indicates that the relative error in calculated vapour phase composition and calculated pressure is still significantly large with the *WSMR* i.e. not a significant improvement over the results with the *1-fluid van Der Waals* mixing rule. This would suggest an inconsistency with the vapour phase compositions in the regression with the mixing rules. The best-fit for the n-pentane + ethanol data was achieved with the *SRK-EOS-WSMR(WILSON)* model-see Figure 8.5 and Table 8.8. Although the relative error in bubble pressure was lower with the *SRK-EOS-WSMR(WILSON)*, the pure component vapour pressures were over predicted.

Table 8.8: **The percentage relative error in bubble pressure and n-pentane vapour composition for the *WSMR* regression**

<i>MODEL</i>	%Error y_1	%Error P
<i>PRSV-WSMR-NRTL</i>	5.8987	7.0407
<i>SRK-WSMR-WILSON</i>	5.6158	4.0872

Table 8.9: **The *PRSV-WSMR-NRTL* interaction parameters calculated for pentane(1) + ethanol(2) at 100.14°C**

parameter	Value
k_{12}	0.669
τ_{12}	3.75
τ_{21}	3
α	0.115

Table 8.10: The *SRK-WSMR-WILSON* interaction parameters calculated for pentane(1) + ethanol(2) at 100.14°C

parameter	Value
k_{12}	0.58
τ_{12}	1.25
τ_{21}	1.33

Table 8.11: The pentane(1) + ethanol(2) experimental data at 100.14°C compared with the *PRSV-EOS-WSMR(NRTL)* regression, where x^* , P^* , and y^* are measured.

x_1^*	y_1^*	$P(\text{bar})^*$	y_1^{cal}	$P(\text{bar})^{\text{cal}}$
0	0	2.26	0	2.73
0.0802	0.4983	4.14	0.2289	3.31
0.2049	0.6390	5.59	0.4357	4.02
0.2953	0.6800	6.21	0.5328	4.44
0.4564	0.7258	6.48	0.6583	5.04
0.5199	0.7386	6.77	0.6995	5.25
0.8253	0.7983	6.82	0.8854	6.11
0.9516	0.8526	6.52	0.9671	6.44
1	1	5.89	1	6.56

Table 8.12: The pentane(1) + ethanol(2) experimental data at 100.14°C compared with the *SRK-EOS-WSMR(WILSON)* regression, where x^* , P^* , and y^* are measured.

x_1^*	y_1^*	$P(\text{bar})^*$	y_1^{cal}	$P(\text{bar})^{\text{cal}}$
0	0	2.26	0	2.73
0.0802	0.4983	4.14	0.385	4.18
0.2049	0.6390	5.59	0.58757	5.62
0.2953	0.6800	6.21	0.6413	6.12
0.4564	0.7258	6.48	0.6768	6.43
0.5199	0.7386	6.77	0.6864	6.83
0.8253	0.7983	6.82	0.8234	6.70
0.9516	0.8526	6.52	0.9449	6.62
1	1	5.89	1	6.56

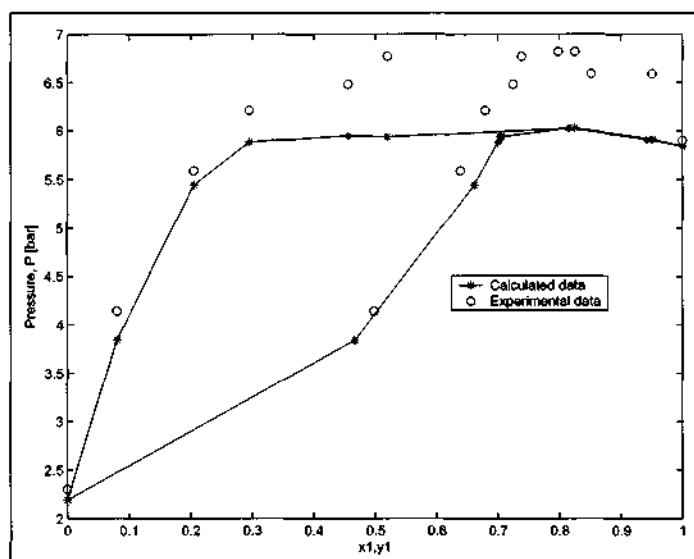


Figure 8.3: The n-pentane(1) + ethanol(2) isothermal P-x-y regression at 100.41°C with the *PRSV-EOS* and *WSMR-NRTL* mixing rules

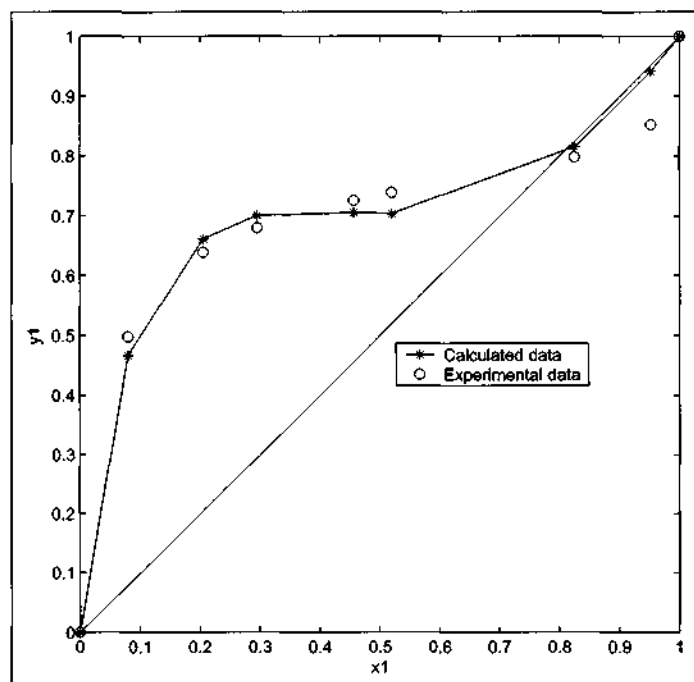


Figure 8.4: The n-pentane(1) + ethanol(2) $x_i - y_i$ diagram at 100.41°C with *PRSV-EOS* and *WSMR-NRTL* mixing rules

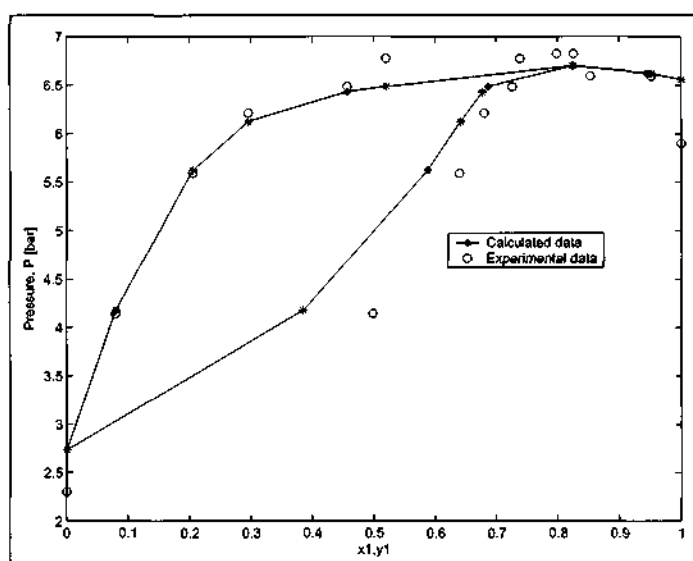


Figure 8.5: The n-pentane(1) + ethanol(2) isothermal P-x-y regression at 100.41°C with the *SRK-EOS* and *WSMR-WILSON* mixing rules

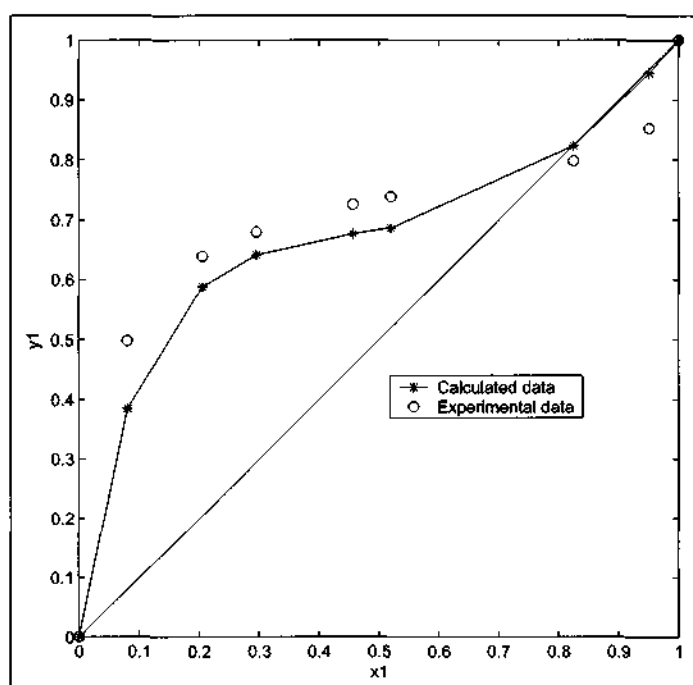


Figure 8.6: The n-pentane(1) + ethanol(2) $x_i - y_i$ diagram at 100.41°C with *SRK-EOS* and *WSMR-WILSON* mixing rules

2-Methyl-2-Butene(1) + TAME(2) system

The regression of the isothermal data for the 2-methyl-2-butene(1) + TAME(2) system was poor in general similar to the test system. An improvement in

the results with the *WSMR* was neither achieved. Errors in the vapour phase composition and bubble pressure were as large as 35% and 60% respectively. Tables (8.13)-(8.15) tabulate the calculated 2-methyl-2-butene vapour compositions and bubble pressures against the experimentally measured values for each isotherm. The P-x-y and x-y diagrams for the respective *PRSV-EOS-1 fluid van Der Waals mixing rule* isotherms are given on pages: (87), (88) and (90).

Table 8.13: The 2-methyl-2-butene(1) + TAME(2) experimental measurements at 70°C against the calculated values with *PRSV-1 fluid van der Waals mixing rule*, where x^* , P^* , and y^* are measured.

x_1^*	y_1^*	$P(\text{bar})^*$	y_1^{cal}	$P(\text{bar})^{\text{cal}}$
0	0	0.6	0	1.22
0.379	0.622	1.22	0.609	2.22
0.556	0.772	1.58	0.7241	2.49
0.728	0.888	1.95	0.8285	2.72
1	1	2.54	1	3.05

Table 8.14: The 2-methyl-2-butene(1) + TAME(2) experimental measurements at 94.6°C against the calculated values with *PRSV-1 fluid van der Waals mixing rule*, where x^* , P^* , and y^* are measured.

x_1^*	y_1^*	$P(\text{bar})^*$	y_1^{cal}	$P(\text{bar})^{\text{cal}}$
0	0	1.29	0	2.58
0.2391	0.6958	1.88	0.4451	3.81
0.4099	0.7954	2.43	0.5917	4.34
0.5093	0.8106	2.90	0.6638	4.60
0.6207	0.8434	3.29	0.7402	4.87
1	1	4.92	1	5.67

Table 8.15: The 2-methyl-2-butene(1) + TAME(2) experimental measurements at 104.5°C against the calculated values with *PRSV-1 fluid van der Waals mixing rule*, where x^* , P^* , and y^* are measured.

x_1^*	y_1^*	$P(\text{bar})^*$	y_1^{cal}	$P(\text{bar})^{\text{cal}}$
0	0	1.73	0	3.47
0.1708	0.5580	2.93	0.3474	4.62
0.3918	0.7740	3.42	0.5624	5.53
0.6065	0.8986	4.18	0.7200	6.21
1	1	6.50	1	7.22

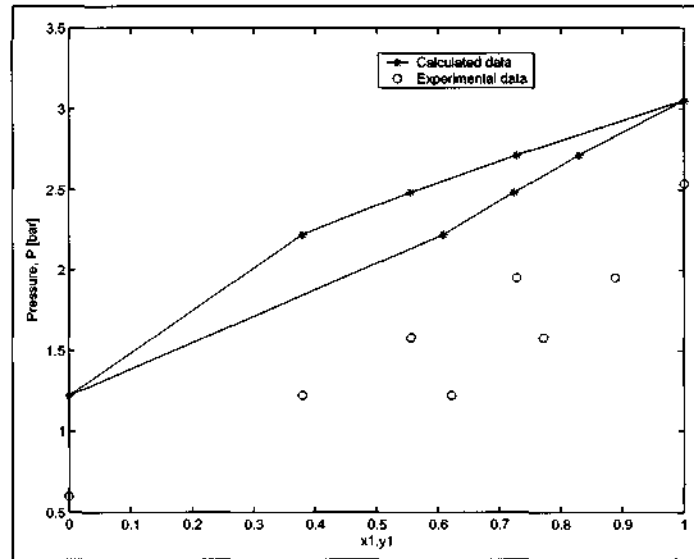


Figure 8.7: The 2-methyl-2-butene(1) + TAME(2) isothermal P-x-y regression at 70°C with the *PRSV-EOS-1fluid van Der Waals mixing rules*

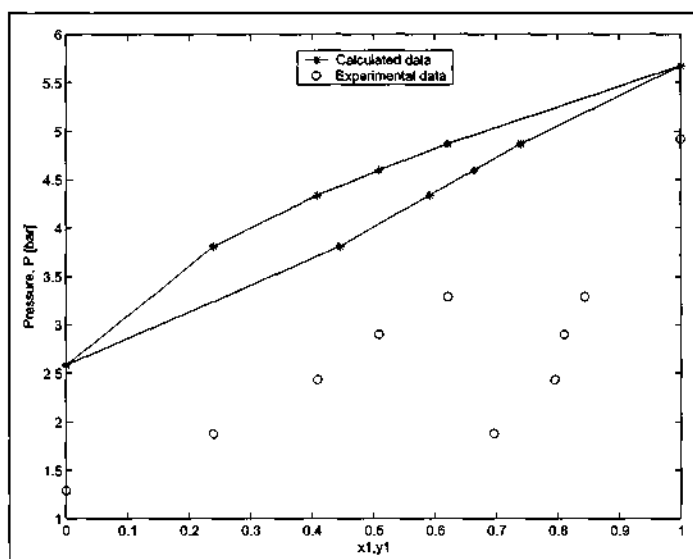


Figure 8.8: The 2-methyl-2-butene(1) + TAME(2) isothermal P-x-y regression at 94.6°C with the *PRSV-EOS-1fluid van Der Waals mixing rules*

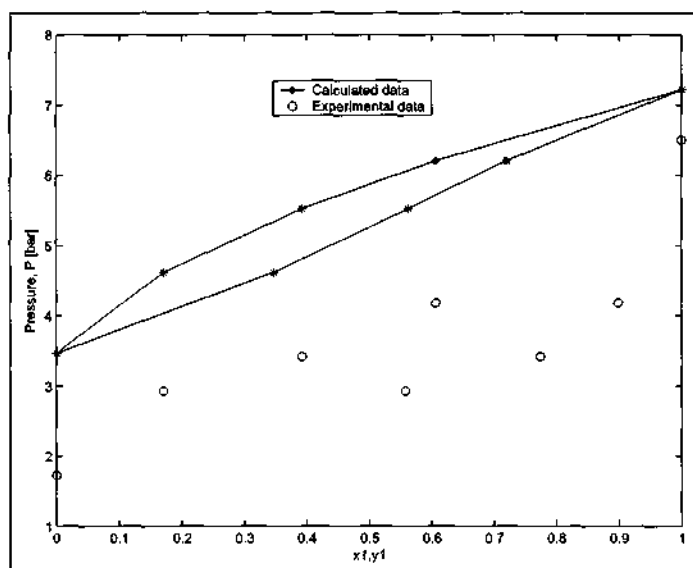


Figure 8.9: The 2-methyl-2-butene(1) + TAME(2) isothermal P-x-y regression at 105.4°C with the *PRSV-EOS-1fluid van Der Waals mixing rules*

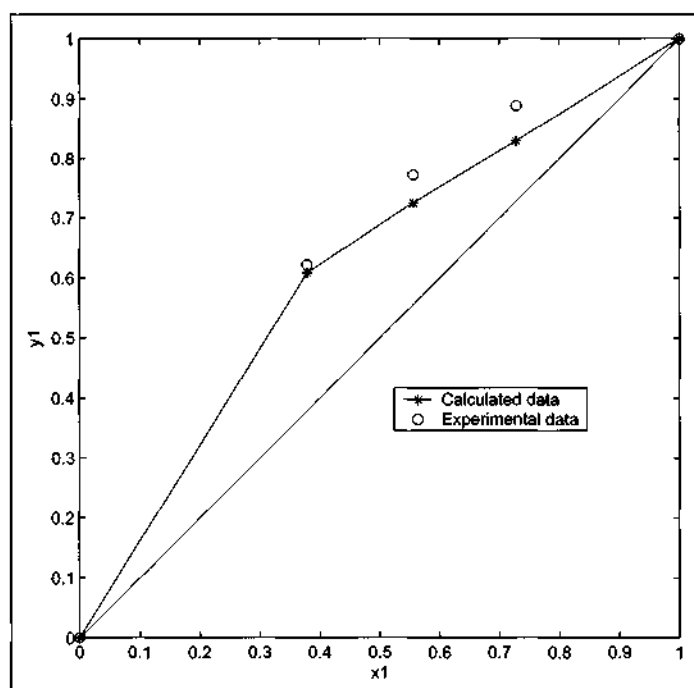


Figure 8.10: The 2-methyl-2-butene(1) + TAME(2) isothermal x-y diagram at 70°C with the *PRSV-EOS-1fluid van Der Waals mixing rules* regression

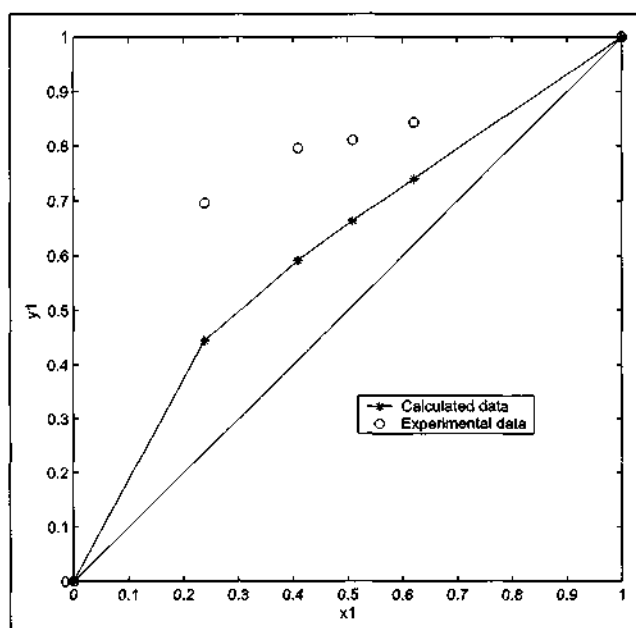


Figure 8.11: The 2-methyl-2-butene(1) + TAME(2) isothermal x-y diagram at 94.6°C with the *PRSV-EOS-1fluid van Der Waals mixing rules* regression

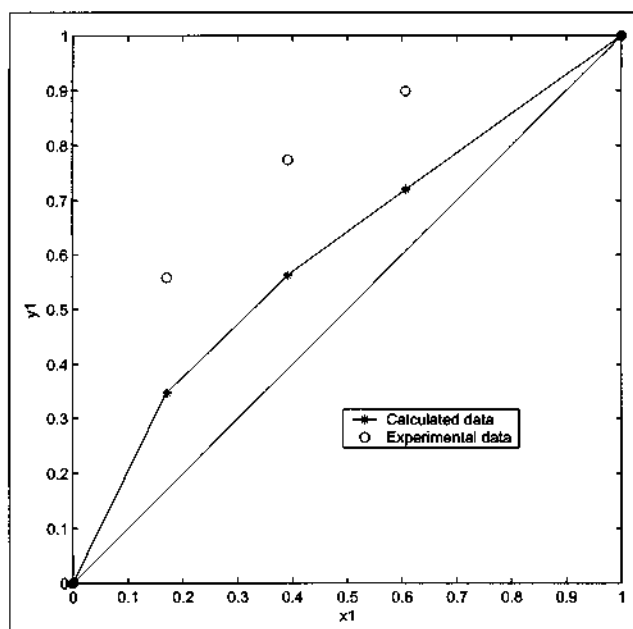


Figure 8.12: The 2-methyl-2-butene(1) + TAME(2) isothermal x-y diagram at 105.4°C with the *PRSV-EOS-1 fluid van Der Waals mixing rules* regression

The regressed parameters for the *PRSV-EOS-1 fluid van Der Waals mixing rule* and *SRK-EOS-1 fluid van Der Waals mixing rule* are tabulated in table 8.16 below. The calculated 2-methyl-2-butene vapour composition and the calculated binary system bubble pressures determined with the *SRK-EOS-1 fluid van Der Waals mixing rule* model did not differ from that determined with the *PRSV-EOS* substituted. The relative error in the 2-methyl-2-butene vapour composition and calculated bubble pressure for the respective isotherms is given in table 8.17.

Table 8.16: The 2-methyl-2-butene(1) + TAME(2) k_{12} parameter for *PRSV-EOS-1 fluid van Der Waals mixing rule* and *SRK-EOS-1 fluid van Der Waals mixing rule*

MODEL	70°C	94.6°C	104.4°C
<i>PRSV-1 fluid vdW</i>	1.21E ⁻⁰⁴	1.10E ⁻⁰⁴	8.90E ⁻⁰⁵
<i>SRK-1 fluid vdW</i>	1.11E ⁻⁰⁴	1.00E ⁻⁰⁴	9.25E ⁻⁰⁵

The regression with the *WSMR* did not yield a significant improvement in the results compared to the *1-fluid van Der Waals mixing rule* results. The error in vapour composition and bubble pressures calculated were slightly lower i.e. 10% in the vapour and 12% in the pressure. Fur-

Table 8.17: The relative errors in 2-methyl-2-butene(1) vapour composition and in the calculated bubble pressures for the respective isotherms

TEMPERATURE (°C)	% Error y_1	% Error P
70	3.75	60.47
94.6	18.39	67.17
104.5	21.24	56.00

thermore it was noticed that the choice of equation of state or G^E model did not produce any significant change in the results either, $\pm 1\%$ in the vapour compositions and $\pm 1.2\%$ in the bubble pressure. The model that yielded the lowest relative error with regard to vapour composition and bubble pressure was the *PRSV-WSMR-NRTL*. Tables (8.18)-(8.20), tabulate the calculated 2-methyl-2-butene vapour compositions and calculated bubble pressures against the experimental measurements. Table 8.21 tabulates the relative errors for the *PRSV-WSMR-NRTL* model of the respective isotherms. The P-x-y and x-y diagrams were not attached as these did not differ from visual inspection to those obtained with the *1-fluid van Der Waals mixing rule*. The regressed parameters for the *PRSV-WSMR-NRTL* model are given in table 8.22.

Table 8.18: The 2-methyl-2-butene(1) + TAME(2) experimental measurements at 70°C against the calculated values with *PRSV-WSMR-NRTL*, where x^* , P^* , and y^* are measured.

x_1^*	y_1^*	$P(\text{bar})^*$	y_1^{cal}	$P(\text{bar})^{\text{cal}}$
0	0	0.6	0	1.22
0.379	0.622	1.22	0.595	1.92
0.556	0.772	1.58	0.7474	2.24
0.728	0.888	1.95	0.8609	2.255
1	1	2.54	1	3.05

Table 8.19: The 2-methyl-2-butene(1) + TAME(2) experimental measurements at 94.6°C against the calculated values with *PRSV-WSMR-NRTL*, where x^* , P^* , and y^* are measured.

x_1^*	y_1^*	$P(\text{bar})^*$	y_1^{cal}	$P(\text{bar})^{\text{cal}}$
0	0	1.29	0	2.58
0.2391	0.6958	1.88	0.3968	3.32
0.4099	0.7954	2.43	0.5876	3.85
0.5093	0.8106	2.90	0.6785	4.15
0.6207	0.8434	3.29	0.7668	4.49
1	1	4.92	1	5.67

Table 8.20: The 2-methyl-2-butene(1) + TAME(2) experimental measurements at 104.5°C against the calculated values with *PRSV-WSMR-NRTL*, where x^* , P^* , and y^* are measured.

x_1^*	y_1^*	$P(\text{bar})^*$	y_1^{cal}	$P(\text{bar})^{\text{cal}}$
0	0	1.73	0	3.47
0.1708	0.5580	2.93	0.2898	4.11
0.3918	0.7740	3.42	0.5553	4.93
0.6065	0.8986	4.18	0.7445	5.73
1	1	6.50	1	7.22

Table 8.21: The relative errors in 2-methyl-2-butene(1) vapour composition and in the calculated bubble pressures with the *PRSV-WSMR-NRTL* model

TEMPERATURE (°C)	% Error y_1	% Error P
70	2.64	50.73
94.6	18.89	55.05
104.5	23.27	46.71

Table 8.22: The *PRSV-WSMR-NRTL* interaction parameters determined for 2-methyl-2-butene(1) + ethanol(2) for the respective isotherms

parameter	70°C	94.6°C	104.4°C
k_{12}	1E^{-04}	1.1E^{-05}	1.2E^{-05}
τ_{12}	2.3	4.3	2
τ_{21}	0.98	1.5	1.89
α	0.23	0.23	0.23

In summary, the poor *VLE* thermodynamic computation results may be attributed to the experimental equipment design and the experimental methods. Specifically the design of the isothermal bath, the sampling method and the few data points obtained for regression analysis (2-methyl-2-butene + TAME system).

It was found that during experimentation the equilibrium cell was in fact not isothermal. Temperature gradients across the cell would cause the liquid and vapour phases to be at different temperatures. Baffles were placed into the air-bath to distribute air flow. This improved the isothermal environment and reduced the temperature gradient across the equilibrium cell to 1.5 – 2.35°C. Ramjugernath (2000) states that a maximum temperature difference across the cell of 0.2°C is acceptable. Therefore the vapour phase and liquid phase compositions in this study were not in equilibrium.

The concern around the sampling method can be attributed to the length of tubing from the vapour sample point on the cell to the GC and the numerous fittings along the length of tubing (such as valves). Partial condensation of the sample along the line or at the fittings was the major concern. If condensation of the sample did occur, the measured composition (liquid phase) would be incorrect. Recall that the respective sample is vapourised at the jet-mixers.

As a general rule of thumb, a minimum of five data points should be measured (excluding the pure component vapour pressures). The number of

data points obtained for the 2-methyl-2 butene + TAME system were less than five for the respective isotherms. A number of points were excluded due to inaccuracy with the composition measurement. These points were not repeated because of time constraints. The low number of data points therefore also contributed to the poor regression.

Chapter 9

CONCLUSION

A high pressure vapour liquid equilibrium (HPVLE) study was undertaken on a static apparatus. The apparatus was designed by Professor J. D. Raal and has a history of HPVLE studies-(Mühlbauer, 1990); (Ramjugernath, 2000); (Kissun, 2001) and (Naidoo, 2004). The study entailed isothermal measurements on sub-critical binary systems and subsequently regression analysis of the data with thermodynamic models. The systems investigated were n-Pentane + ethanol and 2-methyl-2-butene + TAME or tert-amyl-methyl ether. The operating conditions of the study were $50^{\circ}\text{C} - 106^{\circ}\text{C}$ and pressures were measured up to 7 bar.

The experimental procedure used in this VLE study was similar to the methods of Naidoo (2004). The main difference in the procedure was the use of the degassing apparatus and injection of the second component into the equilibrium cell since the respective components were subcritical. The injection apparatus was fabricated from stainless steel in the laboratory workshop. Problems with the syringe sealing ("O"-ring) were encountered during numerous runs. This is attributed to air being introduced into the equilibrium cell-consequently affecting the system vapour pressure. The equilibrium cell was housed within an insulated air-bath. It was found that the air-bath was not isothermal, heat gradients existed within the bath and therefore caused temperature gradients on the equilibrium cell. Baffles were inserted into the bath to minimize these gradients, however the temperature probes on the equilibrium cell differed by more than 1°C (across the equilibrium cell).

n-Pentane + Ethanol

This system was used as the test system of the study i.e. as a first experimental run to determine the equipment integrity. The respective pure component vapour pressure measurements were accurate to 1.38% and 1.64%

for n-pentane and ethanol respectively. The binary system was measured at a single isotherm and the results compared with reference data from the literature survey, (Campbell et al., 1987). The $P - x - y$ data of the test system was measured at 99.55°C and did not yield significant deviation from literature with respect to pressure. It is well known that in general static cells provide vapour mole fractions that are difficult to measure and therefore less reliable.

2-Methyl-2-butene + TAME

This system was measured at three isotherms not previously measured, 70°C , 94.6°C and 105.6°C respectively. The pure component vapour pressure measurements at these temperatures did not yield significant deviation compared with the Antoine vapour pressure correlation. Due to the high volatility of the olefin 2-methyl-2-butene, considerable problems were encountered with the binary system VLE measurements.

As a general rule of thumb, a minimum of five data points should be measured (excluding the pure component vapour pressures). Due to the significant inaccuracy with a large number of the data points measured, where the inaccurate points were determined by being inconsistent with the general $P - x - y$ trend. A maximum of four data points was obtained for this system (the 94.5°C isotherm).

Data Regression

The binary HPVLE data measured were modeled using the direct method. The combination of the thermodynamic models used were: *PRSV-EOS-1fluid van der Waals*; *SRK-EOS-1fluid van der Waals*; *PRSV-WSMR(NRTL)*; *SRK-WSMR(NRTL)*; *PRSV-WSMR(WILSON)* and *SRK-WSMR(WILSON)*.

There was no significant difference in the correlation results employing either of the two cubic equations of state, PRSV and SRK. This finding was not expected since the PRSV was designed to improve the accuracy of the liquid volumes and vapour pressures over that obtained with the SRK. The modified $\alpha(T)$ function of Twu et al. (1991) was substituted into both EOS and yield an improvement in the pure component vapour pressure predictions using the respective EOS. The WILSON model was expected to be sufficient since neither binary system resulted in two liquid phases. The NRTL model is in general sufficient for most polar systems as well as partially miscible systems. The regression analysis in general yielded poor results with the model combinations mentioned above i.e. absolute relative errors in the pressure and vapour compositions were as much as 60% and 23% respectively.

Bibliography

- Abbott, M. M. (1979), 'Cubic equations of state An interpretative review', *Adv. Chem. Ser.* **182**(47-70).
- Abrams, D. S. and Prausnitz, J. M. (Jan 1975), 'Statistical thermodynamics of liquid mixtures: a new expression for the excess gibbs energy of partly or completely miscible systems', *AICHE* **21**(1), 116-128.
- Anderson, T. F. and Prausnitz, J. M. (1980), 'Computational methods for high-pressure phase equilibria and other fluid-phase properties using a partition function. 1. pure fluids', *Ind. Eng. Chem. Process Des. Dev.* **19**, 1-8.
- Ashcroft, S. J., Shearn, R. B. and Williams, G. J. J. (1983), 'A visual equilibrium cell for multiphase systems at pressures up to 690 bar', *Chem Eng Res Des* **61**, 51-55.
- Baba-Ahmed, A., Guilbot, P. and Richon, D. (1999), 'New equipment using a static analytic method for the study of vapour-liquid equilibria at temperatures down to 77 k', *Fluid Phase Equilib.* **166**, 225-236.
- Besserer, G. J. and Robinson, D. B. (1971), 'A high pressure autocollimating refractometer for determining coexisting liquid and vapor phase densities', *The Canadian Journal of Chemical Engineering* **49**, 651-656.
- Boublik, T. (1981), 'Statistical thermodynamics of nonspherical molecule fluids', *Ber. Bunsenges. Phys. Chem* **70**(11), 2233-2257.
- Campbell, S. W., Wilsak, R. A. and Thodos, G. (1987), '(vapor + liquid) equilibrium behavior of (n-pentane + ethanol) at 372.7, 379.7 and 422.6 k.', *J. Chem. Thermodyn.* **19**, 449.
- Carnahan, N. F. and Starling, K. E. (1969), 'Equation of state for nonattracting rigid spheres', *J. Chem. Phys.* **51**, 635-636.
- Castier, M. and Sandler, S. I. (1997), 'Critical points with Wong-Sandler mixing rule II. calculations with a modified peng-robinson equation of state', *Chem. Eng. Sci.* **52**(20), 3579-3588.

- Chao, K. C. and Seader, J. D. (1961), 'A general correlation of vapor-liquid equilibria in hydrocarbon mixtures', *AIChE J.* **7**, 598-605.
- Chueh, P. L., Muirbrook, N. K. and Prausnitz, J. M. (1965), 'Part 2. thermodynamic analysis', *AIChE J.* **11**(6), 1097-1102.
- Coutsikos, P., Kalospiros, N. S. and Tassios, D. P. (1995), 'Capabilities and limitations of the Wong-Sandler mixing rules', *Fluid Phase Equilib.* **108**, 59-78.
- Deiters, U. K. and Schneider, G. M. (1986), 'High pressure phase equilibria: Experimental methods', *Fluid Phase Equilib* **29**(1), 145-160.
- Figuiere, P., Hom, J. F., Laugier, S., Renon, H., Richon, D. and Szwarc, H. (1980), 'Vapour-liquid equilibria up to 40 000 kPa and 400 °C: A new static method', *AIChE* **26**(5), 872-875.
- Fontalba, F., Richon, D. and Renon, H. (June 1984), 'Simultaneous determination of vapor-liquid equilibria and saturated densities up to 45 MPa and 433 K', *Rev. Sci. Instrum.* **55**(6), 944-951.
- Fuller, G. G. (1976), 'A modified Redlich-Kwong-Soave equation of state capable of representing the liquid phase', *Ind. Eng. Chem. Fund.* **15**, 254-257.
- Galicia-Luma, L. A. and Ortega-Rodriguez, A. (2000), 'New apparatus for the fast determination of high-pressure vapor-liquid equilibria of mixtures and of accurate critical pressures', *J. Chem. Eng. Data* **2000** **45**, 265-271.
- Gasem, K. A. M., Gao, W., Pan, Z. and Robinson, R. L. (2001), 'A modified temperature dependence for the Peng-Robinson equation of state', *Fluid Phase Equilib.* **181**, 113-125.
- Gmehling, J. (1995), 'From UNIFAC to modified UNIFAC to PSRK with the help of DDB', *Fluid Phase Equilib.* **107**(1995)1-29 **107**, 1-29.
- Guggenheim, E. A. (1965), 'Variations on van der Waals Equation of State for high densities', *Mol. Phys.* **9**, 199.
- Harmens, A. and Knapp, H. (1980), 'Three-parameter cubic equation of state for normal substances', *Ind. Eng. Chem. Fund.* **19**, 291-294.
- Hayden, G. J. and O'Connell, J. P. (1975), 'A generalized method for predicting second virial coefficients', *Ind. Eng. Chem., Process Des. Dev.* **14**(3), 209-216.
- Heidemann, R. A. (1983), 'Computation of high pressure phase equilibria', *Fluid Phase Equilib* **14**, 55-78.

- Huang, H. and Sandler, S. I. (1993), 'Prediction of vapor-liquid equilibria at high pressures using activity coefficient parameters obtained from low-pressure data: a comparison of two equations of state mixing rules', *Ind.Eng.Chem.Res.* **32**, 1498–1503.
- Huron, M.-J. and Vidal, J. (1979), 'New mixing rules in simple equations of state for representing vapour-liquid equilibria of strongly non-ideal mixtures', *Fluid Phase Equilibria* **3**, 255–271.
- Inomata, H., Arai, K. and Saito, S. (1986), 'Measurement of vapour-liquid equilibria at elevated temperatures and pressures using a flow type apparatus', *Fluid Phase Equilib* **29**, 225–232.
- Ishii, N. (1935), *J. Soc. Chem. Ind. Jap.* **38**(12), 705–710.
- Japas, M. L. and Frank, E. V. (1985), 'High pressure phase equilibria and PVT- data of the water-nitrogen system 673 K and 250 MPa.', *Ber.Bunsenges.Phys. Chem.* **89**, 793–800.
- Joseph, M. A. (2002), Computer-aided measurement of vapour-liquid equilibria in a dynamic still at sub-atmospheric pressures, Master's thesis, Chemical Engineering.
- Kissun, S. M. (2001), Measurement and thermodynamic interpretation of high-pressure vapour-liquid equilibrium at sub-ambient temperatures, Master's thesis, Chemical Engineering University Of Natal, Durban, South Africa.
- Knudsen, K., Stenby, E. H. and Fredenslund, A. (1993), 'A comprehensive comparison of mixing rules for calculation of phase equilibria in complex systems', *Fluid Phase Equilib.* **82**, 361–368.
- Konrad, R., Swaid, I. and Schneider, G. M. (1983), 'High-pressure phase studies on fluid mixtures of low-volatile organic substances with supercritical carbon dioxide', *Fluid Phase Equilibria* **10**, 307–314.
- Laugier, S. and Richon, D. (1986), 'New apparatus to perform fast determination of mixture vapor-liquid equilibria up to 10 MPa and 423 K', *Rev.Sc.Instrum* **57**(3), 469–472.
- Legret, D., Richon, D. and Renon, H. (March 1981), 'Vapor liquid equilibria up to 100 MPa: A new apparatus', *AICHE* **27**(2), 203–207.
- Maria, A. and Sandler, S. I. (1994), 'Vapor-liquid equilibria of hydrocarbons and tert-amyl methyl ether', *J.Chem.Eng.Data* **39**, 584–587.
- Martin, T. M., Lateef, A. A. and Roberts, C. B. (1999), 'Measurements and modeling of cloud point behavior for polypropylene/n-pentane and

- polypropylene/n-pentane/carbon dioxide mixtures at high pressure', *Fluid Phase Equilib* **154**, 241–259.
- Meskei-Lesavre, M., Richon, D. and Renon, H. (1981), 'New variable volume cell for determining vapor-liquid equilibria and saturated liquid molar volumes by the static method', *Ind. Eng. Chem. Fundam.* **20**, 284–289.
- Mollerup, J. (1980), 'Thermodynamic properties from corresponding states theory', *Fluid Phase Equilib.* (4), 11–34.
- Mollerup, J. (1986), 'A note on the derivation of mixing rules from excess Gibbs energy models', *Fluid Phase Equilib* **25**, 323–327.
- Mollerup, J. M. and Michelsen, M. L. (1992), 'Calculation of thermodynamic equilibrium properties', *Fluid Phase Equilib.* *74(1992)1-15* **74**, 1–15.
- Mühlbauer, A. L. (1990), Measurement and Thermodynamic Interpretation of High pressure Vapour-Liquid Equilibrium Data, PhD thesis, Department Of Chemical Engineering, Durban, University Of Natal.
- Mühlbauer, A. L. and Raal, J. D. (1991), 'Measurement and thermodynamic interpretation of high-pressure vapour-liquid equilibria in the toluene- CO_2 system.', *Fluid Phase Equilib.* **64**, 213–236.
- Mühlbauer, A. L. and Raal, J. D. (1995), 'Computation and thermodynamic interpretation of high-pressure vapour-liquid equilibrium-a review', *The Chemical Engineering Journal* **60**, 1–29.
- Naidoo, P. (2004), High-Pressure Vapour-Liquid Equilibrium Studies, PhD thesis, Chemical Engineering University Of Kwa-Zulu Natal, Durban, South Africa.
- Nakayama, T., Sagara, H., Arai, K. and Saito, S. (1987), 'High Pressure Liquid-Liquid Equilibria for the system of water, ethanol and 1,1-difluoroethane at 323.2 K', *Fluid Phase Equilib* **38**(1), 109–127.
- Ness, H. C. V., Byer, S. M. and Gibbs, R. E. (1973), 'Vapor-liquid equilibrium: Part1. an appraisal of data reduction methods', *AICHE J.* **19**, 238–244.
- Orbey, H. and Sandler, S. I. (1995a), 'Reformulation of Wong-Sandler mixing rule for cubic equations of state', *AICHE Journal* **41**(3), 683–690.
- Orbey, H. and Sandler, S. I. (1996), 'Analysis of excess free energy based equations of state models', *AICHE* **42**(8), 2327–2334.
- Orbey, H. and Sandler, S. I. (1997), 'A comparison of Huron-Vidal type mixing rules of mixtures of compounds with large size differences and a new mixing rule', *Fluid Phase Equilib* **132**, 1–14.

- Orbey, H. and Sandler, S. I. (1998), *Modeling Vapor-Liquid Equilibria*, Cambridge University Press, Cambridge.
- Patel, N. C. and Teja, A. S. (1982), 'A new cubic equation of state for fluids and fluid mixtures', *Chem. Eng. Sci.* **37**, 463-473.
- Pavlova, I. P., Saraev, B. A. and Chaplits, D. H. (1981), *Prom.Sint.Kauch* **5**, 2-4.
- Peng, D. and Robinson, D. B. (1976), 'A new two constant equation of state', *Ind. Eng. Chem. Fund* **15**, 59-64.
- Pfhol, O., Riebesell, C. and Dohrn, R. (2002), 'Measurement of high-pressure vapour-liquid-equilibria in the system n-pentane + poly(dimethylsiloxane) at 308.15-423.15 K', *Fluid Phase Equilib* **202**.
- Pierotti, G. J., Deal, C. H. and Derr, E. L. (1959), *Ind. Eng. Chem.* **51**(1), 95-102.
- Prausnitz, J. M. and Chueh, P. L. (1968), *Computer Calculations for High-Pressure Vapor-Liquid Equilibria*, Prentice-Hall, Englewood Cliffs, N. J.
- Qin, J., Li, Z. and Shi, M. (1996), *Muaxue-gongye-yu-gongcheng* **13**(4), 37-41.
- Qin, J., Li, Z. and Shi, M. (1997), *J.Fuel.Chem.Tech* **25**(2), 162-165.
- Raal, J. D. and Mühlbauer, A. L. (1994), 'The measurement of high-pressure vapour-liquid-equilibrium', *Developmants in chemical engineering and mineral precessing* **2**(2/3), 69-104.
- Raal, J. D. and Mühlbauer, A. L. (1998), *Phase Equilibria: Measurement and Computation*, Taylor and Francis, Bristol, P. A.
- Ramjugernath, D. (2000), *High Pressure Phase Equilibrium Studies*, PhD thesis, Chemical Engineering University Of KwaZulu-Natal.
- Ramjugernath, D. and Raal, J. D. (1999a), Modelling, prediction and extrapolation of high pressure vapour-liquid equilibrium data: Direct vs combined methods, Technical report, Warsaw, Poland.
- Ramjugernath, D. and Raal, J. D. (November 1999b), 'Modelling, prediction and extrapolation of high pressure vapour-liquid equilibrium data:direct versus combined methods', *Developmants in Chemical Engineering and Mineral processing* **18-20**.
- Redlich, O. and Kwong, J. N. S. (1949), 'On thermodynamics of solutions v: An equation of state. fugacities of gaseous solutions', *Chem. Rev.* **44**, 233-244.

- Reid, R. C., Prausnitz, J. M. and Poling, B. E. (1987), *The Properties of Gases & Liquids*, 4th edn, McGraw-Hill Book Company, Singapore.
- Reiff, W. E., Peters-Gerth, P. and Lucas, K. (1987), 'A static equilibrium apparatus for (vapor + liquid) equilibrium measurements at high temperatures and pressures', *J. Chem. Thermodynamics* **19**, 467-477.
- Reimers, J. L., Bhethanabotla, V. R. and Campbell, S. W. (1992), 'Total pressure measurement for pentane + methanol + ethanol at 303.15 K', *J. Chem. Eng. Data* **37**, 127.
- Reiss, N. R., Frisch, H. L. and Lebowitz, J. L. (1959), 'Statistical mechanics of rigid spheres', *J. Chem. Phys.* **31**, 369-380.
- Renon, H. and Prausnitz, J. M. (1968a), 'Local compositions in thermodynamic excess functions for liquid mixtures', *AIChE* **14**(1), 135-144.
- Renon, H. and Prausnitz, J. M. (1968b), 'Local compositions in thermodynamic excess functions for liquid mixtures', *AIChE J.* **14**(1), 135-144.
- Rogers, B. L. and Prausnitz, J. M. (1970), 'Sample-extrusion apparatus for high pressure vapor-liquid equilibria', *Industrial And Engineering Chemistry Fundamentals* **9**(1), 174-177.
- Sadus, R. J. (1992), *High Pressure Phase Behaviour Of Multicomponent Fluid Mixtures*, Elsevier Science.
- Sandler, S. I. (1994), *Models for Thermodynamics and Phase Equilibria Calculations*, Marcel Dekker Inc., New York.
- Sandler, S. I. (1999), *Chemical and Engineering Thermodynamics*, John Wiley & Sons, New York.
- Satyro, M. A. and Trebble, M. A. (1996), 'On the applicability of the Wong-Sandler mixing rules for the calculation of thermodynamic excess properties', *Fluid Phase Equilib* **115**, 135-164.
- Schmidt, G. and Wenzel, H. (1980), 'A modified van der waals equation of state', *Chem. Eng. Sci.* **35**, 10503-1512.
- Seo, J., Lee, J. and Kim, H. (2000), 'Isothermal vapor-liquid equilibrium for ethanol and n-pentane system at the near critical region', *Fluid Phase Equilib.* **172**, 211-219.
- Skjold-Jorgensen, S. (1984), 'Gas solubility calculations.ii. application to a new group-contribution equation of state', *Fluid Phase Equilib.* **16**, 317-351.

- Smith, J. M., Ness, H. C. V. and Abbott, M. M. (2001), *Chemical Engineering Thermodynamics*, sixth edn, McGraw Hill.
- Soave, G. (1972), 'Equilibrium constants from a modified Redlich-Kwong equation of state', *Chem. Eng. Science* **72**, 1197-1203.
- Soave, G. (1984), 'Improvements of the van der waals equation of state', *Chem. Eng. Sci.* **39**, 357-369.
- Soave, G. (1993), 'Improving the treatment of heavy hydrocarbons by the SRK EOS', *Fluid Phase Equilib.* **84**, 339-342.
- Solorzano-Zavala, M., Barragan-Aroche, F. and Bazua, E. R. (1996), 'Comparative study of mixing rules for cubic equations of state in the prediction of multicomponent vapor-liquid equilibria', *Fluid Phase Equilib.* **122**, 99-116.
- Souahi, F., Sator, S., Albane, A. S., Kies, K. F. and Chitour, E. C. (1998), 'Development of a new form of the alpha function of the Redlich-Kwong cubic equation of state', *Fluid Phase Equilib.* **153**, 73-80.
- Stradi, B. A., Brennecke, J. F., Kohn, J. P. and Stradterr, M. A. (Jan.2001), 'Reliable computation of mixture critical points', *J.AICHE* **47**(1), 212-221.
- Stryjek, R. and Vera, J. H. (1986a), 'PRSV: An improved Peng-Robinson equation of state for pure compounds and mixtures', *Can. J. Chem. Eng.* **64**, 323-333.
- Stryjek, R. and Vera, J. H. (1986b), 'Prsv2: A cubic equation of state for accurate vapour-liquid equilibrium calculations', *Can. J. Chem. Eng.* **64**, 820-826.
- Stryjek, R. and Vera, J. H. (Apr.1986), 'PRSV: An improved Peng-Robinson equation of state for pure compounds and mixtures', *Can. J. Of Chem. Eng.* **64**, 323-333.
- Thiele, E. (1963), 'Equation of state for hard spheres', *J. Chem. Phys.* **39**, 474-479.
- Tochigi, K. (1995), 'Prediction of high-pressure vapor-liquid equilibria using ASOG', *Fluid Phase Equilib* **104**, 253-260.
- Tochigi, K., Kolar, P., Iizumi, T. and Kojima, K. (1994), 'A note on a modified Huron-Vidal mixing rule consistent with the second virial coefficient condition', *Fluid Phase Equilib* **96**, 215-221.
- Treble, M. A. and Bishnoi, P. R. (1987), 'Development of a new four-parameter cubic equation of state', *Fluid Phase Equilib.* **35**(1), 1-18.

- Tsai, U.-C. and Chen, Y.-P. (1998), 'Application of a volume-translated Peng-Robinson equation of state on vapor-liquid equilibrium calculations', *Fluid Phase Equilib* **145**, 193-215.
- Tsonopoulos, C. (Mar.1974), 'An empirical correlation of second virial coefficients', *AIChE* **20**(2), 263-272.
- Twu, C. H., Bluck, D., Cunningham, J. R. and Coon, J. E. (1991), 'A cubic equation of state with a new alpha function and a new mixing rule', *Fluid Phase Equilib.* **69**, 33-50.
- Twu, C. H., Bluck, D., Cunningham, J. R. and Coon, J. E. (1992a), 'A cubic equation of state: Correlation between binary interaction parameters and infinite dilution activity coefficients', *Fluid Phase Equilib.* **72**, 25-39.
- Twu, C. H. and Coon, J. E. (1995), 'Accurately estimate binary interaction parameters', *Chem. Eng. Prog.* (1995) 46-53 pp. 46-53.
- Twu, C. H., Coon, J. E. and Cunningham, J. R. (1995b), 'A new generalized alpha function for a cubic equation of state part 1. peng-robinson equation', *Fluid Phase Equilib.* **105**, 49-59.
- Twu, C. H., Coon, J. E. and Cunningham, J. R. (1992b), 'A new cubic equation of state', *Fluid Phase Equilib.* **75**, 65-79.
- Twu, C. H., Coon, J. E. and Cunningham, J. R. (1994), 'A generalized vapor pressure equation for heavy hydrocarbons', *Fluid Phase Equilib.* **96**, 19-31.
- Twu, C. H., Coon, J. E. and Cunningham, J. R. (1995), 'An approach for the extension of a 3-parameter cubic equation of state to heavy hydrocarbons', *Fluid Phase Equilib* **104**, 83-96.
- Twu, C. H., Sim, W. D. and Tassone, V. (2000), 'An extension of $ceos/a^E$ zero pressure mixing rule for an optimum two-parameter cubic equation-of-state, in 'In Proceedings of the 3rd China/USA Chemical Engineering Conference', Beijing China.
- Vetere, A. (2000), 'A simple modification of the NRTL equation', *Fluid Phase Equilib.* **173**, 57-64.
- Voros, N. G. and Tassios, D. P. (1993), 'Vapor-liquid equilibria in nonpolar/weakly polar systems with different types of mixing rules', *Fluid Phase Equilib.* **91**, 1-29.
- Wagner, Z. and Wichterle, I. (1987), 'High-pressure vapour-liquid equilibrium in systems containing carbon dioxide, 1-hexene, and n-hexene', *Fluid Phase Equilib* **33**(1), 109-123.

- Wang, W., Qu, Y., Twu, C. H. and Coon, J. E. (n.d.), 'Comprehensive comparison and evaluation of the mixing rules of WS, MHV2, AND TWU ET AL., volume = 116, year = 1996', *Fluid Phase Equilib.* pp. 488–494.
- Wei-Rong, J. and Lempe, D. A. (1997), 'Density improvement of the SRK equation of state', *Fluid Phase Equilib.* **130**, 49–63.
- Wei, Y. S. and Sadus, R. J. (2000), 'Equations of state for the calculation of fluid-phase equilibria', *AICHE* **46**(1), 169–196.
- Wichterle, I. (1978b), 'High pressure vapour-liquid equilibria. v- quantitative description. part 3', *Fluid Phase Equilib.* **2**.
- Wilson, G. M. (1964), 'Vapor-liquid equilibrium xi. a new expression for the excess free energy of mixing', *J.Am.Chem.Soc.* **86**.
- Wong, D. S. H. and Sandler, S. I. (1984), 'Calculation of vapor-liquid equilibrium with cubic equations of state and a corresponding states principle', *Ind.Eng.Chem.Fundam* **23**, 348–354.
- Wong, D. S. H. and Sandler, S. I. (1992b), 'A theoretically correct mixing rule for cubic eos', *AICHE Journal* **38**(5).
- Wong, D. S. H. and Sandler, S. I. (May 1992a), 'A theoretically correct mixing rule for cubic equations of state', *J.AICHE* **38**(5), 671–678.
- Wong, D. S., Orbey, H. and Sandler, S. I. (1992), 'Equation of state mixing rule for nonideal mixtures using available activity coefficient model parameters and that allows extrapolation over large ranges of temperature and pressure', *Ind.Eng.Chem.Res.* **31**, 2033–2039.
- Wong, D. S., Orbey, H., Sandler, S. I. and Teja, A. S. (1984a), 'Vapor-liquid equilibrium calculations by use of a generalized corresponding states principle.1.new mixing rules', *Ind.Eng.Chem.Fundam.* **23**, 38–44.
- Wong, D. S., Orbey, H., Sandler, S. I. and Teja, A. S. (1984b), 'Vapor-liquid equilibrium calculations by use of a generalized corresponding states principle.2.comparison with other methods', *Ind.Eng.Chem.Fundam.* **23**, 45–49.
- Yu, J. M. and Lu, B. C. (1987), 'A three parameter cubic equation of state for asymmetric mixture density calculations', *Fluid Phase Equilib.* **34**, 1–19.

Appendix A

Phase Equilibrium Theory

A.1 Criteria for phase equilibria

The *Gibbs* free energy in any *closed system* is related to temperature and pressure by:

$$d(nG) = (nV)dP - (nS)dT \quad (\text{A.1})$$

Smith et al. (2001) state that equation (A.1) may be applied to a single-phase fluid in a closed system wherein no chemical reactions occur. A more general equation may be written for the case where the system can interact with its surroundings- interaction between vapour and liquid.

$$d(G) = (V)dP - (S)dT + \sum_i \mu_i dx_i \quad (\text{A.2})$$

$$\mu_i \equiv \left[\frac{\partial(nG)}{\partial(n_i)} \right]_{T,P,n_j} \quad (\text{A.3})$$

The chemical potential, μ_i , is defined by equation (A.3). The individual phases of a closed system can be described by equation (A.2). For a two phase system the governing property relations are:

$$\begin{aligned} d(nG)^\alpha &= (nV)^\alpha dP - (nS)^\alpha dT + \sum_i \mu_i^\alpha dn_i^\alpha \\ d(nG)^\beta &= (nV)^\beta dP - (nS)^\beta dT + \sum_i \mu_i^\beta dn_i^\beta \end{aligned}$$

The change in the total *Gibbs* energy of the system can be expressed as the summation of these relations. Therefore the sum of the respective phase relations or the total *Gibbs* energy of the system is:

$$d(nG) = (nV)dT - (nS)dT + \sum_i \mu_i^\alpha dn_i^\alpha + \sum_i \mu_i^\beta dn_i^\beta$$

The comparison of the equation above with equation (A.1), shows that the equilibrium condition for a two phase system is:

$$\sum_i \mu_i^\beta dn_i^\beta + \sum_i \mu_i^\alpha dn_i^\alpha = 0$$

Recall that, at equilibrium, there is no change in the overall macroscopic properties of the system. Therefore, the changes in dn_i^α and dn_i^β between the phases resulting from mass transfer requires:

$$\begin{aligned} dn_i^\alpha &= -dn_i^\beta \\ \sum_i (\mu_i^\alpha - \mu_i^\beta) dn_i^\alpha &= 0 \end{aligned}$$

Therefore, the equilibrium the criterion for the two phases considered is:

$$\mu_i^\alpha = \mu_i^\beta \quad (\text{A.4})$$

This fundamental relation given by equation (A.4) represents the condition for a two-phase system. This condition can be generalized for a heterogeneous closed system consisting of two or more phases(π) and N components:

$$\mu_1^\alpha = \mu_1^\beta = \dots = \mu_1^\pi (i = 1, 2, \dots, N) \quad (\text{A.5})$$

Smith et al. (2001) described the criterion for phase equilibria simply as: “Multiple phases at the same T and P are in equilibrium when the chemical potential of each of the species is the same in all phases.”

The relations described in this section have been written for pure components only. These fundamental relations can be applied to mixtures by considering partial molar properties.

A.1.1 Partial Molar Properties

The general thermodynamic property M of a homogeneous phase can be expressed as a function of temperature, pressure and the number of moles of the respective species constituting the phase. Equation (A.6) below illustrates such a function.

$$nM = m(T, P, n_1, n_2, n_3, \dots, n_i, \dots) \quad (\text{A.6})$$

The definition of a partial molar property \overline{M}_i of a species(i) in solution(mixture)

is defined as:

$$\overline{M}_i \equiv \left[\frac{\partial(nM_i)}{\partial n_i} \right]_{P,T,n_j} \quad (\text{A.7})$$

This relationship in equation (A.7) is defined as a response function, (Smith et al., 2001). The function represents the change of the total property M from addition addition at constant T and P of a differential amount of species i to a finite quantity of solution. The total differential of nM is:

$$d(nM) = \left[\frac{\partial(nM)}{\partial P} \right]_{T,n_j} + \left[\frac{\partial(nM)}{\partial T} \right]_{P,n_j} + \left[\frac{\partial(nM)}{\partial n_i} \right]_{P,T,n_j} \quad (\text{A.8})$$

Smith et al. (2001) state that the definition of the partial molar property provides an equation for the calculation of partial properties from solution-property data and the determination of solution properties from partial properties.

A.1.2 Fugacity

It was shown earlier that the definition of the chemical potential (μ_i) provides the fundamental criterion (equation (A.5)) for phase equilibria. This criterion extends to the case of chemical reaction equilibria. However, chemical potential is a difficult property to measure and therefore its use is not common. This can be attributed to the fact that μ , an abstract concept, is not easily related to measurable quantities. The *Gibbs* energy is related to the internal energy(U) and entropy(S), which are primitive quantities for which the absolute values are unknown-hence μ_i .

Therefore it is more desirable to express the chemical potential in terms of an auxiliary function, which can be more easily expressed as a physical quantity. The concept of *fugacity* was introduced, which is a physical quantity with units of pressure. The relation between the chemical potential of a species and its fugacity, begin with the definition of the chemical potential as given in equation (A.3):

$$\mu_i \equiv \left[\frac{\partial(nG)}{\partial(n_i)} \right]_{T,P,n_j}$$

$$\mu = \mu(P, T, n_1, n_2, \dots, n_N)$$

The chemical potential is related to temperature and pressure, for an ideal

gas *in solution*, by the differential equation (A.9).

$$d\mu = -\bar{S}_i^{ig} dT + \bar{V}_i^{ig} dP \quad (\text{A.9})$$

Therefore, at constant temperature ($dT = 0$):

$$\begin{aligned} d\mu &= \bar{V}_i^{ig} dP \\ &= \left(\frac{RT}{P}\right) dP \end{aligned} \quad (\text{A.10})$$

Integrating equation (A.10) from an arbitrary reference state to pressure(P) gives:

$$d\mu = d\mu^\circ + RT \ln \frac{P}{P^\circ} \quad (\text{A.11})$$

The ratio P/P° in equation (A.11) is replaced by *fugacity*(f) with the units of pressure. Hence for a species in solution at isothermal conditions in any system (ideal or nonideal):

$$\mu - \mu^\circ = RT \ln \frac{\hat{f}}{f^\circ} \quad (\text{A.12})$$

Fugacity may be considered as a corrected pressure, where the corrections account for the non-idealities between the state of interest and the standard state. The equilibrium criterion below can be imposed on the fugacities of species (i) in phases, $\alpha, \beta, \dots, \pi$:

$$\hat{f}_i^\alpha = \hat{f}_i^\beta = \dots = \hat{f}_i^\pi \quad (\text{A.13})$$

Hence for vapour-liquid equilibrium of a mixture:

$$\hat{f}_i^v = \hat{f}_i^l \quad (\text{A.14})$$

Where \hat{f}_i is not a partial molar property. Smith et al. (2001) derive the equilibrium condition (equation (A.14)) from the pure species relations:

$$\begin{aligned} G_i^v &= \Gamma_i(T) + RT \ln f_i^v \\ G_i^l &= \Gamma_i(T) + RT \ln f_i^l \\ \Leftrightarrow f_i^v &= f_i^l \end{aligned}$$

The relationship between component fugacities (equation (A.13)) does not give a quantitative description of VLE equilibrium, the problem is relating these fugacities to measurable properties e.g. temperature, pressure and composition. This problem of relating fugacity to measurable quantities is overcome in vapour-liquid equilibria by the use of thermodynamic auxiliary functions i.e. activity coefficient γ_i and fugacity coefficient ϕ_i .

A.2 Fugacity Coefficient and activity coefficient

There are three auxiliary functions, the fugacity coefficient ϕ , the activity coefficient γ and the liquid phase standard-state fugacity f^{OL} . Fugacity can be related to functions of measurable quantities as follows:

$$\begin{aligned}\hat{f}_i^V &= g(T, P, y_1 \dots y_n) \\ \hat{f}_i^L &= g(T, P, x_1 \dots x_n)\end{aligned}$$

The fugacity coefficient ϕ is defined as a dimensionless number:

$$\phi = \left[\frac{f}{P} \right]$$

For, a component in solution, in the vapour and liquid phase, respectively:

$$\hat{\phi}_i^V = \left[\frac{\hat{f}_i^V}{y_i P} \right] \quad (\text{A.15})$$

$$\hat{\phi}_i^L = \left[\frac{\hat{f}_i^L}{x_i P} \right] \quad (\text{A.16})$$

The definitions of the fugacity coefficient in solution above can be related to measurable quantities by considering the residual *Gibbs* free energy (\bar{G}_i^R) (Smith et al., 2001). Assuming isothermal conditions, for the vapour phase:

$$\mu_i \equiv \bar{G}_i = \Gamma_i(T) + RT \ln \hat{f}_i \quad (\text{A.17})$$

$$\mu_i^{ig} \equiv \bar{G}_i^{ig} = \Gamma_i(T) + RT \ln y_i P \quad (\text{A.18})$$

$$\bar{G}_i^R = \mu_i - \mu_i^{ig} \quad (\text{A.19})$$

$$= RT \ln \frac{\hat{f}_i^V}{y_i P} \quad (\text{A.20})$$

$$= RT \ln \hat{\phi}_i^V \quad (\text{A.21})$$

The fugacity coefficient in solution is related to temperature, pressure and composition through the identification of the fugacity coefficient with $\frac{\bar{G}_i^R}{RT}$:

$$\ln \hat{\phi}_i = \int_0^P (\bar{Z}_i - 1) \frac{dP}{P} \quad (\text{const T}) \quad (\text{A.22})$$

Where \bar{Z}_i refers to the liquid or vapour compressibility of the system. For the vapour phase, \bar{Z}_i is based on the liquid volume \bar{V}_i .

The activity coefficient (γ) , relates the liquid phase fugacity \hat{f}_i^L to the liquid mole fraction x_i and to the standard-state fugacity f_i^{OL} . The activity coefficient is defined by:

$$\gamma_i = \frac{\hat{f}_i^L}{x_i f_i^{OL}} \quad (\text{A.23})$$

$$\Leftrightarrow \gamma_i \text{ is a partial molar property} \quad (\text{A.24})$$

The activity coefficient is related to \bar{G}_i by the concept of *excess molar properties* (M^E) where for a general property M :

$$M^E = M - M^{id} \quad (\text{A.25})$$

where, M^{id} is the ideal solution property.

The ideal solution property has been defined such that the concept facilitates the description of nonideal solution behavior. It serves as the reference standard for the liquid phase. Raal and Mühlbauer (1998) derive the relationship between the activity coefficient (γ_i) and the excess Gibbs energy (\bar{G}_i^E) for gas mixtures from statistical mechanics. The relationship between γ_i and \bar{G}_i^E is analogous to the relationship between the residual Gibbs energy (\bar{G}_i^R) and the fugacity coefficient in solution ($\hat{\phi}_i$):

$$\frac{\bar{G}_i^E}{RT} = \ln \gamma_i \quad (\text{A.26})$$

The relationship between the auxiliary functions (γ_i and $\hat{\phi}_i$) and their respective Gibbs energy functions (excess and residual) allow the vapour-liquid equilibrium constraint, equation (A.14), to be rewritten in the form of measurable quantities:

$$\begin{aligned} \hat{f}_i^V &= \hat{\phi}_i^V y_i P \\ &= \hat{f}_i^L \\ &= \gamma_i x_i f_i^{OL} \\ &= \hat{\phi}_i^L x_i P \end{aligned}$$

Where,

$$f_i^{OL} \equiv \text{standard state fugacity}$$

The fugacity (\hat{f}_i^L) of component i in the liquid phase, can be determined by equation (A.27). A rigorous derivation is given in Raal and Mühlbauer (1998).

$$\hat{f}_i^L = f_i^{OL} = \phi_i^{sat} P_i^{sat} \exp \left[\frac{1}{RT} \int_{P_i^{sat}}^P V_i^L dP \right] \quad (\text{A.27})$$

Appendix B

Auxiliary Equipment

B.1 Degassing apparatus

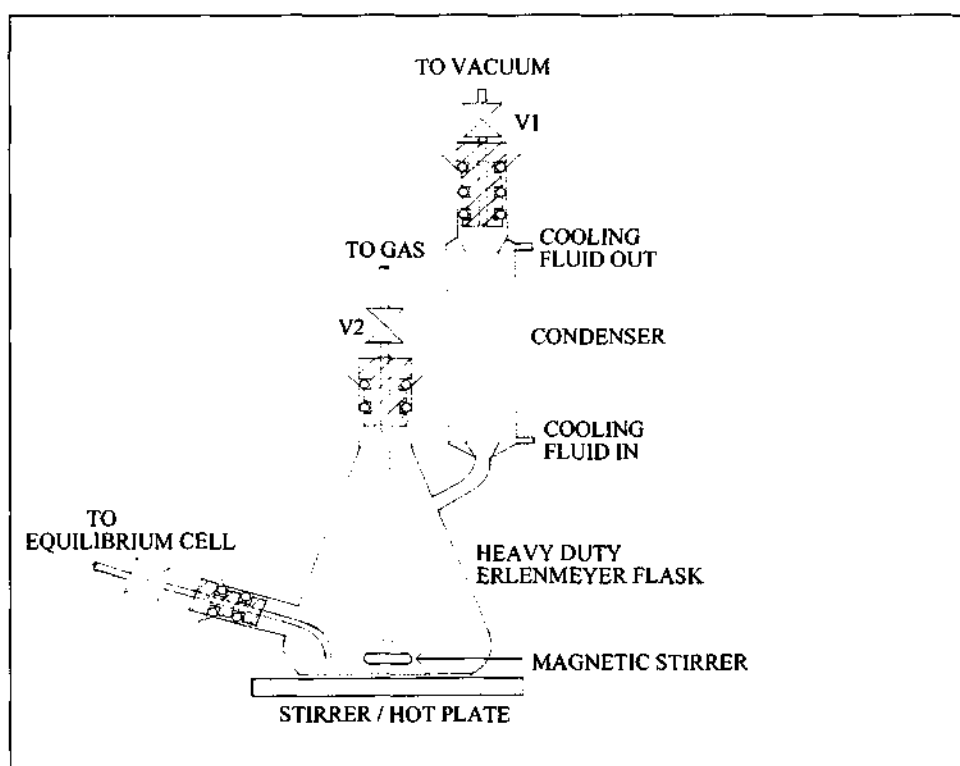


Figure B.1: Degassing apparatus layout (Naidoo, 2004)

The degassing procedure was undertaken in a custom made heavy duty Elynmeyer flask. The degassing apparatus was connected to a cooling circuit. The cooling circuit circulated a cold mixture of ethylene glycol and water through the degassing condenser. The circuit consisted of a water

bath, a water pump and a Julabo FT200 cold finger (refrigerator)

- the Julabo cold finger was switched on and the temperature of the cooling medium was monitored until it reached 0°C.
- The water pump was switched on and the cooling solution was circulated through the condenser.
- Approximately 150ml of component was poured into the degassing apparatus via a 200ml volumetric cylinder.
- The temperature on the hot-plate was set slightly above the boiling point of the component to be degassed. The hot-plate stirrer motor was also switched on and set to a moderate speed.
- The vacuum was applied on the condenser side of the degassing apparatus.
- Degassing was allowed for approximately thirty minutes.

B.2 Determination of Jet-Mixer operating temperature

The jet-mixer has been discussed as a phase homogenisation device. The withdrawn sample from the equilibrium cell must be homogeneous and vapourised for accurate composition analysis. Therefore the operating temperature of the jet-mixer must be higher than the saturation temperature of the less volatile liquid component at the pressure within the jet-mixer.

A few assumptions are made in the determination of the jet-mixer operating temperature:

- the jet-mixer contains only the non-volatile component
- the non-volatile component behaves as an ideal gas.

As discussed in the experimental procedure chapter, the sampling lines are heated in increments sectionally. Therefore the jet-mixer (internal and external) temperatures were determined by undertaking the calculations for the internal (large) liquid jet-mixer. With the dimensions of the internal liquid jet-mixer, a simple calculation with the non-volatile component properties (density) results in the jet-mixer operating range. The intersection between this operating line and the vapour pressure curve (vapour pressure correlation) gives the jet-mixer operating temperature.

The equations used were:

$$P = \frac{nRT}{V_{jm}} \quad (\text{B.1})$$

where

$$n = \frac{pV_s}{M} \quad (\text{B.2})$$

$$(\text{B.3})$$

The dimensions of the sample loop, (Naidoo, 2004)are:

$$\Phi_{ID} = 0.1\text{cm}$$

$$L = 21\text{cm}$$

And

$$\begin{aligned} V &= \frac{\pi\Phi_{ID}^2 L}{4} \\ &= 0.165\text{cm}^3 \end{aligned}$$

- P, vapour pressure[bar]
- n, number of moles
- T, temperature [K]
- R, universal gas constant [$\text{cm}^3.\text{bar}/\text{mol}.K$]
- V_{jm} , jet-mixer volume [cm^3]
- V_s , volume of the sample loop [cm^3]
- p , density [g/cm^3]
- M , molar volume [g/mol]
- L , length of the sample loop
- Φ_{ID} , the internal diameter of the sample loop tubing

Figure B.2 illustrates the operating point of the jet-mixer for the n-pentane + ethanol system. The actual operating temperature set on the jet-mixer controller is determined as 10% of the intersection pressure from the plot. Hence the temperature is read from the plot by extrapolating the vapour pressure curve.

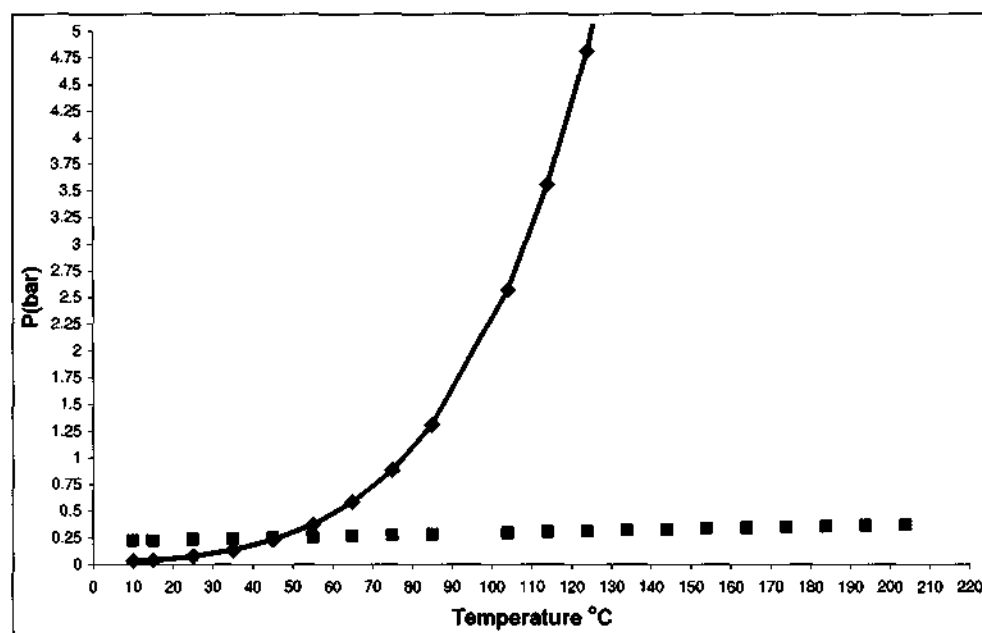


Figure B.2: A plot of the jet-mixer pressure against the component saturation pressure. In this figure, the plot was done for ethanol.

B.3 Temperature and pressure calibration

B.3.1 Temperature calibration

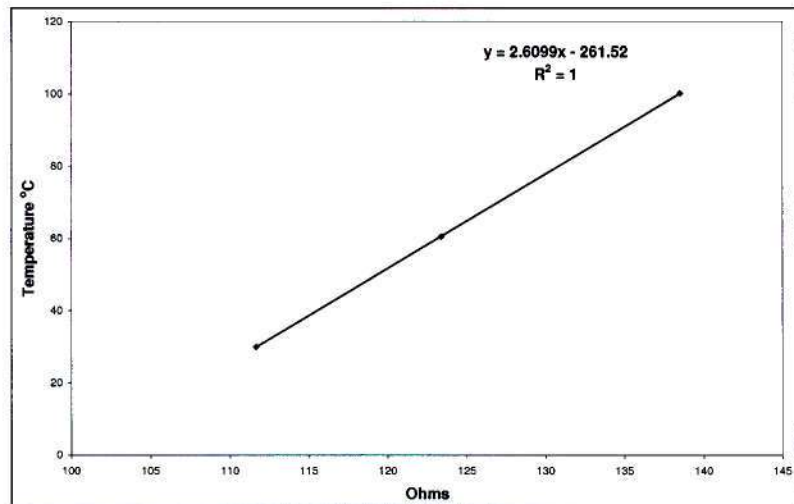


Figure B.3: PT-100 standard calibration chart

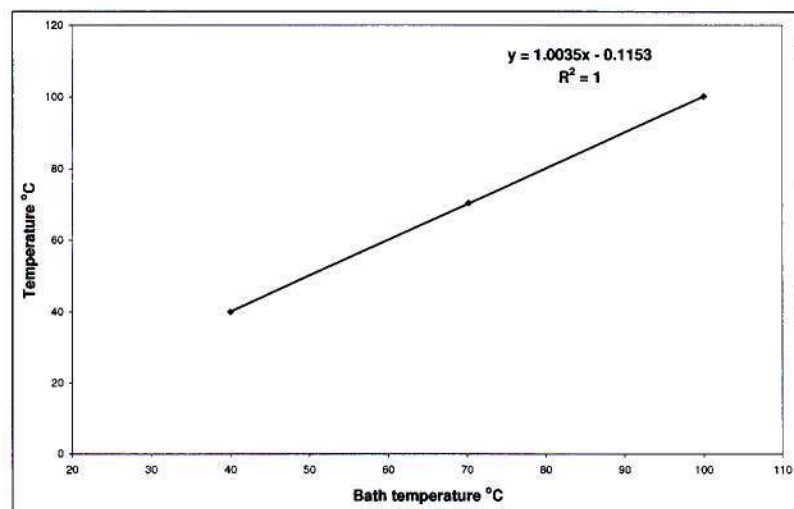
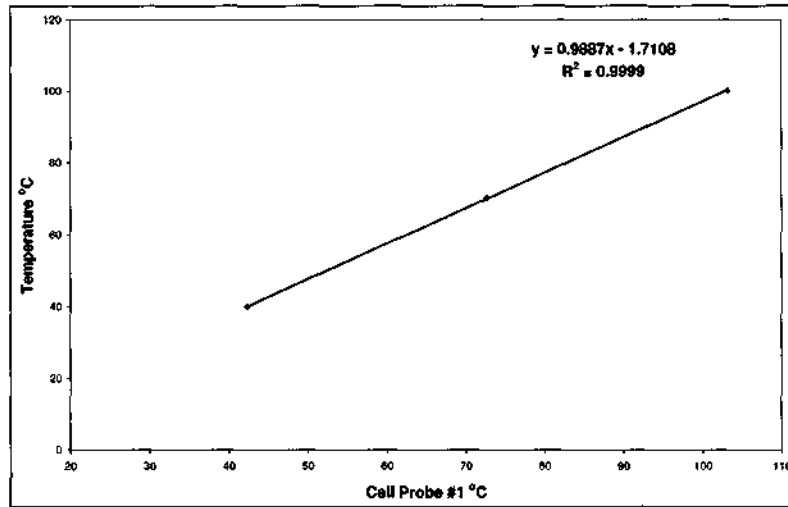
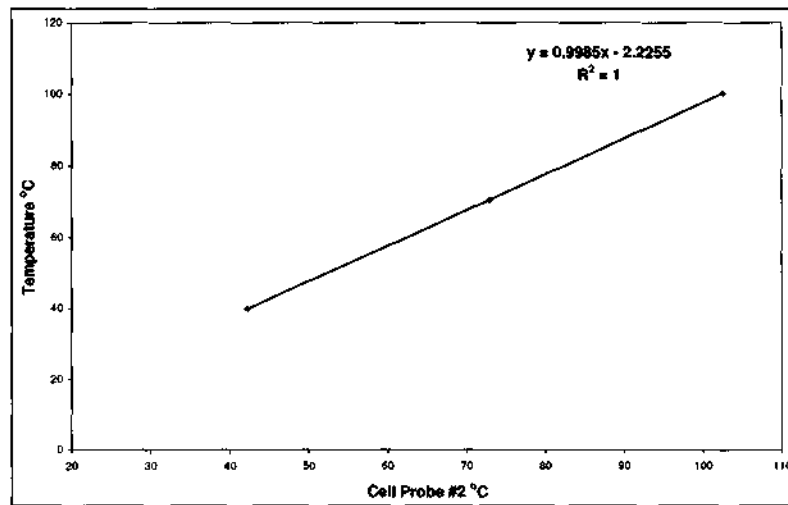
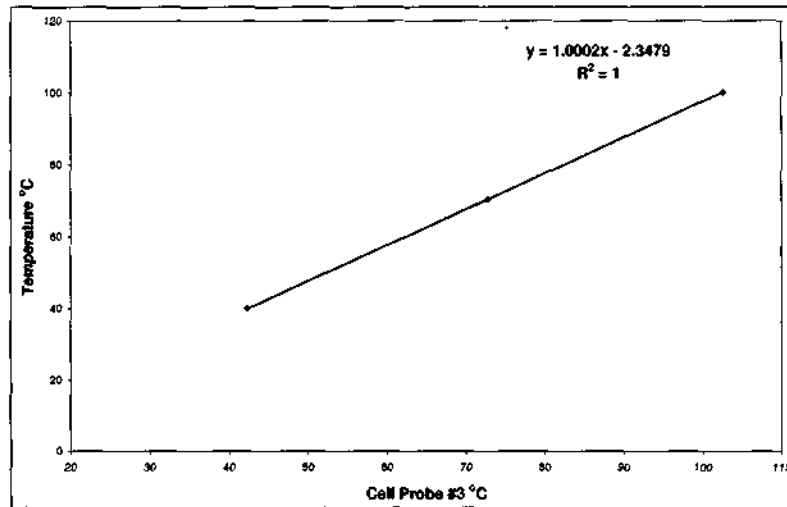
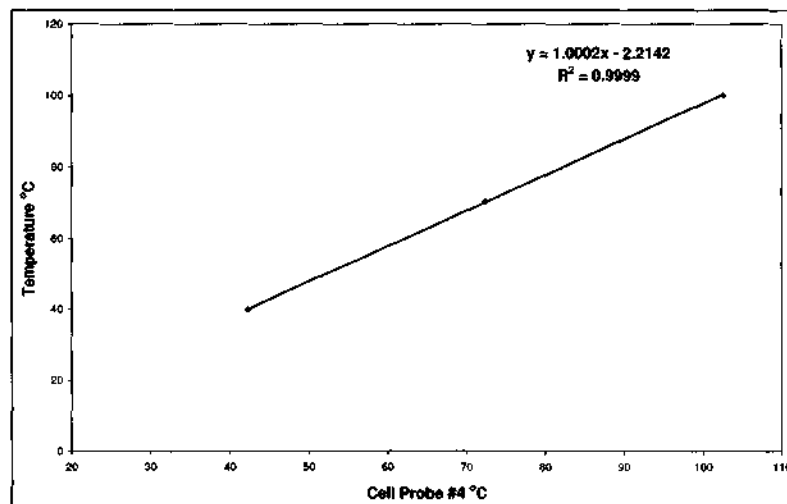


Figure B.4: Air-bath temperature sensor calibration, T_B

Figure B.5: Equilibrium temperature sensor calibration, T_1 Figure B.6: Equilibrium temperature sensor calibration, T_2

Figure B.7: Equilibrium temperature sensor calibration, T_3 Figure B.8: Equilibrium temperature sensor calibration, T_4

B.3.2 Pressure calibration

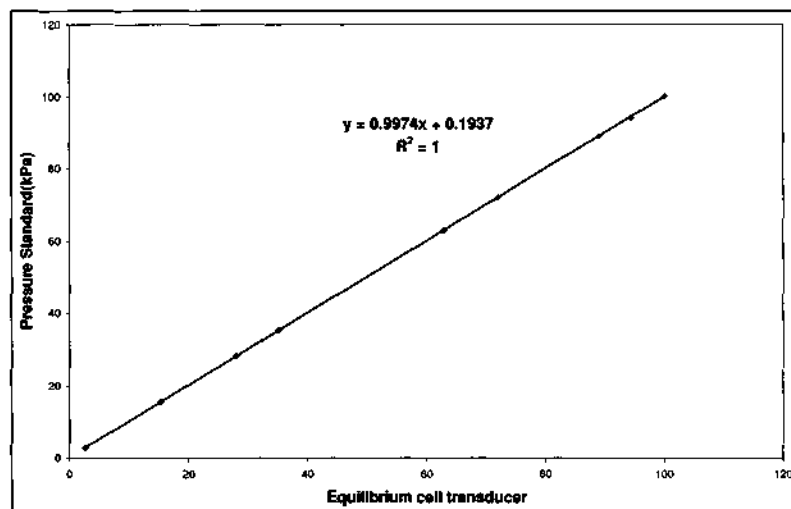


Figure B.9: Equilibrium cell pressure transducer calibration

B.4 Gas Chromatograph Specifications

B.4.1 GC settings and calibration

The samples made-up for GC calibration were injected with a $1\mu\text{ml}$ SGE syringe. The syringe was first rinsed with the sample approximately seven times. A minimum of three injections were undertaken to determine average area ratios. The response factor charts for the two binary systems is given below.

Table B.1: GC operating settings for the Chrompak CP9000 column

Specifications	n-pentane + ethanol	2-methyl-2-butene + TAME
Injector Temperature ($^{\circ}\text{C}$)	220	220
Oven Temperature ($^{\circ}\text{C}$)	160	180
Detector Temperature ($^{\circ}\text{C}$)	240	240
Reference Gas flow (ml/min)	39	39
Carrier Gas flow (ml/min)	39	39

n-Pentane(1) + Ethanol(2) calibration

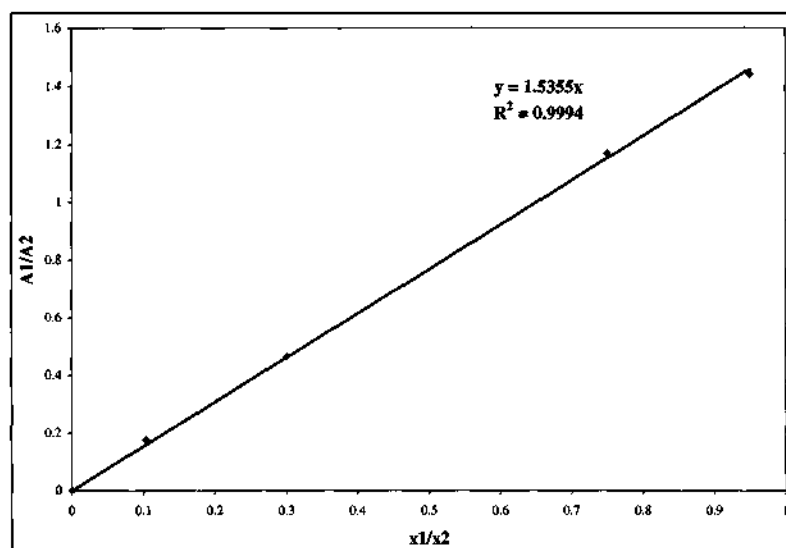


Figure B.10: Response factor chart for the ethanol rich region

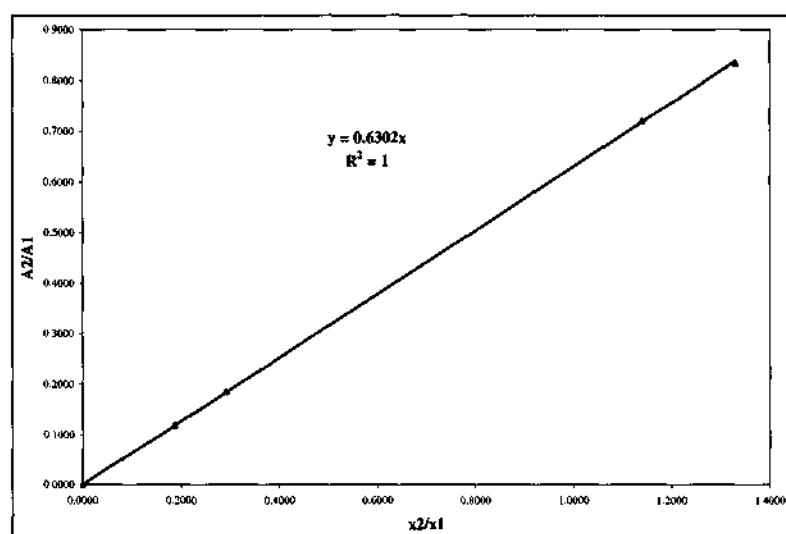


Figure B.11: Response factor chart for the pentane rich region

2-Methyl-2-butene(1) + TAME(2) calibration

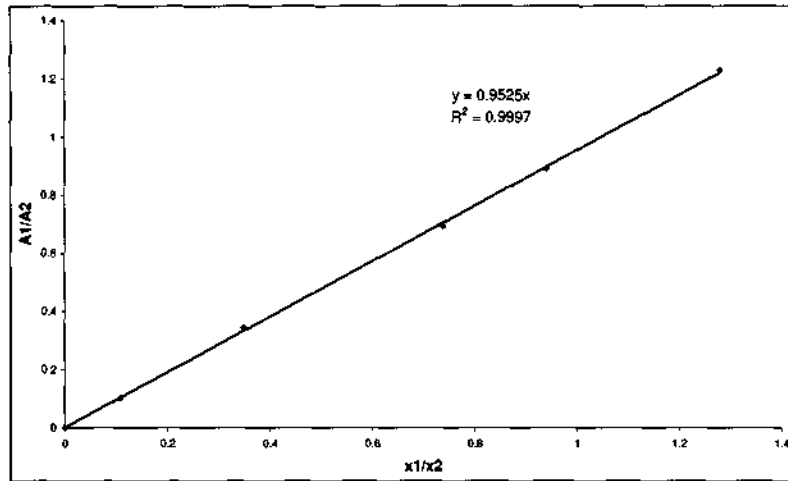


Figure B.12: Response factor chart for the TAME rich region

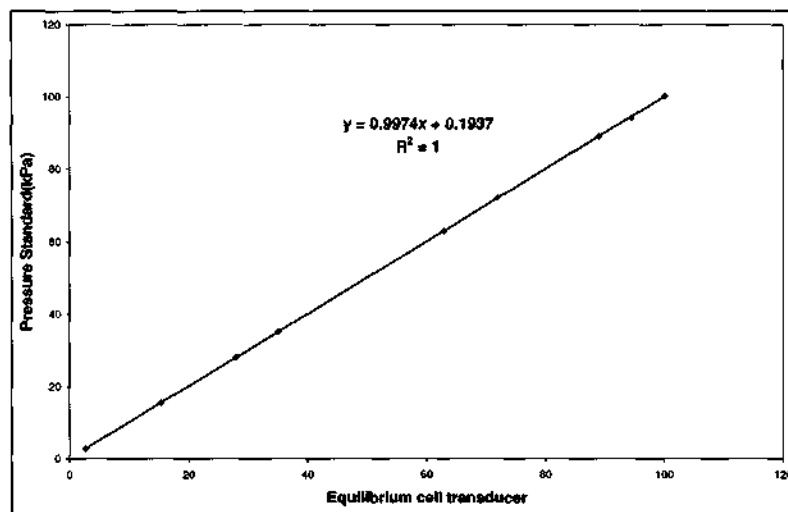


Figure B.13: Response factor chart for the 2-methyl-2-butene rich region

Appendix C

PHYSICAL PROPERTIES AND LITERATURE DATA OF SYSTEMS MEASURED

C.1 Physical Properties Of Components

C.1.1 General Physical Properties

Table C.1: Physical properties of the pure components of the respective binary systems

<i>Component</i>	$T_C(K)$	$P_C(bar)$	ω	$V_C(\frac{cm^3}{mol})$
<i>n - Pentane</i>	469.7	33.69	0.2510	304
<i>Ethanol</i>	516.2	63.83	0.6350	167
<i>2 - methyl - 2 - Butene</i>	0.6390	5.59	0.5798	6.23
<i>TAME</i>	0.6800	6.21	0.5967	6.40

Critical properties from Reid et al. (1987)

$Z_{RA} = 0.29056 - 0.08775\omega$, where ω is the acentric factor.

C.1.2 Vapour Pressures

Table C.2: Vapour pressure parameters of the respective binary system components

<i>Component</i>	<i>A</i>	<i>B</i>	<i>C</i>	<i>D</i>	<i>Equation</i>
<i>n - Pentane</i>	-7.28936	1.53679	-3.08367	-1.02456	1
<i>Ethanol</i>	-851838	.34163	-5.73683	8.32581	1
<i>2methyl - 2Butene</i>	-7.71438	1.95946	-3.15710	-2.22515	1
<i>TAME</i>	7.93490	2030.58	315.517	-	2

Where equation 1, is the Wagner correlation from Reid et al. (1987):

$$\ln\left(\frac{P}{P_C}\right) = (1-x)^{-1} \left[Ax + Bx^{1.5} + Cx^3 + Dx^6 \right] \dots\dots\dots(1)$$

P = pressure [bar]

P_C = critical pressure [bar]

T = temperature [K]

T_C = critical temperature [K]

And, equation 2 is the Antoine equation with parameters retrieved from DDB:

$$\log_{10}P = A - \frac{B}{(T-273.15)+C} \dots\dots\dots(2)$$